


# Synthesis, Characterization and Catalytic Activity of Graphene Promoted Metal / Metal Oxide Composite Catalysts on Direct Propylene Oxidation

**By**

**Sultan A. Alshuhri**

**711502**

**Wolfson College**

**Supervisor**

**Professor S. C. Edman Tsang**

**A dissertation submitted for the degree of Master of Science (by research) at the Inorganic Chemistry Laboratory, Department of Chemistry**

**University of Oxford**

**2017**

# Contents

1 Chapter 1: Introduction ..... 2

1.1 Catalysis ..... 2

1.2 Catalysts Classification ..... 3

1.3 Catalyst Selection ..... 5

1.4 Propylene Oxidation ..... 8

1.4.1 Acrolein ..... 16

1.4.2 Other Products ..... 19

1.5 Objective and Outline ..... 21

2 Chapter 2: Analytical techniques ..... 24

2.1 Gas Chromatography ..... 24

2.2 X-ray diffraction (XRD) ..... 25

2.3 Transition electron microscopy (TEM) ..... 28

2.4 Thermogravimetric analysis (TGA) ..... 31

2.5 Temperature programmed desorption (TPD) ..... 32

2.6 X-ray photoelectron spectroscopy (XPS) ..... 32

3 Chapter 3 Experimental: ..... 36

3.1 Graphene Synthesis: 36

3.2 Preparation of the composite catalysts: 36

3.3 GC Method Development 38

3.4 Reaction setup: 39

4 Chapter 4: Results and Discussion 41

4.1 XRD Measurements 41

4.2 TGA 43

4.3 Catalytic performance 44

4.3.1 Support performance 45

4.3.2 Ag Catalysts 49

4.3.3 Au catalysts 55

4.3.4 Cu catalysts 59

4.4 Graphene; a promoter or a poison? 64

4.4.1 Graphene as a support 66

4.5 Water addition: 72

4.5.1 Cu-G catalyst 72

4.5.2 Ag–G catalyst 73

4.5.3 Au-G catalyst ..... 74

4.6 Summary of Catalysts Performances towards Acrolein Production ..... 75

4.7 Summary ..... 77

4.8 TEM ..... 78

4.9 XPS ..... 81

4.10 Ammonia TPD ..... 86

5 Chapter 5: Conclusions and perspectives ..... 89

6 References ..... 93

7 Appendix A : Catalytic Results ..... 103

## Declaration

I confirm that this is my own work and the use of all materials from other sources has been properly and fully acknowledged.

Sultan A. Alshuhri

# Dedication

To my family.

# Acknowledgements

First and foremost, I would like to thank my supervisor Professor Edman Tsang for the help and guidance throughout my time in Oxford.

I would like to thank Professor Hamid Al-megren for the support and advice with the admission process, Prof. Abdulaziz Baqabs for the assistance and knowledge he provided, and Dr. Abdulhamid Alsaygh for encouraging me to pursue this path.

To my friends, Khaled Alghamdi and Feras Alshehri, I am so grateful that our paths have crossed. Thank you for the support you provided.

During my time in Oxford, I have had the privilege of meeting and working with great individuals. They contributed to my life and studies in many ways. Each one of them offered me sincere efforts to reach my goals and overcome obstacles. I will mention them in a historical manner:

Dr. Simon Fairclough, he was the first one to meet me at Oxford. He introduced me to my friends in the lab and guided me throughout my early days.

Bin Yu, my teammate and refined taste friend. We had great times together in the lab and in college. He offered me all the support throughout my days in Oxford.

Dr. Abdullah Khan, My neighbor in the office. Beautiful memories we made from the joy we had together.

Elizabeth Raine, great friend and the fun organizer of the group. Thank you for the continuous flow of TEM images.

Dr. Tugce Ayvali, the great team leader and friend. Thank you for your sincere help and advice.

Dr. Ian McPherson, beautiful soul and joy to talk to. Thank you for many hours of IR measurements and laughter.

Dr. Haohong Duan, Thank you for all the help and advice with my work.

Dr. Robert Jacobs and Dr. Ashley Shepard for the XPS analysis

I would like also to thank Ivo Teixeira, The great couple Molly & Jacob. Hanna Kreissl, Dr. Hanif Mahdi, Dr. Iuean Ellis, Simson Wu. Prof. Zhenyu Sun, Dr Jianwei, and all Edman's group members past and present for their friendship and support.

Finally, Many thanks to King Abdulaziz City for Science and Technology (KACST) for their generous financial support for my studies.

# Abstract

The catalytic oxidation of hydrocarbons such as propylene is of a major economic importance. The products of their oxidation are used daily in our life and the uses are expanding to other products. However, the oxidation processes are sometimes accompanied by various by-products that are environmentally unfriendly. Nowadays, the calling for greener production processes is louder than ever due to the emission of greenhouse gases and the other environmental pollutants. Therefore, a search for a capable catalyst to improve the process with a minimal environmental impact was set as a goal in this project.

We report herein the use of graphene as a promoter for different supports for the direct gaseous oxidation of propylene. Graphene, when added to the catalyst, can facilitate the production of acrolein through synergetic effects. Despite the fact that acrolein can be produced solely on graphene, the activity of the graphene was greatly improved when it was used as a support for the metals. The conversion had risen from 1% for graphene to 11% when graphene is loaded with 5% Cu. The increase of metal content can clearly increase the conversion.

Typically, Cu-G-$Al_2O_3$ and Cu-G produced acrolein with up to 52% selectivity and 11% conversion. TEM, XPS and $NH_3$-TPD characterization showed enhanced metal support interaction with acidic sites of graphene.

**List of Figures**

Figure 1-1: Generic potential energy diagram showing the effect of a catalyst in a hypothetical exothermic chemical reaction.[2] ..... 2

Figure 1-2: The catalytic cycle. ..... 3

Figure 1-3: catalysts classification (reproduced from [3] ). ..... 4

Figure 1-4: propylene oxidation on Ag.[22] ..... 10

Figure 1-5: ethylene oxidation on Ag.[22] ..... 11

Figure 1-6: Acrolein Products.[57] ..... 17

Figure 1-7: Propylene products. Reproduced from[72] ..... 20

Figure 2-1: GC components ..... 25

Figure 2-2: X-ray interference with matter. ..... 27

Figure 2-3: TEM components. Reproduced from [83]. ..... 30

Figure 2-4: The photoemission process for XPS. ..... 34

Figure 3-1: Reaction setup. ..... 39

Figure 4-1: XRD pattern of GO and Graphene. ..... 42

Figure 4-2: XRD pattern of $TiO_2$. ..... 42

Figure 4-3: XRD pattern of 1Au-1G-$TiO_2$. ..... 43

Figure 4-4: TGA of 1Au-$TiO_2$ / 1Au-5G-$TiO_2$. ..... 44

Figure 4-5: Conversion profiles of $Al_2O_3$ / $ZrO_2$ / $TiO_2$ supports. ..... 46

Figure 4-6: Selectivity profiles of $ZrO_2$ / 1G-$ZrO_2$/ 5G-$ZrO_2$ to partial oxidation products in the temperature range of 160 °C - 430 °C. ..... 47

Figure 4-7: Selectivity profiles of $TiO_2$ / 1G-$TiO_2$/ 5G-$TiO_2$ to partial oxidation products in the temperature range of 160 °C - 430 °C. ..... 48

Figure 4-8: Selectivity profiles of $Al_2O_3$ / 1G-$Al_2O_3$/ 5G-$Al_2O_3$ to partial oxidation products in the temperature range of 160 °C - 430 °C. ..... 49

Figure 4-9: Conversion profiles of 1Ag-1G-$Al_2O_3$/ 1Ag-5G-$Al_2O_3$/ 1Ag-$Al_2O_3$/ 5Ag-1G-$Al_2O_3$/ 5Ag-5G-$Al_2O_3$ catalysts in the temperature range of 160 °C - 430 °C. ..... 50

Figure 4-10: Conversion profiles of 1Ag-1G-$TiO_2$/ 1Ag-5G-$TiO_2$/ 1Ag-$TiO_2$/ 5Ag-1G-$TiO_2$/ 5Ag-5G-$TiO_2$ catalysts in the temperature range of 160 °C - 430 °C. ..... 52

Figure 4-11: Conversion profiles of 1Ag-1G-$ZrO_2$/ 1Ag-5G-$ZrO_2$/ 1Ag-$ZrO_2$/ 5Ag-1G-$ZrO_2$/ 5Ag-5G-$ZrO_2$ catalysts in the temperature range of 160 °C - 430 °C. ..... 54

Figure 4-12: Conversion profiles of 1Au-1G-$Al_2O_3$/ 1Au-5G-$Al_2O_3$/ 1Au-$Al_2O_3$/ 5Au-1G-$Al_2O_3$/ 5Au-5G-$Al_2O_3$ catalysts in the temperature range of 160 °C - 430 °C. ..... 56

Figure 4-13: Conversion profiles of 1Au-1G-$TiO_2$/ 1Au-5G-$TiO_2$/ 1Au-$TiO_2$/ 5Au-1G-$TiO_2$/ 5Au-5G-$TiO_2$ catalysts in the temperature range of 160 °C - 430 °C. ..... 57

Figure 4-14: Conversion profiles of 1Au-1G-$ZrO_2$/ 1Au-5G-$ZrO_2$/ 1Au-$ZrO_2$/ 5Au-1G-$ZrO_2$/ 5Au-5G-$ZrO_2$ catalysts in the temperature range of 160 °C - 430 °C. ..... 58

Figure 4-15: Conversion of 1Cu-1G-$Al_2O_3$/ 1Cu -$Al_2O_3$/ 5Cu -1G-$Al_2O_3$/ 5Cu -5G-$Al_2O_3$ catalysts in the temperature range of 160 °C - 430 °C. ..... 60

Figure 4-16: Conversion profiles of 1Cu-1G-$TiO_2$/ 1Cu-5G-$TiO_2$/ 1Cu-$TiO_2$/ 5Cu-1G-$TiO_2$/ 5Cu-5G-$TiO_2$ catalysts in the temperature range of 160 °C - 430 °C. ..... 61

Figure 4-17: Conversion profiles of 1Cu-1G-$ZrO_2$/ 1Cu-5G-$ZrO_2$/ 1Cu-$ZrO_2$/ 5Cu-1G-$ZrO_2$/ 5Cu-5G-$ZrO_2$ catalysts in the temperature range of 160 °C - 430 °C. ..... 63

Figure 4-18 : Acrolein selectivity obtained with different catalysts..... 66

Figure 4-19: Conversion and products selectivity of graphene in the temperature range of 160 °C - 430 °C. ..... 67

Figure 4-20: Conversion profiles of 1Ag-G/ 5Ag-G catalysts in the temperature range of 160 °C - 430 °C. ..... 68

Figure 4-21: Conversion profiles of 1Au-G/ 5Au-G catalysts in the temperature range of 160 °C - 430 °C. ..... 69

Figure 4-22: Conversion profiles of 1Cu-G/ 5Cu-G catalysts in the temperature range of 160 °C - 430 °C. ..... 71

Figure 4-23: Conversion profile of 1Cu-G+$H_2O$ catalyst in the temperature range of 160 °C - 430 °C. ..... 72

Figure 4-24: Selectivity of 1Cu-G/ 1Cu-G+$H_2O$ catalysts. ..... 73

Figure 4-25: Conversion profile of 1Ag-G+$H_2O$ catalyst in the temperature range of 160 °C - 430 °C. ..... 73

Figure 4-26: Selectivity of 1Ag-G/ 1Ag-G+$H_2O$ catalysts..... 74

Figure 4-27: Conversion profile of 1Au-G+$H_2O$ catalyst in the temperature range of 160 °C - 430 °C. ..... 74

Figure 4-28: Selectivity of 1Au-G/ 1Au-G+$H_2O$ catalysts..... 75

Figure 4-29: TEM images of 5Cu-5G-$Al_2O_3$ catalyst before and after the reaction. ..... 78

Figure 4-30: Cu particle size distribution before and after the reaction for 5Cu-5G-$Al_2O_3$ catalyst. ..... 79

Figure 4-31: TEM images for 5Cu-G catalyst before and after the reaction. ..... 80

Figure 4-32: Cu particle size distribution before and after the reaction for 5Cu-G catalyst. 80

Figure 4-33: Survey and High-resolution XPS Spectra of 5Cu-5G-$Al_2O_3$ catalyst before reaction. ..... 81

Figure 4-34: Survey and High-Resolution XPS spectra of 5Cu-5G-$Al_2O_3$ catalyst after reaction. ..... 82

Figure 4-35: Survey and High-Resolution XPS spectra of 5Cu-G catalyst before reaction. 83

Figure 4-36: Survey and High-Resolution XPS spectra of 5Cu-G. catalyst after reaction. .. 85

Figure 4-37: $NH_3$ TPD for 5Cu-$Al_2O_3$ and 5Cu-G catalysts in the range of 60 °C - 430 °C. 87

**List of Tables**

Table 1: Corresponding retention time of the products. ..... 38

Table 2: Selectivity of 1Ag-1G-$Al_2O_3$/ 1Ag-5G-$Al_2O_3$/1Ag-$Al_2O_3$/ 5Ag-1G-$Al_2O_3$/ 5Ag-5G-$Al_2O_3$ catalysts. ..... 51

Table 3: Selectivity of 1Ag-1G-$TiO_2$/ 1Ag-5G-$TiO_2$/ 1Ag-$TiO_2$/ 5Ag-1G-$TiO_2$/ 5Ag-5G-$TiO_2$ catalysts..... 53

Table 4: Selectivity of 1Ag-1G-$ZrO_2$/ 1Ag-5G-$ZrO_2$/ 1Ag-$ZrO_2$/ 5Ag-1G-$ZrO_2$/ 5Ag-5G-$ZrO_2$ catalysts..... 54

Table 5: Selectivity of 1Au-1G-$Al_2O_3$/ 1Au-5G-$Al_2O_3$/ 1Au-$Al_2O_3$/ 5Au-1G-$Al_2O_3$/ 5Au-5G-$Al_2O_3$ catalysts. ..... 56

Table 6: Selectivity of 1Au-1G-$TiO_2$/ 1Au-5G- $TiO_2$/ 1Au- $TiO_2$/ 5Au-1G $TiO_2$/ 5Au-5G-$TiO_2$ catalysts. ..... 58

Table 7: Selectivity of 1Au-1G-$ZrO_2$/ 1Au-5G- $ZrO_2$/ 1Au- $ZrO_2$/ 5Au-1G $ZrO_2$/ 5Au-5G-$ZrO_2$ catalysts..... 59

Table 8: Selectivity of1Cu-1G-$Al_2O_3$/ 1Cu -$Al_2O_3$/ 5Cu -1G-$Al_2O_3$/ 5Cu -5G-$Al_2O_3$ catalysts. ..... 61

Table 9: Selectivity of 1Cu-1G-$TiO_2$/ 1Cu-5G-$TiO_2$/ 1Cu-$TiO_2$/ 5Cu-1G-$TiO_2$/ 5Cu-5G-$TiO_2$ catalysts..... 62

Table 10: Selectivity of 1Cu-1G-$ZrO_2$/ 1Cu-5G-$ZrO_2$/ 1Cu-$ZrO_2$/ 5Cu-1G-$ZrO_2$/ 5Cu-5G-$ZrO_2$ catalysts..... 63

Table 11: Acrolein selectivity and corresponding temperature on different supports..... 65

Table 12: Acrolein selectivity and corresponding temperature on selected catalysts. ..... 65

Table 13: Selectivity of 1Ag-G/ 5Ag-G catalysts..... 69

Table 14: Selectivity of 1Au-G/ 5Au-G catalysts..... 70

Table 15: Selectivity of 1Cu-G/ 5Cu-G catalysts. ..... 71

Table 16: Yield percentages of the tested catalysts. ..... 76

Table 17: Yield percentages of different catalysts from literature. ..... 77

**List of abbreviations and symbols**

$m_o$ - Electron's mass

A = Concentration of solute

BE - Binding energy

CO - Carbon monoxide

d - Interplanar spacing

$e$ - Elementary charge

GC – Gas chromatography

$h$ - Planck's constant

Kc - Distribution constant

M - Mobile phase

Max - Temperature at which the highest selectivity was recorded

OS - On-set (The temperature at which the product is detected on the reaction set up)

S - Stationary phase

TEM – Transmission electron microscopy

TGA – Thermogravimetric analysis

TOF – Turn over frequency

TON – Turn over number

TPD – Temperature programmed desorption

$V$ - Accelerating voltage

XPS – X-ray photoelectron spectroscopy

XRD – X-ray diffraction

ΔG - Change in Gibb's free energy

θ - Diffraction angle

λ - Wavelength

n : Integer

L : mean size of the crystal

K : constant

β : Line broadening

FWHM : Full width at half maximum

V : Volt

C : Celsius

$\phi_s$ = work function of the spectrometer

K.E : Kinetic energy

Sample nomenclature:

1M-1G-MO

- 1 wt.% metal (Metal (M): Ag, Au or Cu),

1 wt.% graphene (G: Graphene)

MO: Metal oxide (MO: $Al_2O_3$, $TiO_2$ or $ZrO_2$)

For example: 1Ag-1G-$Al_2O_3$ represents 1 wt.% Ag and 1wt.% graphene, that are loaded on $Al_2O_3$.

Chapter 1 :

# Introduction

# 1 Chapter 1: Introduction

## 1.1 Catalysis

*Catalysis* is the process where a substance *(catalyst)* increases the rate of a reaction without modifying the overall standard Gibbs energy.[1] Catalysts work by providing an alternative molecular path (mechanism) for the reaction involving a different transition state and lower activation energy (Figure 1-1). Since activation energy is defined as the minimum energy that must be overcome to have a reaction, lowering the activation energy barrier leads to more molecular collisions having the energy needed to reach the transition state. Hence, catalysts can enable reactions that would otherwise be blocked or slowed by a kinetic barrier. The catalyst may increase reaction rate or selectivity, or enable the reaction at lower temperatures.

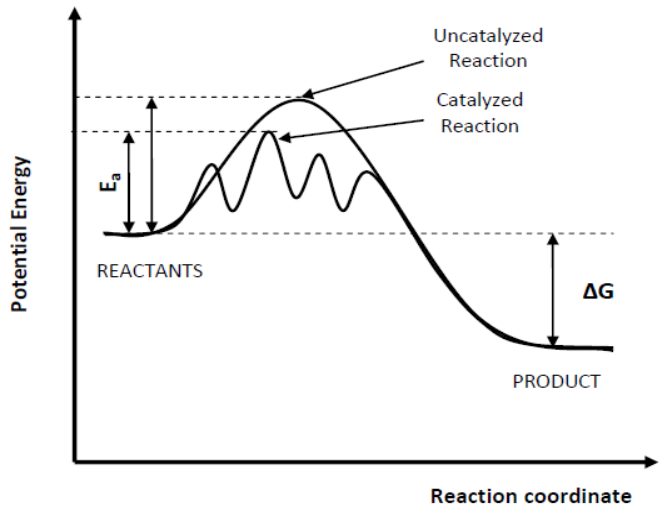



*Figure 1-1: Generic potential energy diagram showing the effect of a catalyst in a hypothetical exothermic chemical reaction.*[2]

In addition, as catalysts, in principal, emerge from the reaction as unchanged, they can take part in many repeated cycles. Figure 1-2 illustrates the phenomenon of a catalytic cycle in which the reactants attach to the catalyst's surface and react, then, desorb in a form of new products. After that, the catalyst can then host new molecules for further reactions. Catalysis is a very important concept to the industry. It aims to increase the yield of the desired product with a minimum number of byproducts, offering a safer and low-cost production.

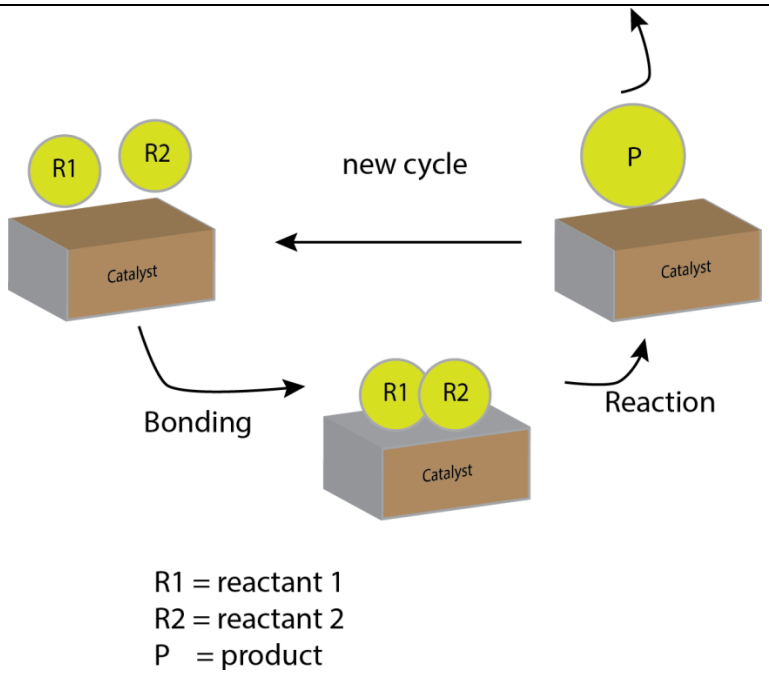



*Figure 1-2: The catalytic cycle.*

## 1.2 Catalysts Classification

The classification of catalysts falls into three main groups as *heterogeneous*, *homogeneous*, and *biological*, as represented in Figure 1-3.

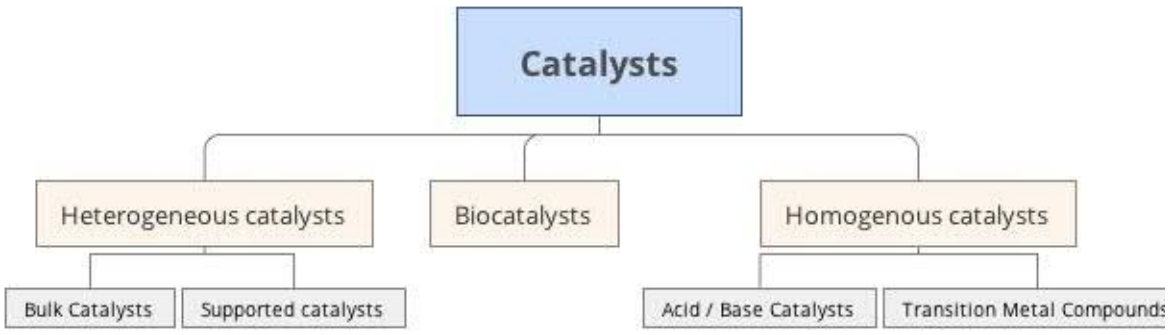



*Figure 1-3: catalysts classification (reproduced from* [3] *).*

Homogeneous and heterogeneous classification is depending on whether the catalyst exists in the same phase as the substrate. Catalytic processes that take place in a uniform phase, for instance liquid catalysts in liquid reactants, are classified as *homogeneous catalysis*. *Heterogeneous catalysts* are those that act in different phase than substrates. Heterogeneous catalysis is crucial to chemical technology. Most catalytic processes are heterogeneous in nature, typically involving a solid catalyst and gas or liquid-phase reactants. Today, the majority of industrial processes involve heterogeneous catalysis.[4]

Homogenous catalysts usually consist of structurally defined materials or coordination complexes. They are better dispersed and have more opportunity to be active, since each atom can interact with the medium, while for the heterogonous catalysts only the surface atoms have access to the surroundings. In addition, the homogenous catalysis usually requires less energy and concentration of the catalyst since the reactants can approach the catalytic center from any direction. Higher selectivity can be achieved using homogenous catalyst, because mass transport does not play a major rule for the catalytic cycle, unlike that of the

heterogeneous catalyst where mass transport is projecting heavily over the catalytic cycle. The study of the mechanism is also relatively easier for the homogeneous catalyst, since the reaction site is better defined, while it is cumbersome for the heterogeneous catalyst. On the other hand, the heterogeneous catalyst is easier to separate from the reaction medium, centrifuging or filtration would be sufficient. While for homogenous catalysts, more advanced procedures are involved, ion exchange or liquid – liquid extraction to name a few. In addition, thermal stability is a major advantage of heterogeneous catalysts. They can endure higher temperatures while lower temperatures must be used for the homogenous catalysts.[5]

Besides homogeneous and heterogeneous catalysts, another group of catalysts that cannot be categorized according to phase difference exist, namely *biocatalysts*, also known as enzymes. Enzymes possess the highest level of complexity among the three types of catalysts. They are nature's own catalysts and fundamental for life, as they catalyze essentially all biological processes.[6]

## 1.3 Catalyst Selection

The suitability of a catalyst in order to satisfy industry demands depends mainly on the following three criteria,[6]

- Activity
- Selectivity
- Stability

Designing a long-lived, efficient, selective, well-defined, isolable and reusable catalyst is under investigation in various research groups in today's world. In order to achieve such an *ideal* catalyst, all these three criteria need to be satisfied.

**Activity** is a measure of how fast one or more reactions proceed in the presence of the catalyst. The catalyst activity can be given by *Turnover Number* (TON) or/and *Turnover Frequency* (TOF) values. TON is defined as total number of moles of product formed per number of active sites until deactivation (Equation 1). TOF is the catalytic turnover number per unit time (the number of moles of product per number of active sites per unit time)[7] (Equation 2).

$$\mathrm{TON} = \frac{\text{mole of product}}{\text{number of active sites}} \qquad (1)$$

$$\mathrm{TOF} = \frac{\text{mole of product}}{\text{number of active sites } x \text{ time}} \qquad (2)$$

There are two major active species for heterogeneous catalysts: metals and metal oxides. This classification can extend to have mixtures of both. The surface of the catalyst is defined as the active phase since it is the only part that can interact with the surrounding environment. Therefore, the smaller the size of the catalyst is, the larger the exposure to the surroundings leading to higher interactions, and so better activity. Since the number of atoms on the surface of a bulk metal or metal oxide is extremely small compared to the number of atoms in the interior, bulk materials are often too costly to use in a catalytic process. Therefore, most of the active phase particles are loaded and dispersed on a carrier, called *support* to increase the

effective surface area of a valuable catalytic material such as a transition metal. The support interacts with the active metal and influences its behavior and stability.

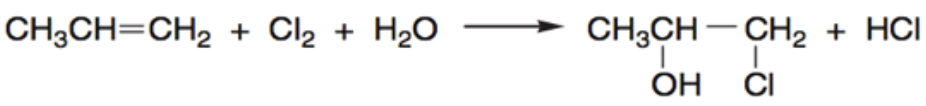
The **selectivity** of a reaction is the fraction of the starting material that is converted to the desired product. A selective catalyst yields a high proportion of the desired product with minimum amount of the side products. High selectivity plays an important role in industry to reduce waste, the work-up equipment of a plant, and to ensure more effective use of feedstock.[3]

The chemical, thermal and mechanical **stability** of a catalyst determine its lifetime in industrial reactors. Catalyst stability is influenced by deactivation of the catalyst which usually occurs after the catalytic cycle due to aging, poisoning or coking. When the activity of the catalyst is diminished by chemisorption of materials that are not easily removed, the deactivation process is termed as *poisoning.* The degree of poisoning depends on the adsorption strength of the poison on the active site when compared to that of the reactants that are competing for the same catalytic site.[8] The catalytic site may also get blocked due to the deposition of some species from the fluid phase. This process is prominent with porous catalysts since it leads to the blockage of the pores and channels of the catalyst.[9] The bond linking the catalyst and the poison are often strong and highly specific. Consequently, the process is usually irreversible. However, in some cases, change in the temperature or the composition of the gas to which the catalyst is exposed might be sufficient to restore catalyst activity. In addition to poisoning, there is a second catalyst deactivation process, *aging,* that is commonly encountered in industrial processes. Aging involves a loss in activity due to a loss in catalyst surface area arising from crystal growth or sintering. This process becomes

faster as the temperature rises. Other factors may also control the extent of sintering. For instance, oxygen facilitates faster sintering, while hydrogen exhibits less of an effect in that regard.[10] In addition, the interaction between the metal and the support has an inverse correlation with sintering, the stronger the interaction the less the sintering.[11] Defects on the surface of the support can also help anchor the metal particles, which in turn reduces their agglomeration.[12] The deactivation process is highly undesirable by the industry, because high costs are usually associated with halting the processes to regenerate or change the catalyst.

## 1.4 Propylene Oxidation

Propylene is produced as a byproduct of the steam cracking process used for ethylene production.[13] It is a starting material for many beneficial materials. Oxidation of propylene can produce propylene epoxide (PO) which is a chemical intermediate used in vast industrial and consumer products. It is used in the production of polyether polyols which are used in the production of urethane. The urethane is then used in the manufacturing of rigid foams, flexible foams, coatings and adhesives. In addition, it is also used in the production of propylene glycol for fiberglass polyester resins and hydraulic fluids.[14] Commercial production of propylene oxide was established in the 1930s with the chlorohydrin process. In this process, propylene is reacted with chlorine and water to form chlorohydrin (reaction 1), followed by a reaction with calcium hydroxide to form propylene oxide and large amounts of calcium chloride as a byproduct (reaction 2), which requires disposal.[15]



(1)



(2)

Following the chlorohydrin process, different processes, such as hydrogen peroxide and cumene recycling processes,[15] were developed for the production of propylene oxide, all of which suffered from drawbacks such as undesired byproducts or the use of dangerous oxidants. The latest commercial process was established by Dow-BASF in 2008 using hydrogen peroxide as an oxidant in the presence of TS-1, titanosilicate, as a catalyst and methanol as the solvent. This process is considered more environmentally friendly as water is the only byproduct and more flexible towards market demands. However, the on-site synthesis of $H_2O_2$ is indispensable as it is expensive and dangerous to transport. In addition, large amount of methanol is required to be used for stable operation to avoid a biphasic liquid, which then needs to be separated from the reaction medium and recycled.[16,17]

Due to the drawbacks of the mentioned PO production routes (*vida supra*), researchers and industrial companies have recently started to search for alternative ways for the production of PO.[18] The drive of the research is to find a direct, one step propylene to propylene oxide reaction. This aim was encouraged with the success of the currently used process of direct ethylene to ethylene oxide production using Ag loaded on $Al_2O_3$ as the catalyst. This catalyst can produce ethylene epoxide with oxygen only, giving selectivity near 50%, and when promoters are used, the selectivity increases to over 80%. The high selectivity is attributed to Ag being able to dissociate oxygen easily, leading to the formation of oxygen adatoms, while the role of promoters is suggested to enhance the electrophilic properties of the oxygen, leading to its insertion to the double bond, forming the epoxide.[19] It is well accepted that the

valance charge state of the atomically adsorbed oxygen ($O_{ad}$) can control the outcome of the reaction. According to XPS experiments performed by Bukhtiyarov *et.al*[20], two adsorbed oxygen spices with $O_{1s}$ binding energies of 528.3 and 530.4 eV were detected and attributed to the nucleophilic and electrophilic oxygen atoms respectively. The $O_{ad}$ with lower valance charge density is suggested to promote the epoxidation reaction, while the $O_{ad}$ with higher valance charge density causes the abstraction of hydrogen leading to combustion.[21]

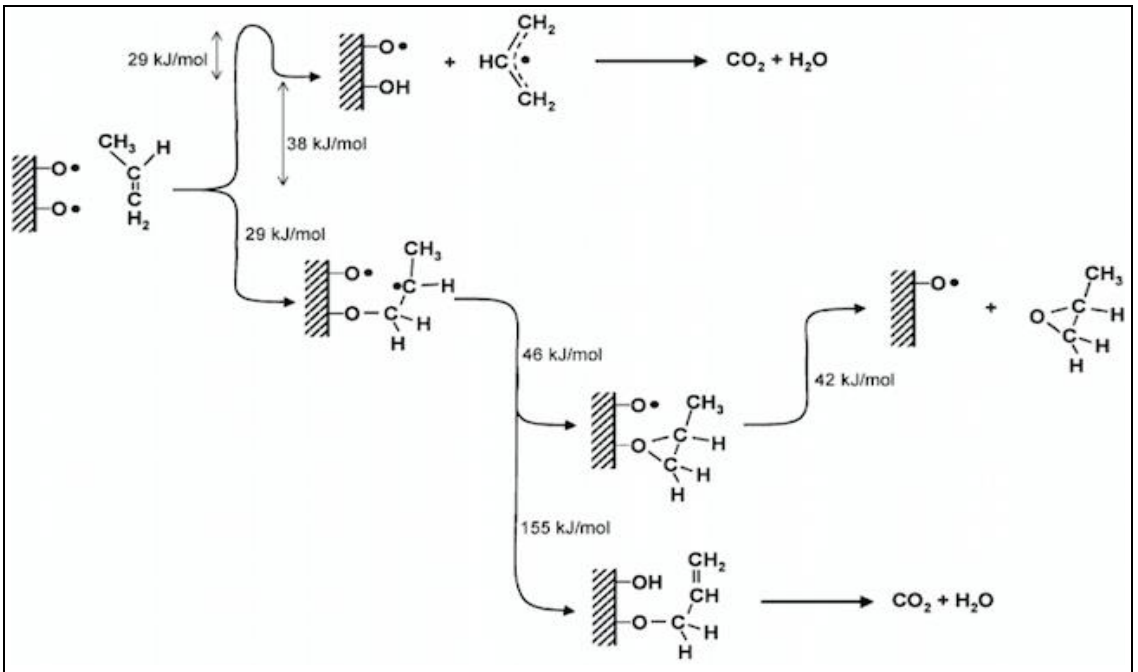



*Figure 1-4: propylene oxidation on Ag.*[22]

The efforts to mimic the ethylene epoxidation process for propylene were faced with low conversion, and selectivity towards combustion products. The difficulties faced with propylene epoxidation on the Ag surface led the researchers to investigate first the possible differences in reaction mechanisms.

DFT calculations examined for propylene (Figure 1-4) and ethylene (Figure 1-5) oxidations on the Ag(111) surface suggests that the low propylene oxide selectivity is due to the allylic hydrogen of propylene, which is weakly bonded when compared to the C-H bond of the ethylene. The cleavage of this bond by the oxygen adatoms to form an allylic intermediate is more favorable, which terminates as combustion products.

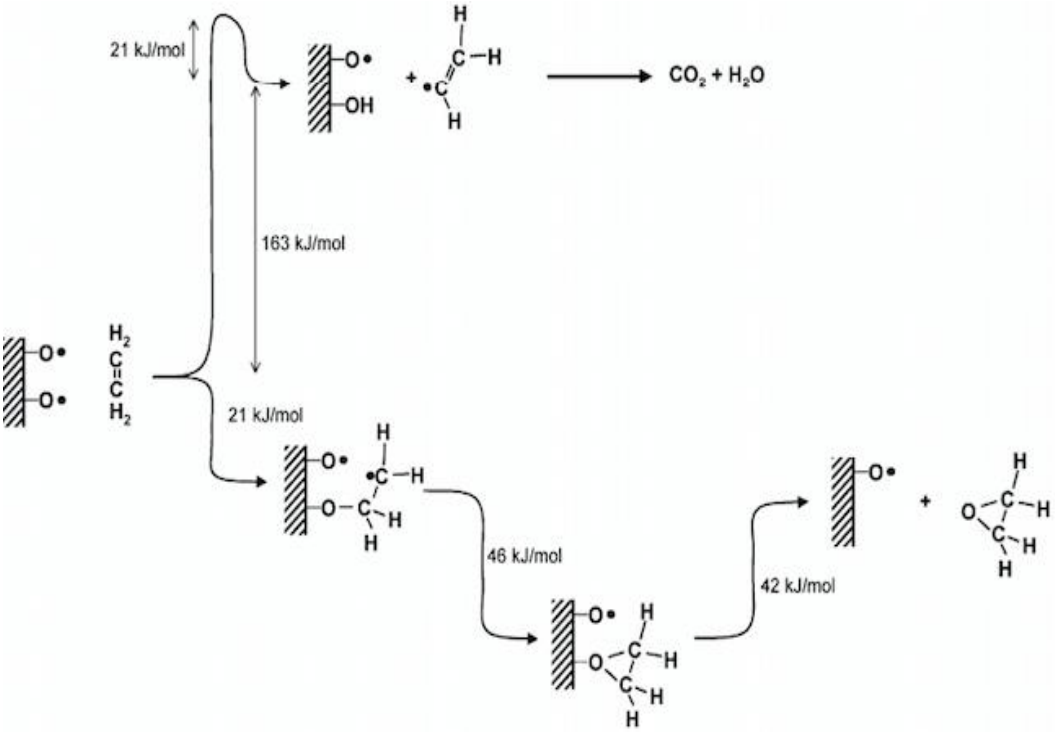



*Figure 1-5: ethylene oxidation on Ag.*[22]

Since then, much effort has been devoted to the enhancement of PO selectivity, mainly focusing on modification of electronic properties of the surface oxygen atoms toward electrophiles by introducing promoters such as chlorine, alkalis, $NO_x$ and metal oxides.[23–26] This increase in selectivity is attributed to the possible electronic effects induced by

minimizing the negative charge on the electron rich oxygen, rendering them being less basic and more attracted to the double bond of propylene instead of the allylic hydrogen as suggested by a DFT study.[27,28]

Researchers continued to investigate other factors that can influence the reactivity of the catalytic system. They found that Ag particle size seems to affect the outcome of the reaction. Schuth *et. al.* reported that Ag supported on anatase $TiO_2$ with a particle size between 2 – 4 nm can produce PO with selectivity up to 90%.[29] They also used different preparation methods but only the deposition precipitation method produced the higher selectivity. The oligomerization of PO on the Ag surface caused the deactivation of the catalyst. Other researchers tested Ag on TS-1 by deposition precipitation method and reported the optimum size of Ag to be 8 nm.[30–32]

In the studies different promoters were used, KOH and $Na_2CO_3$ for example, and it was found that the best result is achieved when using $K_2CO_3$. The group reported a 1.9% propylene conversion and 91% PO selectivity with $H_2$ and $O_2$.

In addition to Ag, Au and Cu have been grouped together as what is called "coinage metals alloys" due to their special properties and reactivity.[33] The d band of coinage metals is completely occupied; however, the low ionization potential of Cu and Ag can lead them to lose an electron easily. This loss creates a vacancy on the d orbital inducing reactivity. Au, on the other hand, has a higher ionization potential resulting in poor interactions with molecules and other elements. [34] Bond and co-workers opened the door for the use of Au as a catalyst when they reported the success of using Au on silica for the hydrogenation of alkenes and alkynes.[35]

This work has encouraged other researchers to explore the Au as a catalyst. $O_2$ adsorption experiments performed by Sault *et. al* [36] on clean Au surfaces suggest that adsorption of $O_2$ is not dissociative, leading to the conclusion that it cannot be used as an oxidation catalyst. However, in 1987 Haruta and co-workers [37] reported that Au can be used as CO oxidation catalyst when the size of the Au catalyst was controlled carefully. After the successful application of Au as an oxidation catalyst, in 1998, Haruta carried out his work on propylene and he reported for the first time the ability of Au nanoparticles deposited on anatase $TiO_2$ to catalyze the oxidation of propylene to propylene oxide in the presence of $O_2$ and $H_2$. In this process,[15,38] $H_2$ was used as sacrificial reductant, which led to in-situ formation of hydroperoxy species ($^{-}$OOH). Applying atmospheric pressure and mild heat could lead to an impressive selectivity of above 90%, but the conversion remained low at around 1%. After this study, many $TiO_2$ and titanosilicate supported, well dispersed Au nanoparticle catalysts have been developed with which, the conversion could rise up to 10% with a selectivity over 90%. Although those results show the best catalytic activity among heterogeneous catalyst systems, and show the use of nanoscale Au to be very promising, several issues still need to be clarified and improved before these catalysts can be employed in practical applications. Firstly, the studies indicate that the selectivity of Au particles is extremely sensitive to their size and shape. [39] The studies of Haruta[40] and Delgass [41] indicate that Au particles smaller than 2.0 nm (1.0-2.0 nm) are stable and active in PO formation while particles larger than that oxidize propylene to total combustion products. In addition, based on theoretical calculation, Joshi *et. al* [42,43] suggested that smaller Au clusters (<0.55 nm) incorporated into the microporous channels of TS-1 could be responsible for high activity. Moreover, it has been found that spherical Au particles lead to the complete combustion and require elevated temperatures

while strongly attached hemispherical nanoparticles lead to the production of PO with near 100% selectivity at lower temperatures. [44] The influence of the shape of the nanoparticles on the activity of the catalyst is attributed to the nanoparticles having different crystallographic structure, density and packing which give rise to different electronic states on their surface. [45] In addition, support-nanoparticle interaction plays a significant role in adsorption of reactants as well as stability of nanoparticles under reaction conditions. For instance, hemispherical shaped nanoparticles have a flatter shape than spherical ones; therefore, the interaction between the support and the nanoparticle is stronger offering to large metal-support interface and high stability.[34,46]

The second concern for this reaction is the requirement for hydrogen which should be as low as possible or, if possible, be suppressed for economic and safety reasons (potential explosion risk of the mixture of $H_2$ and $O_2$). A safer alternative has been reported by Ojeda and Iglesia [47] for *in-situ* formation of hydroperoxy species from $O_2/H_2O$ mixtures with $H_2O$ replacing $H_2$. The third problem is the stability of the catalysts, most of which are deactivated in a short period of time.

As an alternative to Ag and Au, low-cost Cu catalysts have also received major research effort as oxidation catalysts. The multiple oxidation states and the accessibility in-between them gives rise to a rich chemistry between Cu, it's derivatives and reactive molecules.

Lambert *et. al.*[48] presented Cu on silica as an oxidation catalyst for propylene using only molecular oxygen at atmospheric pressure. The selectivity reported to be over 50% at 225 °C with a conversion of 0.25 %. The selectivity declined rapidly reaching negligible levels near 275 °C, but the conversion increased to 1.26%. Other products were observed, including

acetaldehyde and acetone. Lambert also observed that while the selectivity of PO is decreased, the selectivity of acrolein has increased, which suggests that PO is a precursor for acrolein production.

Infrared studies on Cu/silica catalysts showed that propylene adsorbs strongly on $Cu^0$ via C=C stacking and is capable of PO production. The study also showed that the use of promoters can strongly enhance PO selectivity.[49]

$Cu_2O$ was also suggested to be active for PO formation. A report showed that the size of the oxide can influence the selectivity inversely, the smaller the size the higher PO selectivity. The study also showed that the adsorption geometry is similar to that of $Cu^0$ with C=C stacking.[49,50]

Other studies showed that $CuO_x$-$SiO_2$ catalysts prepared by the sol-gel method can produce propylene oxide efficiently by molecular oxygen without prior reduction of the catalyst. The report mentioned that the $Cu^{1+}$ is responsible for the activation of oxygen that leads to the insertion to the double bond followed by the formation of the epoxide. Modification with $K^+$ improved PO selectivity. [50]

In addition, CuOx loaded into SBA-15 support without further reduction showed PO selectivity between 15-50%. The selectivity could be sustained with the increase of conversion from 1% to 12 %. At higher temperature, the production of PO decreased, while acrolein production increased.[51]

Cu oxides are also used in combination with metal oxides to produce PO. CuOx-RuO-NaCl was reported to produce PO selectivity of 40- 50% at propylene conversion of 10 - 20%. The

production of PO was accompanied with acrolein, acetaldehyde and propanal in addition to CO and $CO_2$. The study also showed that the use of the trimetallic system produces the best results when compared to the single and binary systems of the same metals and oxides.[52] The same research group also reported the system SnO2-CuO-NaCl/SiO2 to have a PO selectivity of up to 60% with a conversion between 1-3%.[53]

In order to understand the active copper species responsible for PO production, the researchers performed x-ray experiments under high vacuum using styrene and butadiene as probe molecules due to the low adsorption enthalpy of propylene. The results showed that $Cu^0$ was responsible for the epoxide formation.[54,55] Cu oxidation caused a decrease of the epoxide formation. Further studies were performed on trans methyl styrene, a product that contains an allylic species, and the result showed a similar pattern.[56] Additional studies on styrene by Lambert indicated that oxygen adatoms and Cu metal sites are necessary for styrene adsorption. In addition, he noticed that $CO_2$ production halted during epoxidation under low temperatures leading to higher selectivity for the epoxide. Then he added that even though styrene does adsorb on the Cu (110) – oxygen surface, the catalytic system is inert, whereas in Cu (110); the adsorption is stronger and catalytically active. Finally, the geometry for the adsorption of styrene on the two surfaces was similar, this suggests that the difference in reactivity is not likely due to the difference in adsorption geometry. [55]

### 1.4.1 Acrolein

Acrolein is another chemical produced from the oxidation of propylene. It is the simplest unsaturated aldehyde with the formula $CH_2$=CH-CHO. It accommodates a vinyl group and

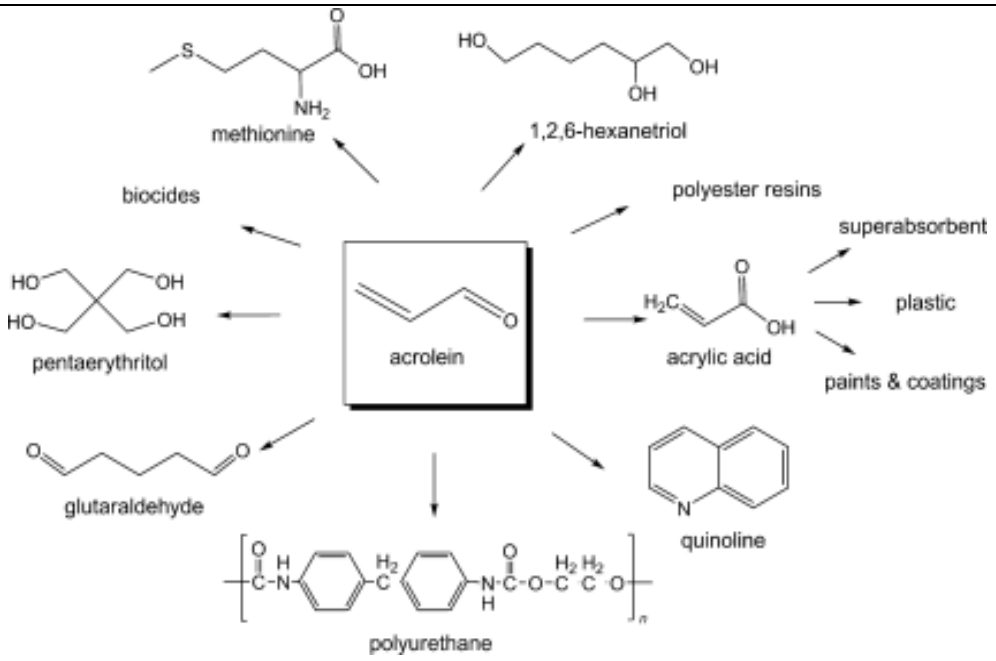



*Figure 1-6: Acrolein Products.*[57]

carbonyl group, giving rise to numerous possibilities for forward integrations. Figure 1-6 provides some products that are produced from acrolein.

Polyacrylic acid is used in the manufacturing of super absorbent materials used in diapers, acrylate plastics, and coatings. Acrylic acid is one of the fastest growing chemicals with an average annual growth of approximately 4%. Further processing of acrolein produces methionine, an amino acid that contains sulfur. Methionine is required by animals, but it is not readily available in natural food resources. In 2006, Belgium built a facility to produce methionine with 120 000-ton annual capacity.[57]

Acrolein was commercially produced using gas phase condensation of acetaldehyde and formaldehyde by Degussa in 1942. Recently, it is produced using heterogeneously catalyzed gas phase oxidation of propylene.[58] It can also be produced from propane, but the selectivity has not reached the levels of economic viability. Many other synthesis methods can be used for acrolein production; for instance, nickel phosphates or silica supported metal oxides are used to react formaldehyde with ethanol to produce acrolein.[59] Oxidative dehydrogenation of allyl alcohol can also establish the production of acrolein.[60] In addition, the partial oxidation of ethane over a silica supported iron catalyst produces the acrolein at elevated temperatures.[61] The previous routes suffer major shortcomings for use at an industrial scale, including low selectivity, excessive energy requirements and costly reactants.

Currently the partial oxidation of propylene to acrolein is the industrial method to produce acrolein. Temperatures between 250 - 400 °C are used for the reaction.[62] One of the earliest catalytic systems used on this oxidation was a Cu and Cu oxide catalyst system. The catalyst has been found to be difficult to characterize since multiple changes occur to the bulk chemical composition when it is under the reaction conditions. The catalyst is easily affected by the reaction mixture, duration and temperature. Further studies showed that a Cu rich oxide leads to the formation of acrolein, while the increase of oxygen facilitates the combustion.[63] The effect of the ratios of the catalyst's components can be extended to the currently used oxidation catalyst for acrolein formation. This catalyst contains multiple components with the formula Mo–Bi–$X^{II}$–$X^{III}$(–$X^{I}$–Y–Z)–O, where, Mo–Bi–$X^{II}$–$X^{III}$ represents the basic structure with four metal components, $X^{II}$ = (Co, Ni,Me,Mg,Pb), and $X^{III}$ = (Fe,Cr,Ce,Al). The major active site is the bismuth molybdate which is located on the surface of the catalyst. The activity of the catalyst is greatly affected by the oxidation states of the metal components, the highest activity

is observed with the simultaneous occurrence of a divalent and trivalent metal ion, for example $Co^{2+}$ and $Fe^{3+}$. For the other components $(–X^{I}–Y–Z)$-O, the factor $X^{I}$ contains an alkaline metal, Y can contain one of Sb,Te,V,W or Nb, while Z can be composed of B or P.[64] The process includes co-feeding of steam to enhance the acrolein production through the occupation of the strong oxidation sites, preventing further oxidation to $CO_2$.[65]

The synergy between the oxidation states of the metals greatly affects the performance of the catalyst.[66] The lattice oxygen is considered responsible for the oxidation leading to acrolein formation, while $CO_2$ forms from the gas phase or lattice oxygens. [67] Regarding the mechanism, it is believed that the intermediate step involves the formation of an allylic species. [68,69] The oxygen center coordinated to Bi, or Bi-O-Mo bridge is responsible for the hydrogen abstraction leading to the oxidation.[69,70] Prolonged adsorption of acrolein leads to the formation of acrylic acid or $CO_2$.[71]

### 1.4.2 Other Products

The oxidation of propylene has many other products. Reactions with oxygen can produce acetone, which could transform into ethanol and acetic acid. The reaction with water leads to the production of propanol and propanal. Figure 1-7 shows a proposed sequence of the propylene oxidation process.

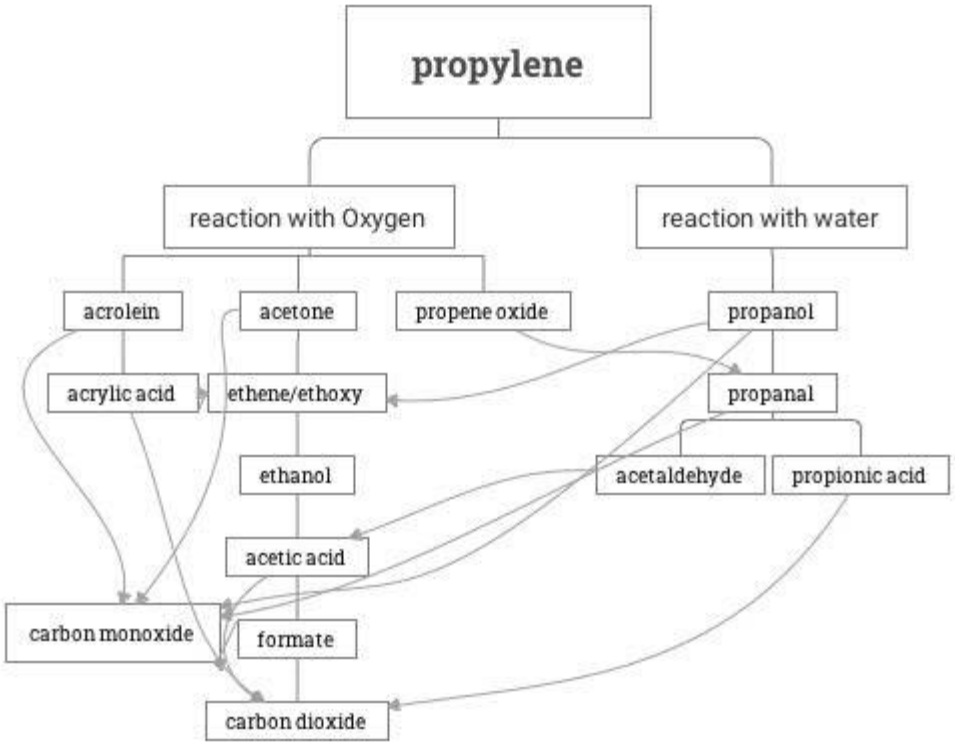



*Figure 1-7: Propylene products. Reproduced from*[72].

## 1.5 Objective and Outline

The importance of the additives and promoters for selective propylene oxidation has been established from the literature survey. The promoters could alter the electronic properties of the dissociated oxygen on the metal surface. When molecular oxygen dissociates, it forms two types of competing reactive oxygen adatoms; one with higher partial charge, which abstracts the weakly bonded allylic hydrogen causing total oxidation to combustion products, and the other less charged oxygen, which leads to oxygen insertion into the double bond leading to higher selectivity towards the oxidation products. Based on this knowledge, we aimed to investigate a support material added to the catalytic system which might help to deter the hydrogen abstraction and lead to selective oxidation of the double bond. Therefore, the availability of electron accepting species on the surface could decrease the electronic charge of the oxygen adatoms making it selective towards oxygen insertion to form the epoxide.[27] In this concern, graphene was thought to be a good promoter candidate due to its intrinsic high conductivity which may act as an efficient electron acceptor,[73] resulting in the loss of electron density from partially charged oxygen. In addition, graphene, could improve the adsorption of some reactants,[74] leading to better conversion. Thus, in this study, incorporation of graphene on the propylene oxidation reaction was carried out to assess the implications of its interaction with the system.

In the following chapter (Chapter 2), general information about the analytical techniques used for the characterization of the synthesized composite catalysts is described.

Chapter 3 reports the experimental procedures of graphene and graphene incorporated composite catalysts synthesis, development of GC method and reaction setup.

Chapter 4 is dedicated to results and discussion of catalytic performances of novel composite catalysts together with comprehensive characterization of catalyst showing best catalytic performance.

Finally, general remarks, conclusions and perspectives of the present work are given in Chapter 5.

Chapter 2:

# Analytical techniques

# 2 Chapter 2: Analytical techniques

## 2.1 Gas Chromatography

Chromatography is a method of physical separation of two or more materials using two phases, a stationary phase and a mobile phase. The stationary phase could be a solid, a gel or a liquid. The mobile phase may be a liquid, a gas or a supercritical fluid. [75]

Gas Chromatography uses gas as the mobile phase and a large surface area solid stationary phase. The separation occurs when the components of a sample are distributed between the mobile phase and the stationary one. The components are eluted from the stationary phase following their interactions with it. The interactions depend on the components relative vapor pressure and affinities for the stationary phase, this affinity is calculated using a distribution coefficient, K, as shown in equation 3.

$$Kc = \frac{[A]_S}{[A]_M} \qquad (3)$$

Where:

Kc = distribution constant
A = concentration of solute
S = stationary phase
M = mobile phase

This constant expresses the relative tendency of a solute to be distributed between the two phases. Each component that acquires a different constant would result in a different elution

time. The components are then delivered to the detector leading to their identification, which is recorded electronically using a computer.[76]

Figure 2-1 shows the basic components of the gas chromatography instrument.

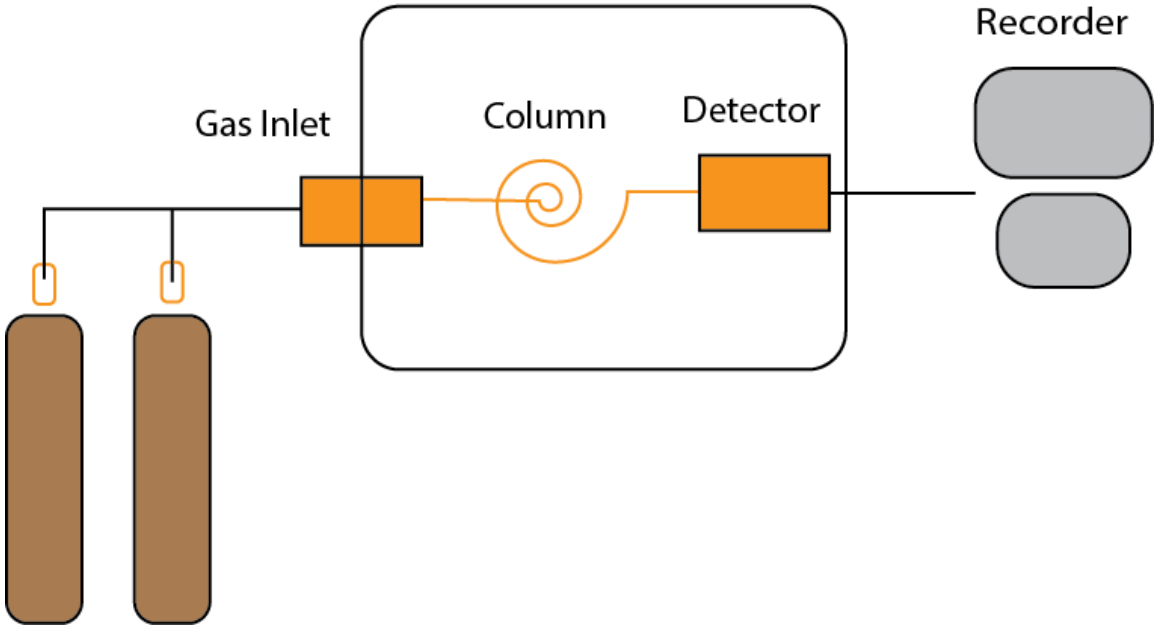



*Figure 2-1: GC components.*

## 2.2 X-ray diffraction (XRD)

X- ray diffraction is one of the most used non-destructive techniques in the field of heterogeneous catalysis. It can be used to determine the structure, phase and orientation of the crystals. In addition, it provides information regarding grain size, crystallinity, crystal defects and strain within the crystal structure.[77]

The crystal determination uses the interactions between the x-ray beam and the matter. When the crystal is targeted with x-ray beams, they tend to reflect from the atoms that make the different layers. The constructive interference, taking place when (a+b)/ λ =n, formed by the reflected beams is representative of the distance between the layers and is called d – spacing (Figure 2-2). This spacing can be derived from Bragg's law (equation 4)[78]. In this law, the incident and diffracted beams are always coplanar and the angle between the diffracted beam and transmitted beam is 2θ. The scattered beams are in phase if the path difference equals a whole number n of wavelengths or if $n\lambda = 2d\ sin\ \theta$.

$$n\lambda = 2d\ sin\ \theta \qquad (4)$$

where:

n = integer
λ = wavelength
d = interplanar spacing
θ = diffraction angle

Bragg's law is satisfied with perfect crystals and with completely paralleled incident beams of monochromatic beams. In reality, perfect crystals are of infinite structure and no beam is strictly monochromatic. Small nanoparticles exhibit deviations from the ideal conditions of Bragg's law due to the differing of the paths of the integral number of wavelengths between two layers of the solid. Complete cancellation of the scattered waves does not occur. The

smaller the size the less the cancellation of the waves occurs, causing broadening of the

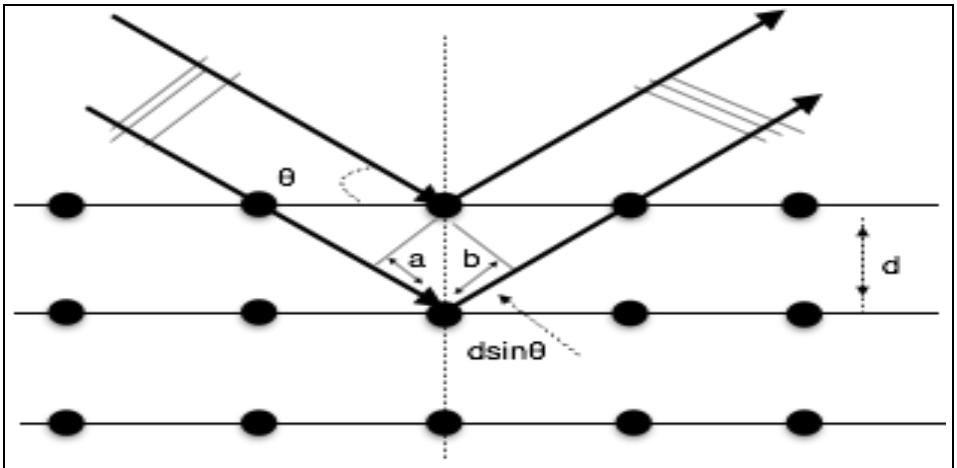



*Figure 2-2: X-ray interference with matter.*

diffracted beams. This indicates that the diffraction occurs at angles close to Bragg's angle. This deviation causes an increase of the width of the diffraction curve with the decrease of the crystal's thickness. The width is indicative of the size of the crystal and Scherrer's equation is used to estimate the size of the particles using full width at half maximum (FWHM), (Equation 5). [79,80]

$$L = \frac{K\lambda}{\beta \cos\theta} \qquad (5)$$

Where

L= mean size of the crystal
K= constant
$\lambda$= wavelength

β = line broadening at FWHM.
Θ = Bragg's angle

## 2.3 Transition electron microscopy (TEM)

The dual wave-particle characteristic of the electron allows for the use of the electron in microscopy, leading to higher resolutions than are available with the use of the optical microscope due to the electrons having a shorter wavelength than visible light.[81] Consequently, the electron microscopy had versatile uses. It can be used for elemental composition, oxidation states of elements, bond distances, symmetry, morphology and nanoporosity.[82]

The operation at high accelerating voltage produces a much shorter wavelength of the electrons compared to the visible light based on equation 6.

$$\lambda = \frac{h}{(2m_o eV)^{\frac{1}{2}}} \qquad (6)$$

where:

λ = wavelength
$h$ = planck's constant
$m_o$ = electron's mass
$V$ = accelerating voltage
$e$ = elementary charge

Transition electron microscope is made up of different components along its optical path, which are as follows: a light source, condenser lenses, specimen stage, objective lenses and projector lenses. Figure 2.3 shows a simple diagram of the components.

The electron gun is used for illumination, by generating a high-energy electron beam. The cathode produces electrons, to be later accelerated by a high voltage to form a high-energy beam. The electron's energy determines the wavelength, so, the acceleration voltage determines the resolution. The higher the acceleration, the higher the resolution. Practically, in order to produce a high-resolution image, the acceleration voltage used is between 100kV to 300kV. When using high voltage for electrons (i.e 1000kV), a more expensive instrumentation is needed. The high energy of the electron could cause some damage to the microstructure of the material under investigation.

Electromagnetic lenses can take advantage of the electron's charge interaction with it to produce a high-energy beam. The electromagnetic lenses are designed as a case and two poles. The case is produced using soft magnetic material which contains a solenoid. The poles are located at the opening of the case. The design leads to produce a powerful magnetic field between the two poles. So, when an electron passes through the field it can be focused by controlling the electrical current used to generate the magnetic field.

The electromagnetic lenses are followed by condensing lenses. Those lenses are used to decrease the magnification of the electron beam produced. They control the convergence angles and the beam diameter targeting the sample. In addition, there are three additional lenses to control magnification, objective, intermediate and projector lenses. For the alternation between the image mode and diffraction mode, the intermediate lenses are used.

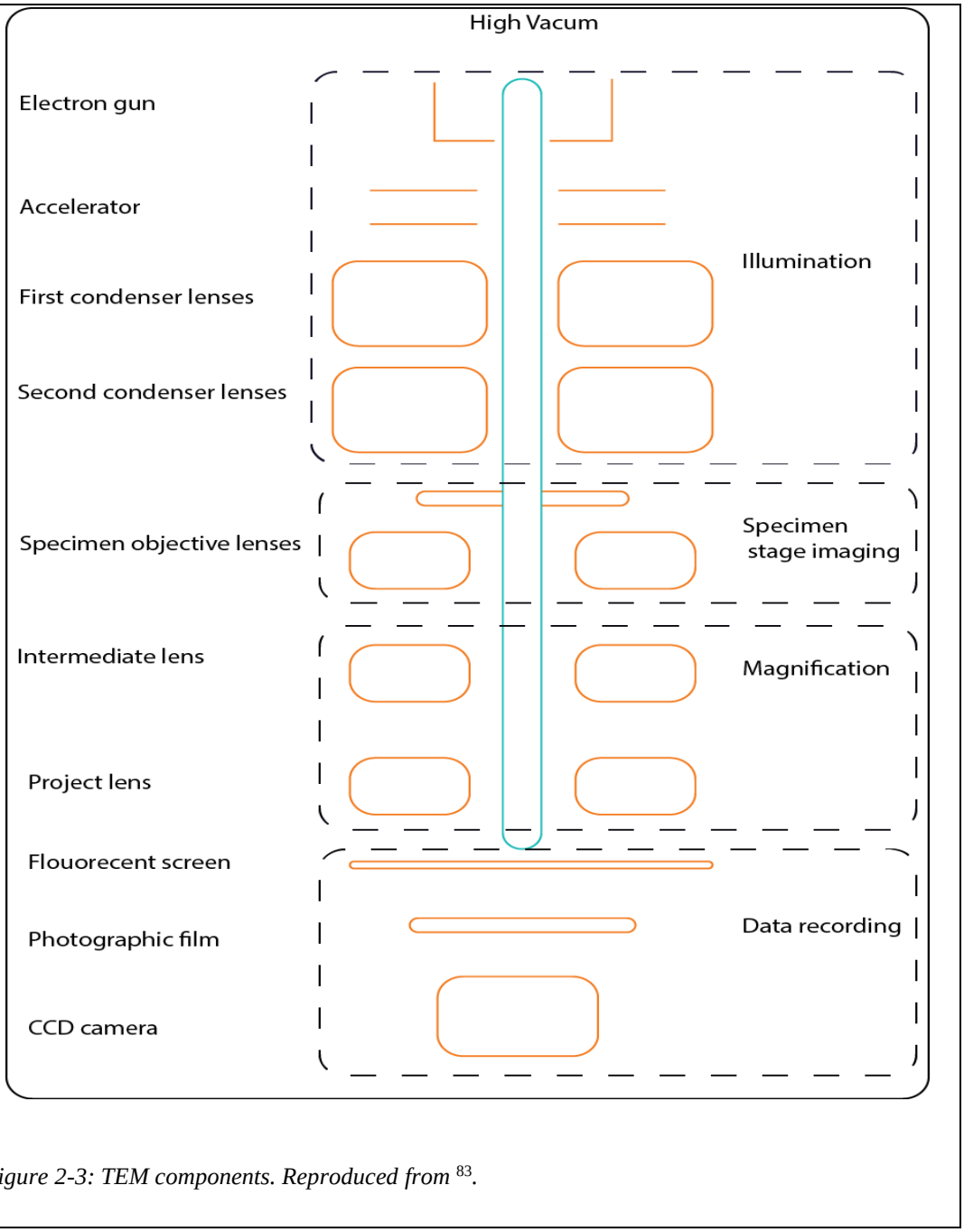



*Figure 2-3: TEM components. Reproduced from* [83].

During the use of the image mode, the intermediate lenses focus on the image plane of the objective lens, while a focus on the back- focal plane of the objective lens is targeted during the diffraction mode.[83]

TEM also can be used for elemental composition using the x-rays that are produced from the interaction of electrons from the beam with the inner electrons of the sample. This interaction ejects an electron from the inner orbital of the sample, leaving a vacancy. Then, an electron from an outer shell relaxes and moves from an outer shell to fill the vacancy leading to x-ray emission that is characteristic of the element. [84]

## 2.4 Thermogravimetric analysis (TGA)

TGA measures the change of a sample's mass as a function of temperature and / or time in a controlled environment. It can provide an indication of mass loss due to drying, reduction, degradation or desorption. Mass gain also can be detected. Those gains could be a result of oxidation, wetting and adsorption.

The TGA analyzer consists of a crucible attached to a very sensitive balance. The crucible is kept in a furnace during the temperature program.

The change of mass versus time can be used to study the reaction rate when the reaction is already known. This leads to the determination of kinetic values

Physiochemical properties of the surface can be probed using the appropriate gas. For example, using pulse TGA, the adsorption isotherm can be created through the injection of successive dosses of the appropriate gas while the weight gain of the sample due to the adsorbed gas is measured.[82]

## 2.5 Temperature programmed desorption (TPD)

TPD is used to study the acidity or basicity of a material through monitoring the amount of desorption of a pre-adsorbed species.

The TPD setup usually consists of a sample holder, furnace and detector.

The analysis method consists of multiple steps. First, the pretreatment, in which a low pressure of a flow of inert gas, is applied with a high temperature to clean the surface of the material. Then, the adsorption of selected probe molecule on the surface of the sample is applied until saturation. Finally, the desorption process is started through a temperature program. The desorbed materials are then carried to the detector with an inert carrier gas. Desorption usually occurs in two steps: physical and chemical. In addition, the decomposition of the adsorbed material could be detected especially at higher temperatures.

The area under the desorbed peak is related to the number of desorbed species and increase proportionally.

$NH_3$ ($pK_a = 9.2$) with its basic characteristics is used to probe the acidity of the catalysts and $CO_2$ ($pK_a \approx 6.4$ ) is used to probe the basicity of the catalysts .[82]

## 2.6 X-ray photoelectron spectroscopy (XPS)

XPS is considered as one of the most popular electron spectroscopic methods. XPS works based on photoelectron emission principle (Figure 2-4) which is described as the process in which the electron that is bound to an atom/ion is ejected by a photon (X-ray). Photons do not possess mass or charge so they are annihilated after the interaction with the electron with a

complete energy transfer to the electron. This transfer, if sufficient, can excite the electron enough to escape from the atom/ion and travel under vacuum to the detector. In a consequent step, quantification of the kinetic energy (*K.E*) remaining on the emitted electron takes place, which depends on the environment and the element. So, *K,E* is the difference between the x-ray photon energy ($h\upsilon$) and the binding energy of the core level electron. The binding energies of energy levels in solids are conventionally measured with respect to the Fermi-level of the solid, rather than the vacuum level. This involves a small correction to the equation in order to account for the work function ($\phi$). Because *K.E* of the photoelectron can be determined experimentally, the energy of the x-ray is known, and the work function is known by calibration, the binding energy of the emitted electron is the result of the following relation:

$$BE = h\upsilon - K.E - \phi_s \qquad (7)$$

Where:

BE = binding energy
$\phi_s$ = work function of the spectrometer

After the photoelectric process, relaxation of the ionized atom may occur by the shake-up or the shake-down process. In this process the electrons in the outer shell are excited to bound and unbound states. Moreover, ions with an unpaired electron may couple with unpaired electrons of the atom which causes peaks splitting at higher binding energies, since it causes multiple possibilities for final state configurations. In addition, when free electrons are excited by the photoelectron, smaller plasmon peaks appear at higher binding energies from the principle peak at equal spacing.[85]

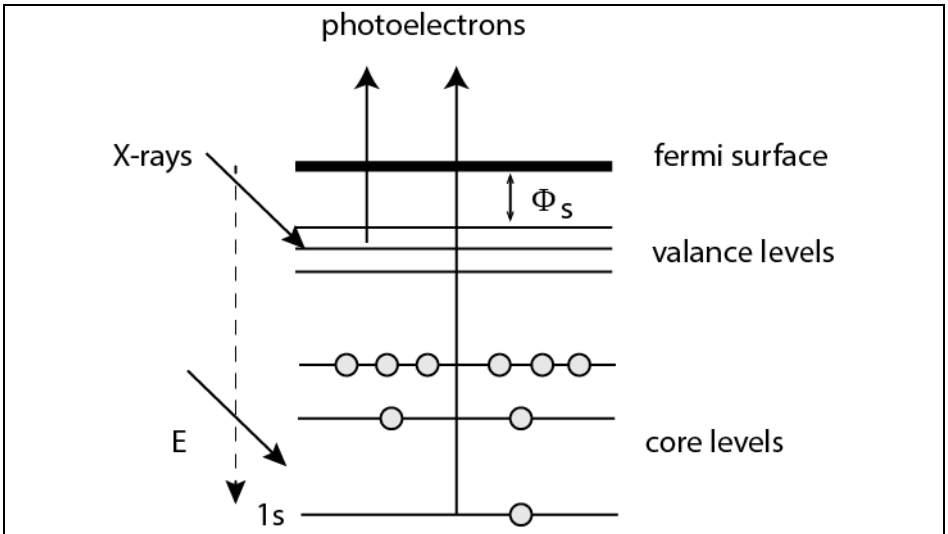


*Figure 2-4: The photoemission process for XPS.*

XPS technique is limited to analyze and quantify the elements at the surface, for up to 10 nm. This limitation is due to the loss of energy of emitted electrons by inelastic collisions, recombination, excitation of the sample, recapture or trapping in various excited states within the material while travelling from inner layers to the outer surface. Thus, the signal measured by XPS is an exponentially surface-weighted signal, and this fact can be used to estimate analyte depths in layered materials.

XPS covers all the elements except hydrogen and helium. Moreover, it can provide the chemical environment the element is associated with.[86]

Chapter 3:

# Experimental

# 3 Chapter 3 Experimental:

## 3.1 Graphene Synthesis:

Graphene was synthesized using Graphene Oxide according to Hummers method.[87,88] 1 g $NaNO_3$ was dissolved in 50 ml 98% $H_2SO_4$ in an ice bath. Then, 2 g graphite was added to the mixture under vigorous stirring for 3 h, followed by the slow addition of 6 g $KMnO_4$. The mixture was stirred for two hours, followed by sonication for one hour, then stirring again for two hours. 1 L $H_2O$ was added slowly to the mixture. The ice bath was removed. The mixture was maintained at 35 ℃ for 1 hour and then diluted by adding 500 ml of warm water. Afterwards, 100 ml 30 % hydrogen peroxide was added to the mixture and stirred for 1 hour. The graphene oxide was separated using the centrifuge at 13500 rpm for 15 minutes. The graphene oxide was dried at 45 ℃ under vacuum. An amount of 2.4 g of graphene oxide was obtained. 480 ml of DI water was added to the graphene oxide followed by sonication. Then 1 ml of hydrazine hydrate was added to the graphene oxide suspension for reduction. The solution was placed inside a microwave and irradiated for 10 seconds followed by stirring for 20 seconds. The previous process was repeated. The graphene was separated by centrifuging at 5000 rpm for 15 minutes, and then dried at 45 ℃ under vacuum for 48 hours.

## 3.2 Preparation of the composite catalysts:

The composite catalysts were prepared in three steps. Ag loaded on $Al_2O_3$ was used as an example for the preparation. The first step was the mixing and grinding of 0.06 g graphene with 5.88 g mesoporous support ($Al_2O_3$, $TiO_2$, $ZrO_2$). Then 20 ml benzene was added to the solid mixture and sonicated for 30 minutes. Afterwards, the suspension was manually stirred inside the fume hood until the complete evaporation of the benzene. Benzene addition,

sonication, stirring and evaporation were repeated three times to ensure a homogenous mixture.

The second step was the wet incipient impregnation. This method is one of the methods that are used to load the metal into the support, which ensures the proper distribution of the active phase into the porous support. For loading Ag nanoparticles over the graphene/support mixture, mixing and grinding of 0.094 g Ag nitrate with graphene /support mixture was performed. Then, the minimum amount of water to make a paste was added and stirred until complete dryness of water. Water addition, stirring and drying were repeated three times. The second step was performed in the dark to avoid Ag reduction.

The third step was the reduction of Ag ions to Ag metal nanoparticles under a flow of 50 ml/min hydrogen at 250 °C for 3 hours with 1 °C/min temperature ramping rate.

The resulting catalyst contained 1 wt. % Ag, 1 wt. % graphene on $Al_2O_3$. The labeling of the catalyst was 1Ag-1G-$Al_2O_3$.

The precursors used were Ag nitrate, Cu acetylacetonate and chloroauric acid for the preparation of the Ag, Cu and Au catalysts. In the case of Cu, chloroform was used as an impregnation medium, and water was used for the Au and Ag catalysts.

The prepared catalysts were characterized using XRD, TEM, TGA and XPS. In the case of XPS, the data collected is corrected to the carbon 1s binding energy for $sp^2$ carbon at 284.5.

## 3.3 GC Method Development

The literature was scanned to list the probable outcome products of the reaction. The materials were then introduced to the reactor using a bubbler. In this bubbler, the desired chemical to be analyzed was added and the propylene gas was bubbled through. Then the gas with the bubbled material was introduced to the GC through a tube. The retention times were registered. Then, a method was developed to ensure the best resolution possible between the products. The result was a 20-minute method. The positions of the possible products are summarized in Table 1: Corresponding retention time of the products.

*Table 1: Corresponding retention time of the products.*

| Product | Retention time (min) |
|---|---|
| Propylene | 5.384 |
| CO | 4.459 |
| $CO_2$ | 4.731 |
| Acetaldehyde | 6.542 |
| Methanol | 6.701 |
| Ethanol | 9.419 |
| Acrolein | 10.646 |
| Acetone | 11.147 |
| Propanal | 11.308 |
| Propylene Oxide | 11.837 |
| 2-propanol | 12.1 |

## 3.4 Reaction setup:

The setup consisted of 5 % (v/v) propylene /He and 5% (v/v) $O_2$ / He cylinders connected to a stainless-steel tube and the flow of gas is controlled with a mass flow controller. The outlet of the tube was connected to the GC with a stainless-steel tube covered with a heating tape to prevent the condensation of the materials. The GC was then connected to a computer for the analysis. Figure 3-1 shows the set-up image.

The performance testing of the catalysts was carried out in a vertically oriented tube reactor at atmospheric pressure. The catalysts were placed in the middle of reactor tube between quartz wool. Total gas flow was 10 ml/min with 2:1 propylene to oxygen molar ratio.



*Figure 3-1: Reaction setup.*

Chapter 4:

# Results and discussion

# 4 Chapter 4: Results and Discussion

The aim of this study was to investigate the effect of graphene in the selective propylene oxidation with molecular oxygen. Therefore, graphene oxide (GO) was firstly prepared via modified Hammers' method and reduced to graphene by microwave irradiation in the presence of hydrazine as described in detail in Chapter 3.1. Afterwards, the quality and stability of as synthesized graphene were investigated by x-ray diffraction (XRD) and thermogravimetric analysis (TGA) methods.

## 4.1 XRD Measurements

Figure 4.1 shows the XRD patterns of GO and graphene. In the XRD pattern of GO, the (002) crystal plane of GO is evident at $2\Theta$ around 10º, which is typical for GO.[89] In contrast to GO, the XRD pattern of graphene, presents a new intense narrower diffraction peak at $2\Theta$ = 24º, which can be indexed to the (002) plane of graphitic structure of carbon indicating the successful synthesis of graphene. The second peak appearing in the XRD pattern of graphene at around 43º can be attributed to the short range order in the stacked graphene layer.[90]

The XRD patterns of the different catalysts composites prepared were also registered. Figure 4-2 shows the XRD pattern of $TiO_2$. The strong diffraction peaks at $2\Theta$ = 25º and $2\Theta$ = 48º are indicative of the anatase phase.[91]

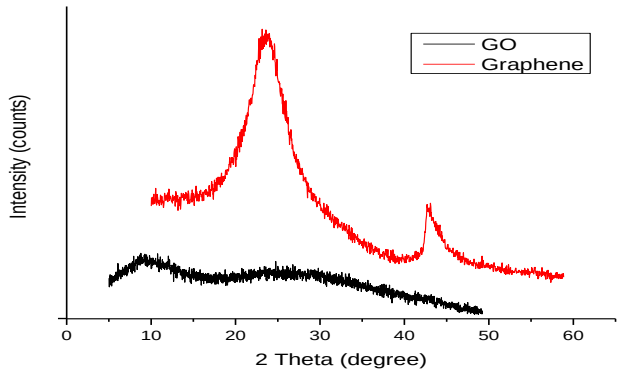



*Figure 4-1: XRD pattern of GO and Graphene.*

After the synthesis of Au on the $TiO_2$, XRD pattern ( Figure 4-3 ) shows an overlap in the earlier peaks, but additional broad and low intense peaks at the diffraction angles 64 and 77,

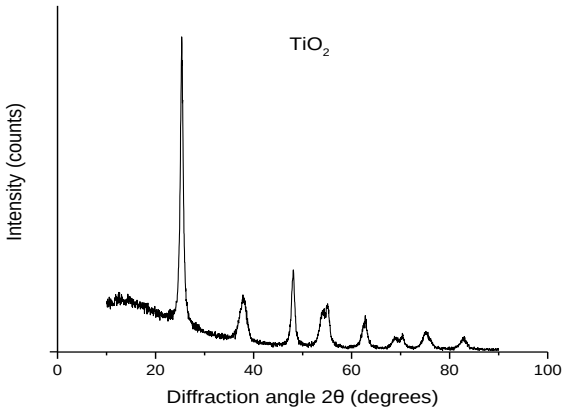



*Figure 4-2: XRD pattern of $TiO_2$.*

which correspond to the (220) and the (311) planes for Au, have appeared. Indicating that the small particles Au was successfully loaded onto the support. There appeared to be no major changes of the $TiO_2$ phase after the reduction process.

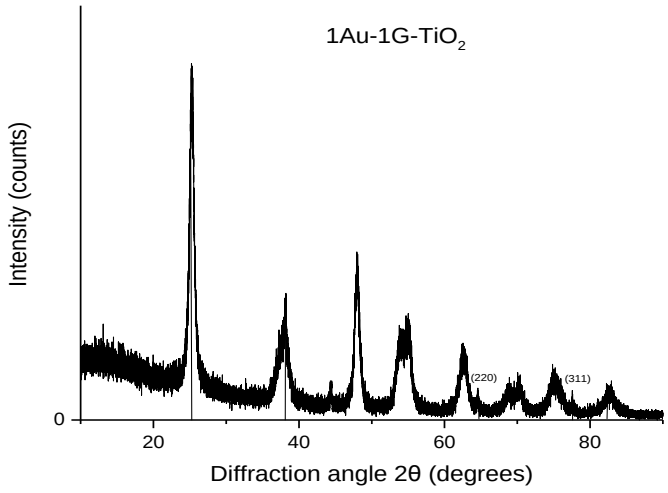



*Figure 4-3: XRD pattern of 1Au-1G-$TiO_2$.*

## 4.2 TGA

The materials used in the study of the composition of the catalyst, must endure the conditions of the catalytic test, therefore TGA analysis was performed for the graphene doped catalyst and compared to the catalyst with no graphene. Figure 4-4 shows TGA experiments of 1Au-$TiO_2$ and 1Au-5G-$TiO_2$ under similar heating conditions to the reaction. The results show a slight increase in mass loss for the graphene doped catalyst, which could be due to the enhanced adsorption of some molecules on graphene before testing.[92] For both catalysts, three distinct regions for the desorption are seen. The regions up to 120 ºC and between 120 ºC and

270 ºC can be attributed to the dehydration of the physically adsorbed water and the release of the hydroxyl group respectively. The region above 270 ºC could be attributed to a loss of some inorganic species and impurities that could have adsorbed through the synthesis process or handling the material.

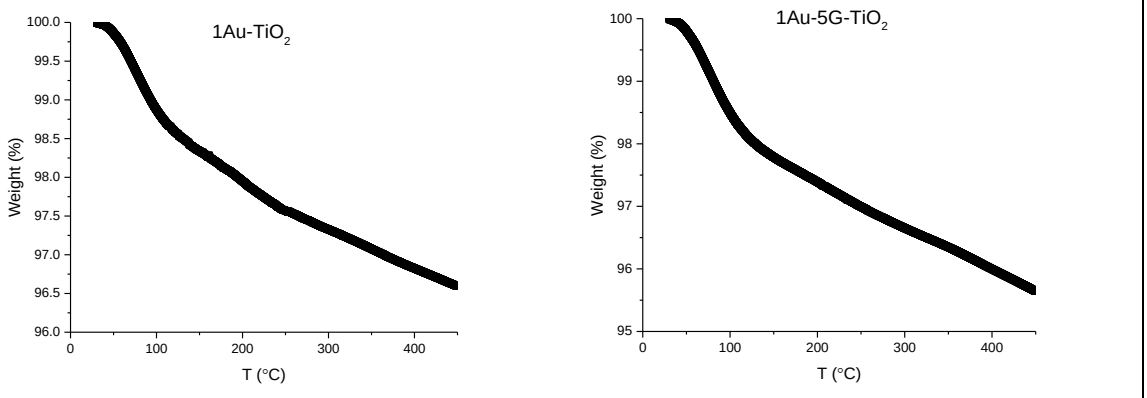



*Figure 4-4: TGA of 1Au-$TiO_2$ / 1Au-5G-$TiO_2$.*

## 4.3 Catalytic performance

In order to investigate the effect of graphene on the selective propylene oxidation with molecular oxygen, different metal/mesoporous oxides/graphene composite materials have been prepared. Three mesoporous oxides ($Al_2O_3$, $TiO_2$, $ZrO_2$) have been selected as supports since they are widely used in the literature for oxidation reactions. Then, these oxide supports were doped with graphene and/or coinage metals (Ag, Au, Cu), which were found to be most active catalysts in propylene oxidation. Later on, graphene was also investigated as the sole catalyst and support for coinage metal nanoparticles in propylene oxidation reaction. After the synthesis of novel solid state materials, their catalytic performance in propylene oxidation was

investigated under flow conditions using a tubular reactor whose outlet was connected to gas chromatography for online analysis of the product distribution at different temperatures. This strategy allowed us to do systematic work in order to examine the effect of the nature and amount of metal/mesoporous oxide support/graphene composites in the activity and selectivity of propylene oxidation with molecular oxygen.

Before the display of the catalytic result, it is important to note that the reactions were performed once for each sample for time constraints. In addition, the CO and $CO_2$ were excluded from most graphs of the products distribution for more clarity. However, the whole product distributions can be found at appendix A. It is also important to note that the products we focused on were PO, Acrolein, Acetone, Acetaldehyde and Propanal. Other products were grouped under "Other".

### 4.3.1 Support performance

Different supports used in the oxidation process were tested in order to determine the effect of the graphene. The temperature profiles of the observed conversion of propylene oxidation with graphene/metal oxide supports are displayed in Figure 4-5. As seen from the figures, $Al_2O_3$ and $ZrO_2$ did not reveal any catalytic activity until 300 $^oC$ after which a rapid increase in rate of propylene oxidation was observed. $TiO_2$, on the contrary, was found to be more active than $Al_2O_3$ and $ZrO_2$ representing a sigmoidal curve, that indicates more changes on the active phase. In addition, the conversion increased rapidly after 200 $^oC$ and plateaued after 400 $^oC$. For all cases, the addition of graphene showed an increase in the conversion of the three supports used for the oxidation process. In addition to the change in conversion, the graphene addition changed the distribution of products and the evolution temperature, which is the temperature at which the product is recorded via GC analysis.

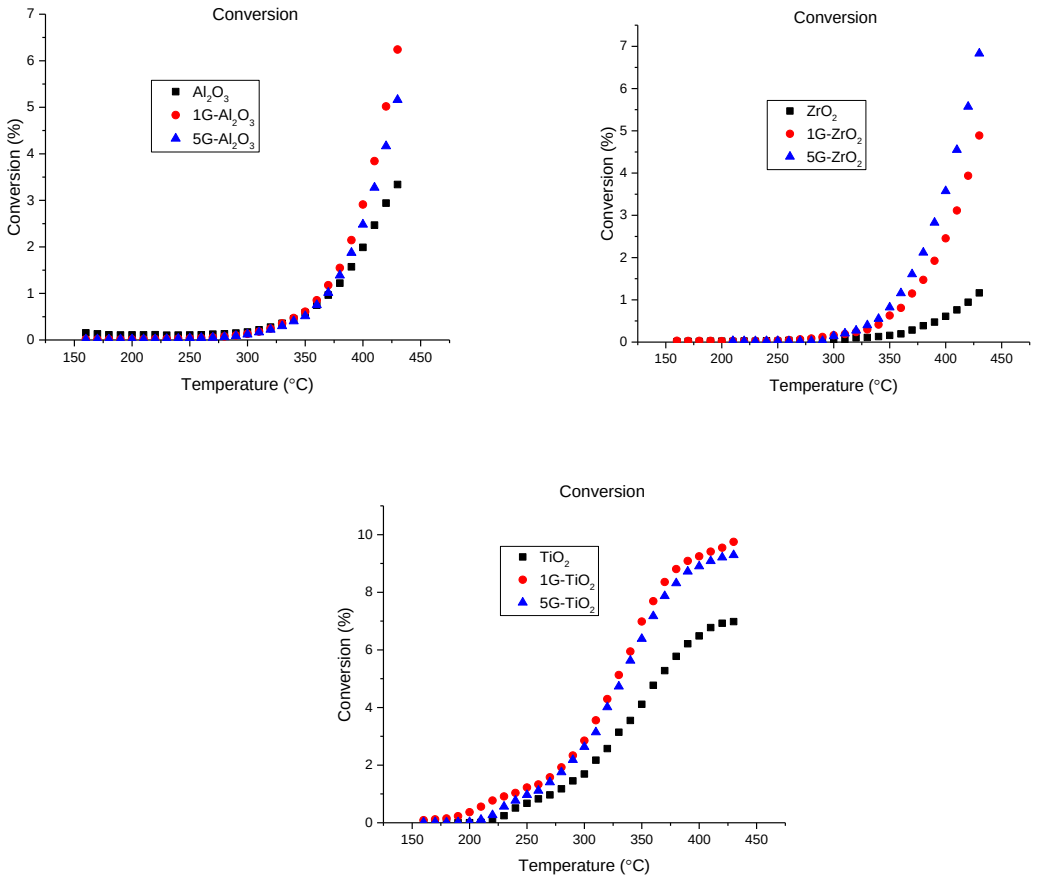



*Figure 4-5: Conversion profiles of $Al_2O_3$ / $ZrO_2$ / $TiO_2$ supports.*

Figure 4-6 shows that $ZrO_2$ is capable of producing acrolein at 360 ºC of up to 7% selectivity. The introduction of 1% graphene added few products, but maintained similar acrolein selectivity. Further increase of the graphene to 5% showed a decrease of the evolution temperature of acrolein without a significant change in selectivity.

$TiO_2$ also showed a similar behavior (Figure 4-7). When 1% graphene was added, the production of acetone at low temperatures was halted and acrolein started to be produced at 360 ºC followed by the acetone at 410 ºC. The increase of the graphene to 5% did not show

any acrolein formation; on the other hand, little amount of acetaldehyde was introduced into the products.

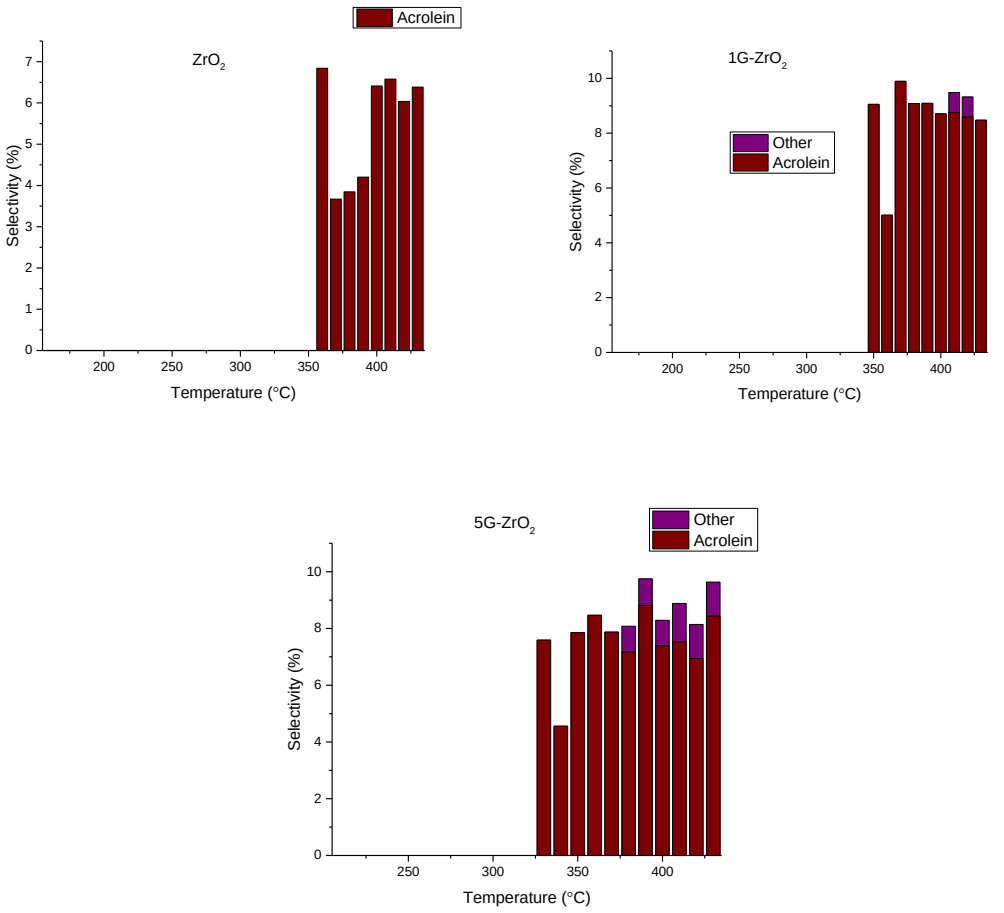



*Figure 4-6: Selectivity profiles of $ZrO_2$ / 1G-$ZrO_2$/ 5G-$ZrO_2$ to partial oxidation products in the temperature range of 160 °C - 430 °C.*

Graphene induced some effects on $Al_2O_3$. Suppression of lower temperature products was observed. Moreover, higher graphene loading produced lower acrolein content. The products distribution was similar with bare and graphene loaded $Al_2O_3$ as can be seen from Figure 4-8.

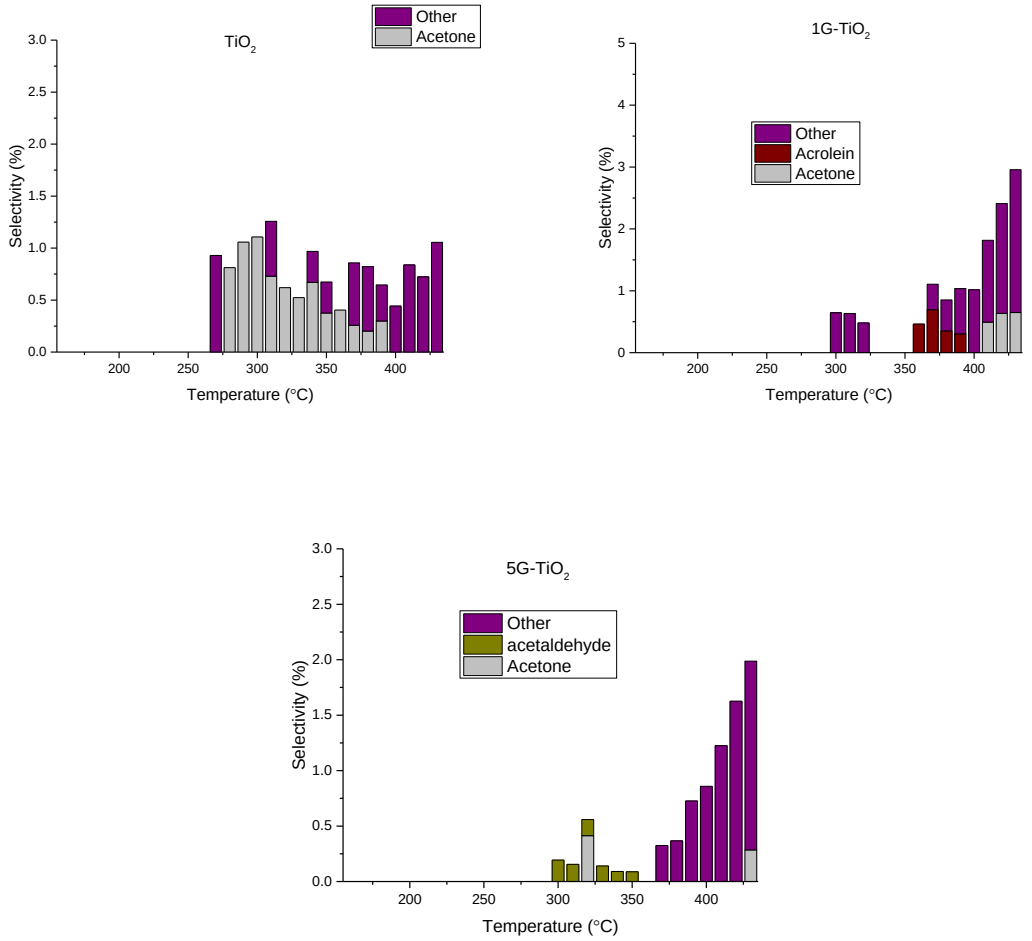



*Figure 4-7: Selectivity profiles of $TiO_2$ / 1G-$TiO_2$/ 5G-$TiO_2$ to partial oxidation products in the temperature range of 160 °C - 430 °C.*

In catalysis, introducing a small quantity of transition metals onto metal oxide supports generally enhances the catalytic activity. For instance, oxidation using Ag catalysts supported on $Al_2O_3$ is currently used in the commercial production of ethylene oxide from ethylene.[13] Therefore, our next objective was to investigate the effect of introducing transition metals into graphene/metal oxide composite systems on the catalytic activity of propylene oxidation. For this purpose, the coinage metals group (Ag, Au, Cu) has been chosen as the literature indicated that they could be cost-effective and active in oxidation of propylene.

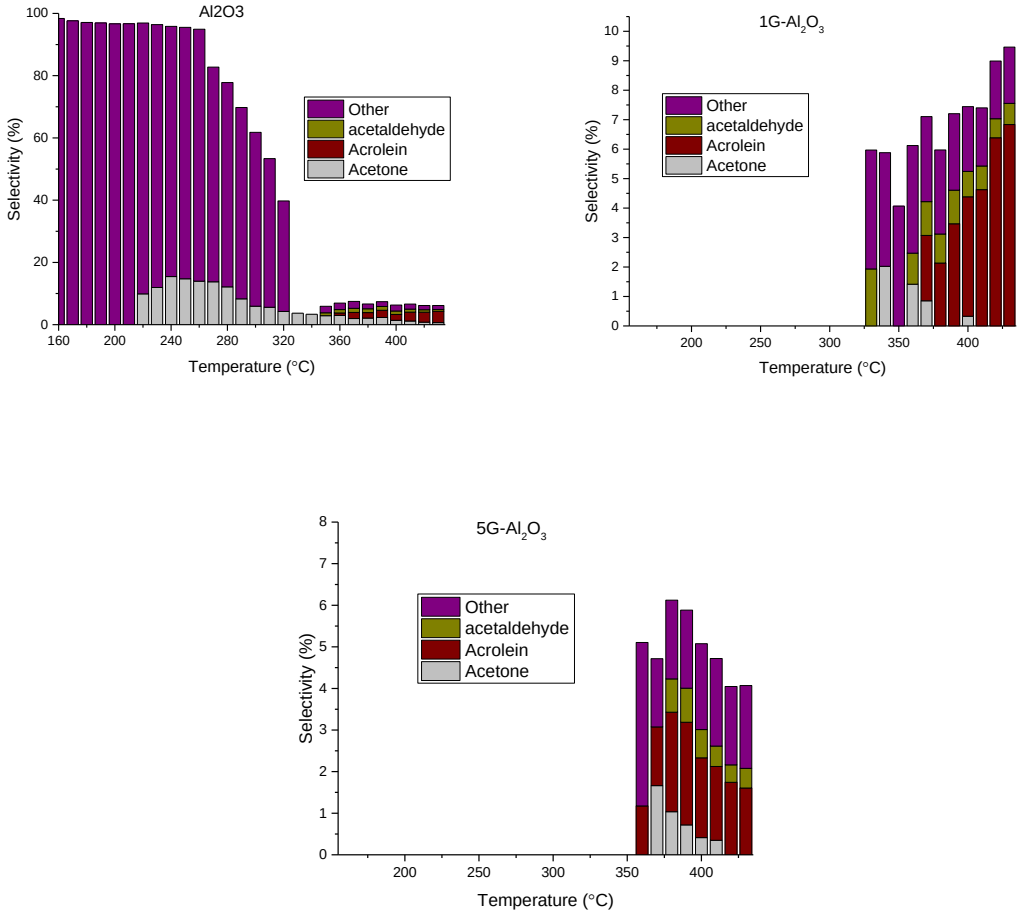



*Figure 4-8: Selectivity profiles of $Al_2O_3$ / 1G-$Al_2O_3$/ 5G-$Al_2O_3$ to partial oxidation products in the temperature range of 160 °C - 430 °C.*

### 4.3.2 Ag Catalysts

The application of the Ag catalysts on the propylene was investigated with different metal/graphene/support loadings as follows:

#### 4.3.2.1 *Ag - $Al_2O_3$*

The catalytic activity of 1 wt.% Ag loaded $Al_2O_3$ was found to be higher compared to bare $Al_2O_3$ as expected due to the capability of transition metals to activate substrates. Interestingly, while high Ag and low graphene loadings show increased reactivity, the graphene addition to the 1%Ag exhibits a decrease in conversion, as can be seen from Figure 4-9.

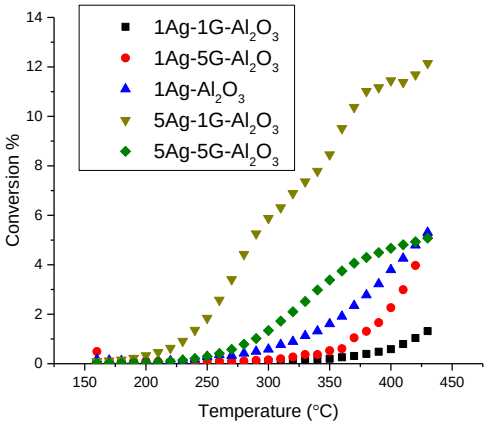



*Figure 4-9: Conversion profiles of 1Ag-1G-$Al_2O_3$/ 1Ag-5G-$Al_2O_3$/ 1Ag-$Al_2O_3$/ 5Ag-1G-$Al_2O_3$/ 5Ag-5G-$Al_2O_3$ catalysts in the temperature range of 160 °C - 430 °C.*

Ag loaded $Al_2O_3$/graphene composites show different activities based on the loading of the Ag and graphene composition as can be seen in Table 2. Lower loading of graphene shows increased selectivity towards the formation of acetone, but acetaldehyde is not produced. Higher Ag and lower graphene loadings show enhanced activities towards the production of acetaldehyde. The introduction of graphene into the catalysts suppressed other products as can

be inferred from the lower percentage of other products of the graphene loaded catalysts when compared to the Ag on bare $Al_2O_3$.

The highest amount of acrolein is produced when there is no graphene and selectivity decreases with the addition of graphene.

*Table 2: Selectivity of 1Ag-1G-$Al_2O_3$/ 1Ag-5G-$Al_2O_3$/1Ag-$Al_2O_3$/ 5Ag-1G-$Al_2O_3$/ 5Ag-5G-$Al_2O_3$ catalysts.*

| Product / Catalyst | Acetone | | Acrolein | | Acetaldehyde | | Other | |
|---|---|---|---|---|---|---|---|---|
| | OS ºC | Max % | OS ºC | Max % | OS ºC | Max % | OS ºC | Max % |
| 1Ag-1G-$Al_2O_3$ | 290 | 16.6 | 380 | 4.6 | - | - | 220 | 58.1 |
| 1Ag-5G-$Al_2O_3$ | 320 | 5.4 | 320 | 6.5 | | | 330 | 5.8 |
| 1Ag-$Al_2O_3$ | 310 | 4.8 | 330 | 7.2 | 310 | 1.8 | 160 | 78.2 |
| 5Ag-1G-$Al_2O_3$ | 320 | 1.2 | 330 | 3.1 | 160 | 22.5 | 320 | 4.6 |
| 5Ag-5G-$Al_2O_3$ | 320 | 1 | 310 | 0.7 | 400 | 0.1 | - | - |

#### 4.3.2.2 *Ag - $TiO_2$*

Variations of Ag and graphene loadings on $TiO_2$ show ambiguous results (Figure 4-10). Introducing a small quantity (1 wt.%) of graphene on 1Ag-$TiO_2$ decreased the conversion to half; on the contrary, more graphene content carried the conversion up to 8%. When the metal content was increased while keeping graphene amount at 1%, a drastic rise in conversion was observed. On the other hand, when graphene content was at 5%, increasing Ag content led to a decline in conversion. These results are complex and difficult to explain as different factors may play role in catalytic activity. But, one might consider that at low metal content, graphene is the dominant promoter to the catalytic activity while the reverse is valid when the metal

content higher. The results suggest that Ag and graphene do not work in cooperation but compete with each other, and so the presence of one might be poisonous for the activity of the other.

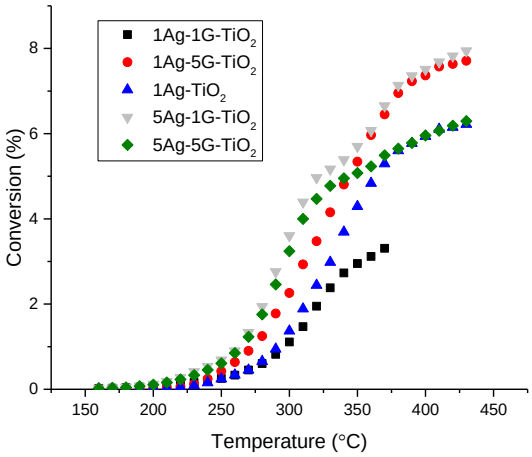



*Figure 4-10*: *Conversion profiles of 1Ag-1G-$TiO_2$/ 1Ag-5G-$TiO_2$/ 1Ag-$TiO_2$/ 5Ag-1G-$TiO_2$/ 5Ag-5G-$TiO_2$ catalysts in the temperature range of 160 °C - 430 °C.*

Selectivity profiles of Ag/G/$TiO_2$ exhibit that main products are CO and $CO_2$. Table 3 shows small amounts of different products with the highest being of 1.6% selectivity to acrolein, while the others were below 1%. These results are very similar to the ones obtained with G/$TiO_2$ as discussed in Section 4.3.1 which show that loading of Ag or Graphene does not have an effect on the selectivity profile of propylene oxidation reaction but influences the conversion.

*Table 3: Selectivity of 1Ag-1G-$TiO_2$/ 1Ag-5G-$TiO_2$/ 1Ag-$TiO_2$/ 5Ag-1G-$TiO_2$/ 5Ag-5G-$TiO_2$ catalysts.*

| Product / Catalyst | Acetone | | Acrolein | | Acetaldehyde | | Other | |
|---|---|---|---|---|---|---|---|---|
| | OS ºC | Max % | OS ºC | Max % | OS ºC | Max % | OS ºC | Max % |
| 1Ag-1G-$TiO_2$ | - | - | 340 | 0.8 | 340 | 0.7 | - | - |
| 1Ag-5G- $TiO_2$ | 290 | 0.7 | 320 | 0.7 | 330 | 0.3 | - | - |
| 1Ag- $TiO_2$ | 280 | 1.6 | 340 | 0.5 | - | - | 320 | 0.5 |
| 5Ag-1G- $TiO_2$ | 360 | 0.5 | 350 | 0.8 | 350 | .1 | 380 | 0.7 |
| 5Ag-5G- $TiO_2$ | 370 | 0.2 | 340 | 0.4 | 360 | 0.4 | - | - |

#### 4.3.2.3 *Ag - $ZrO_2$*

When $ZrO_2$ was used as a support, a similar trend to $Al_2O_3$ was observed in terms of conversion. (Figure 4-11). Introducing 1% graphene into 1%Ag-$ZrO_2$ decreased the reaction rate and conversion; however, further increase in the amount of graphene, recovered the maximum conversion with slower kinetics. The trend with higher metal content was different. As expected, higher Ag content raised the conversion and accelerated the reaction rate. However, increasing graphene content from 1% to 5% while keeping Ag amount at 5% led to a decrease in conversion. Once again, the difference in activities of composite catalysts based on metal or graphene content might be due to their competitiveness which could be poisonous for the activity of the other.

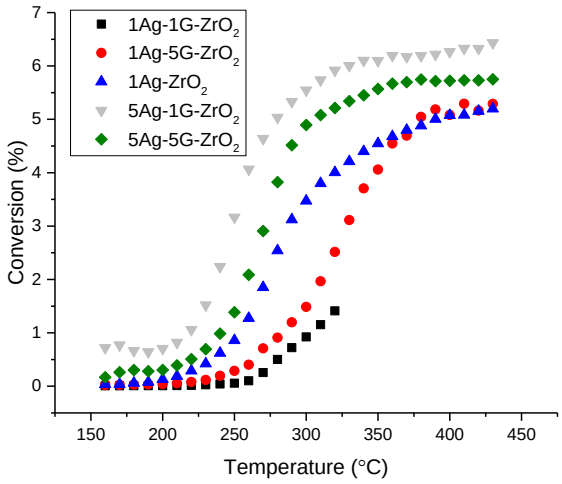



*Figure 4-11: Conversion profiles of 1Ag-1G-$ZrO_2$/ 1Ag-5G-$ZrO_2$/ 1Ag-$ZrO_2$/ 5Ag-1G-$ZrO_2$/ 5Ag-5G-$ZrO_2$ catalysts in the temperature range of 160 °C - 430 °C.*

Fewer products were produced with $ZrO_2$ catalysts, in addition to low selectivity, making the $ZrO_2$ an undesirable support for this reaction (Table 4).

*Table 4: Selectivity of 1Ag-1G-$ZrO_2$/ 1Ag-5G-$ZrO_2$/ 1Ag-$ZrO_2$/ 5Ag-1G-$ZrO_2$/ 5Ag-5G-$ZrO_2$ catalysts.*

| Product / Catalyst | Acetone | | Acrolein | | Acetaldehyde | | Other | |
|---|---|---|---|---|---|---|---|---|
| | OS °C | Max % | OS °C | Max % | OS °C | Max % | OS °C | Max % |
| 1Ag-1G-$ZrO_2$ | - | - | 270 | 3.4 | - | - | - | - |
| 1Ag-5G- $ZrO_2$ | - | - | 360 | 0.3 | | | - | - |
| 1Ag- $ZrO_2$ | 390 | 0.5 | 370 | 0.3 | - | - | - | - |
| 5Ag-1G- $ZrO_2$ | 290 | 1 | 340 | 0.2 | - | - | - | - |
| 5Ag-5G- $ZrO_2$ | 280 | 0.6 | 360 | 1 | - | - | - | - |

### 4.3.3 Au catalysts

Although Au particles supported on Ti-based metal oxides were shown to be active in selective propylene oxidation to propylene oxide[38] with the co-feeding of $H_2$ and $O_2$, their capability for catalyzing direct oxidation of propylene with solely molecular oxygen has hardly been reported. Recently, it was reported that Au catalysts could catalyze propylene oxidation in the absence of sacrificial reductive agents such as $H_2$ and CO if the size of the Au particles are carefully controlled.[93] Being motivated from this study, we decided to investigate the effect of graphene on the catalytic activity of Au for direct propylene oxidation.

#### 4.3.3.1 *Au - $Al_2O_3$*

The propylene conversion doesn't seem to be affected significantly by the existence of graphene and/or Au on $Al_2O_3$ exhibiting a similar behavior even with different loadings as shown in Figure 4-12. However, when the catalytic activities of $Au/G/Al_2O_3$ catalysts were compared with the activities of pure $Al_2O_3$ and $G/Al_2O_3$, a decrease in conversion was observed with the introduction of Au into the system. This might be due to the insertion of Au particles into the defects of the support which are thought to be catalytically active sites and so blocking the reactants approach. As the activity of gold to propylene oxidation depends significantly on its size, any particles larger than 2 nm might be inactive under the applied reaction conditions; however, it can still change the electronic properties of the support that might influence the product selectivity.

Table 5 summarizes the product distributions obtained with $Au/G/Al_2O_3$ composite catalysts. As seen from the table, acetone was the main product when using $Al_2O_3$ as a support for Au. The selectivity seems to be affected by the introduction of graphene. Starting from the 1%Au, a decrease of acetone selectivity is observed with the increase of graphene cover. For the

higher Au coverage, the same trend is observed. Acrolein, on the other hand, showed a high selectivity only with low Au and high graphene loading at lower temperature. In addition to acetone and acrolein, additional products with different percentages are produced, as can be seen from Table 5.

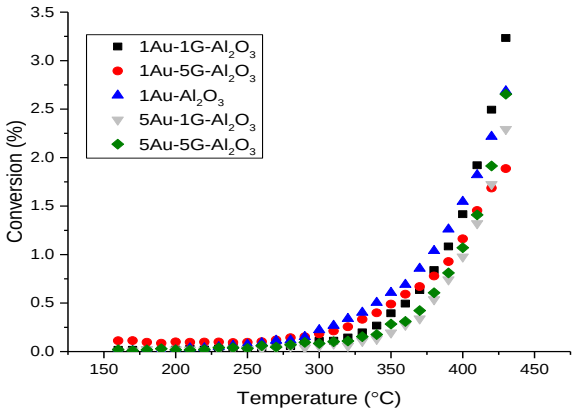



*Figure 4-12: Conversion profiles of 1Au-1G-$Al_2O_3$/ 1Au-5G-$Al_2O_3$/ 1Au-$Al_2O_3$/ 5Au-1G-$Al_2O_3$/ 5Au-5G-$Al_2O_3$ catalysts in the temperature range of 160 °C - 430 °C.*

*Table 5: Selectivity of 1Au-1G-$Al_2O_3$/ 1Au-5G-$Al_2O_3$/ 1Au-$Al_2O_3$/ 5Au-1G-$Al_2O_3$/ 5Au-5G-$Al_2O_3$ catalysts.*

| Product / Catalyst | Acetone | | Acrolein | | Acetaldehyde | | Other | |
|---|---|---|---|---|---|---|---|---|
| | OS ºC | Max % | OS ºC | Max % | OS ºC | Max % | OS ºC | Max % |
| 1Au-1G-$Al_2O_3$ | 210 | 35.5. | 400 | 1.1 | 270 | 1.1 | 270 | 8.2 |
| 1Au-5G-$Al_2O_3$ | 430 | 0.9 | 170 | 52.1 | - | - | 160 | 30.8 |
| 1Au-$Al_2O_3$ | 210 | 59.9 | 370 | 1.8 | 300 | 3.8 | 250 | 9 |
| 5Au-1G-$Al_2O_3$ | 230 | 66.3 | - | - | 380 | 1.3 | 190 | 63.8 |
| 5Au-5G-$Al_2O_3$ | 190 | 43.8 | 410 | 1.8 | 370 | 3.4 | 290 | 22.1 |

#### 4.3.3.2 *Au - $TiO_2$*

The conversions of Au on $TiO_2$-graphene composites are shown on Figure 4-13. The activities of the 5% Au content catalysts are comparable, and the effect of graphene loading is not profound. However, the catalytic activity was diminished with the increase of graphene loading while the amount of Au was 1%.

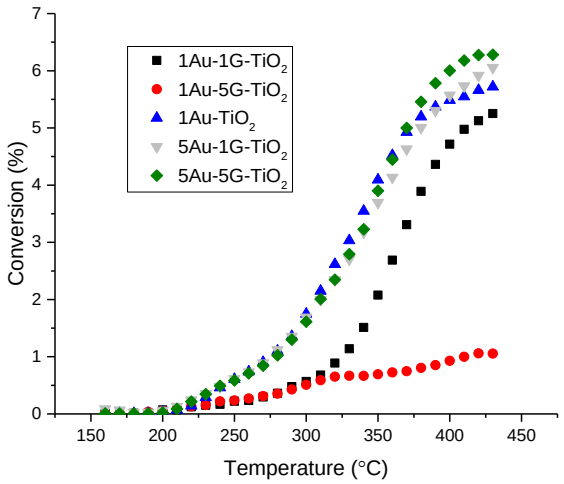



*Figure 4-13: Conversion profiles of 1Au-1G-$TiO_2$/ 1Au-5G-$TiO_2$/ 1Au-$TiO_2$/ 5Au-1G-$TiO_2$/ 5Au-5G-$TiO_2$ catalysts in the temperature range of 160 °C - 430 °C.*

The production of acetone was inhibited with the introduction of graphene while the selectivity increased with higher Au loading. Acrolein, on the other hand, does not show a recognizable trend and acetaldehyde was produced throughout the different catalysts. (Table 6)

*Table 6: Selectivity of 1Au-1G-$TiO_2$/ 1Au-5G- $TiO_2$/ 1Au- $TiO_2$/ 5Au-1G $TiO_2$/ 5Au-5G- $TiO_2$ catalysts.*

| Product / Catalyst | Acetone | | Acrolein | | Acetaldehyde | | Other | |
|---|---|---|---|---|---|---|---|---|
| | OS ºC | Max % | OS ºC | Max % | OS ºC | Max % | OS ºC | Max % |
| 1Au-1G-$TiO_2$ | 200- | 38.6 | 360 | 0.8 | 280 | 2.1 | 200 | 26.4 |
| 1Au-5G- $TiO_2$ | 290 | 2.6 | 190 | 30.8 | 390 | 0.4 | 190 | 37.5 |
| 1Au- $TiO_2$ | 200 | 47.5 | - | - | 250 | 1.1 | 250 | 1.9 |
| 5Au-1G- $TiO_2$ | 160 | 69.6 | 200 | 43.8 | 230 | 1.9 | 160 | 33.3 |
| 5Au-5G- $TiO_2$ | 210 | 35.2 | - | - | 240 | 1.7 | 200 | 42.7 |

### 4.3.3.3 *Au - $ZrO_2$*

Different loading percentages of graphene and the metal does not seem to have a specific trend

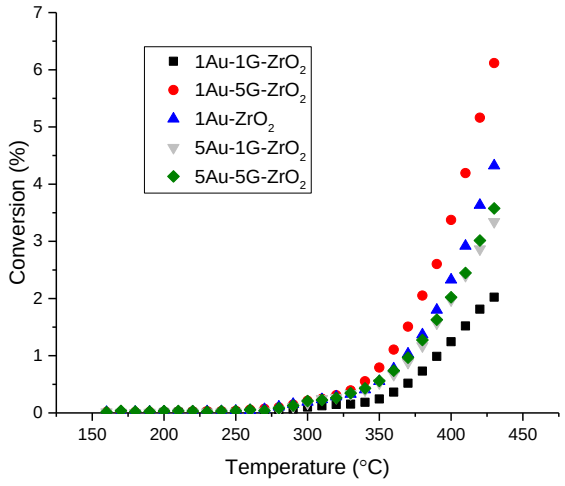



*Figure 4-14: Conversion profiles of 1Au-1G-$ZrO_2$/ 1Au-5G-$ZrO_2$/ 1Au-$ZrO_2$/ 5Au-1G-$ZrO_2$/ 5Au-5G-$ZrO_2$ catalysts in the temperature range of 160 °C - 430 °C.*

for the conversion of the Au/G/$ZrO_2$ catalysts. Figure 4-14 shows the highest and lowest conversions belong to the lowest Au loading on the $ZrO_2$ and graphene composites, while the higher Au loadings have conversions between the two.

Au ratio seems to be of paramount importance when loaded on $ZrO_2$. The highest Au loading shows an increased activity towards acetone production. The addition of graphene shows a change in the product distribution map with the productions of other products (Table 7).

*Table 7: Selectivity of 1Au-1G-$ZrO_2$/ 1Au-5G- $ZrO_2$/ 1Au- $ZrO_2$/ 5Au-1G $ZrO_2$/ 5Au-5G- $ZrO_2$ catalysts.*

| Product / Catalyst | Acetone | | Acrolein | | Acetaldehyde | | Other | |
|---|---|---|---|---|---|---|---|---|
| | OS ºC | Max % | OS ºC | Max % | OS ºC | Max % | OS ºC | Max % |
| 1Au-1G-$ZrO_2$ | 360 | 6.3 | - | - | - | - | 200 | 34.2 |
| 1Au-5G- $ZrO_2$ | - | - | 350 | 5.5 | - | - | 220 | 16.8 |
| 1Au- $ZrO_2$ | 360 | 2.3 | - | - | - | - | - | - |
| 5Au-1G- $ZrO_2$ | 290 | 13.8 | - | - | - | - | 280 | 28.1 |
| 5Au-5G- $ZrO_2$ | 170 | 78.9 | 420 | 0.6 | - | - | 260 | 31.5 |

### 4.3.4 Cu catalysts

Cu was also loaded on different graphene-metal oxide composites and the results are as follows.

#### 4.3.4.1 *Cu - $Al_2O_3$*

Cu on $Al_2O_3$ exhibited slightly enhanced conversion with the addition of graphene, the higher the loading of graphene the more the conversion, as Figure 4-15 shows. In addition, the

sigmoidal curve observed for all Cu-G-$Al_2O_3$ catalysts is evidence that there is saturation of the catalyst surface, while the tailing off is an indication of activity loss, presumably due to poisoning or change of active sites at high temperatures.

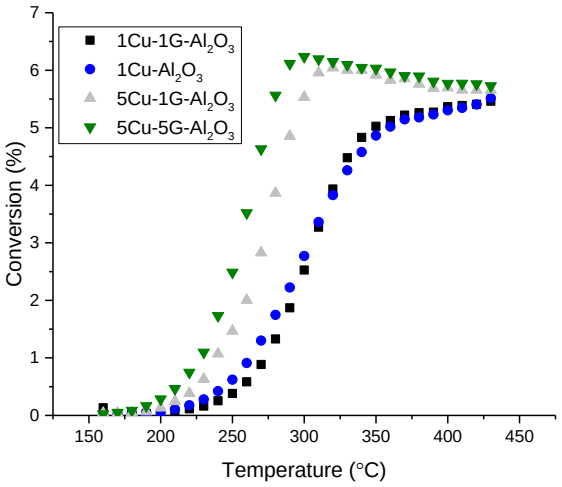



*Figure 4-15: Conversion of 1Cu-1G-$Al_2O_3$/ 1Cu -$Al_2O_3$/ 5Cu -1G-$Al_2O_3$/ 5Cu -5G-$Al_2O_3$ catalysts in the temperature range of 160 °C - 430 °C.*

Propanal, acrolein, and acetaldehyde were found to be the main products of the reaction. The addition of graphene suppressed the propanal and acetaldehyde production, but enhanced acrolein's production. The higher loading of graphene and the metal seems to produce the highest acrolein selectivity. These observations are summarized on Table 8.

*Table 8: Selectivity of1Cu-1G-$Al_2O_3$/ 1Cu -$Al_2O_3$/ 5Cu -1G-$Al_2O_3$/ 5Cu -5G-$Al_2O_3$ catalysts.*

| Product / Catalyst | Propanal | | Acrolein | | Acetaldehyde | | Other | |
|---|---|---|---|---|---|---|---|---|
| | OS ºC | Max % | OS ºC | Max % | OS ºC | Max % | OS ºC | Max % |
| 1Cu-1G-$Al_2O_3$ | 270 | 2.2 | 220 | 16.4 | 240 | 4.7 | 190 | 16.5 |
| 1Cu-$Al_2O_3$ | 250 | 4 | 220 | 14.3 | 210 | 13.4 | 22- | 0.6 |
| 5Cu-1G-$Al_2O_3$ | 200 | 12.1 | 200 | 32.4 | 210 | 6.3 | 190 | 11.3 |
| 5Cu-5G-$Al_2O_3$ | 190 | 8.7 | 170 | 41.4 | 190 | 4.1 | 270 | 1.2 |

### 4.3.4.2 *Cu - $TiO_2$*

Lower conversions are observed when graphene is incorporated into Cu-$TiO_2$ catalytic

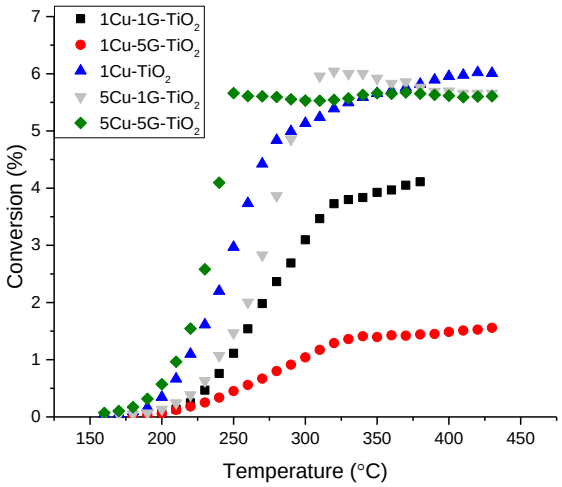



*Figure 4-16: Conversion profiles of 1Cu-1G-$TiO_2$/ 1Cu-5G-$TiO_2$/ 1Cu-$TiO_2$/ 5Cu-1G-$TiO_2$/ 5Cu-5G-$TiO_2$ catalysts in the temperature range of 160 °C - 430 °C.*

systems. Figure 4-16 shows lowest conversion when graphene is used with 1% Cu. In addition, 5% Cu-$TiO_2$ showed lower conversion maxima with higher graphene loading.

In terms of selectivity, acetone exhibited an increased selectivity with higher graphene and metal loadings. Moreover, acrolein is produced when graphene accompanies the support, while acetaldehyde is produced throughout the reaction, as shown on Table 9.

*Table 9: Selectivity of 1Cu-1G-$TiO_2$/ 1Cu-5G-$TiO_2$/ 1Cu-$TiO_2$/ 5Cu-1G-$TiO_2$/ 5Cu-5G-$TiO_2$ catalysts.*

| Product / Catalyst | Acetone | | Acrolein | | Acetaldehyde | | Other | |
|---|---|---|---|---|---|---|---|---|
| | OS ºC | Max % | OS ºC | Max % | OS ºC | Max % | OS ºC | Max % |
| 1Cu-1G-$TiO_2$ | 290 | 1.2 | 300 | 0.6 | 260 | 2.1 | 270 | 1.2 |
| 1Cu-5G- $TiO_2$ | - | - | 370 | 1.3 | 240 | 2.7 | - | - |
| 1Cu- $TiO_2$ | 290 | 1.9 | - | - | 220 | 1.1 | 260 | 1.1 |
| 5Cu-1G- $TiO_2$ | 200 | 12.1 | 200 | 32.4 | 210 | 6.2 | 190 | 11.3 |
| 5Cu-5G- $TiO_2$ | 160 | 37 | 180 | 6.3 | 190 | 4.1 | 190 | 1.8 |

### 4.3.4.3 *Cu - $ZrO_2$*

As in the case of Au/G/$ZrO_2$ (see Section 4.3.3.3) catalysts, the catalytic conversion of Cu/G/$ZrO_2$ showed an increased activity when higher graphene loading is used (Figure 4-17.).

Cu/G/$ZrO_2$ matrixes showed an overall poor performance in producing useful products. Acrolein is only produced with highest metal and graphene loading. Propanal is produced throughout the reactions with higher selectivity towards the higher loadings of metal and

graphene. It is also worth noting that graphene in this case changed the outcome of the reaction with suppressing the other byproducts, as can be shown from Table 10.

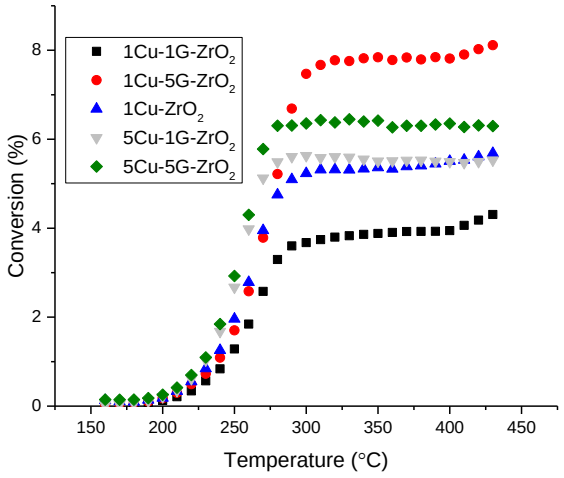



*Figure 4-17: Conversion profiles of 1Cu-1G-$ZrO_2$/ 1Cu-5G-$ZrO_2$/ 1Cu-$ZrO_2$/ 5Cu-1G-$ZrO_2$/ 5Cu-5G-$ZrO_2$ catalysts in the temperature range of 160 °C - 430 °C.*

*Table 10: Selectivity of 1Cu-1G-$ZrO_2$/ 1Cu-5G-$ZrO_2$/ 1Cu-$ZrO_2$/ 5Cu-1G-$ZrO_2$/ 5Cu-5G-$ZrO_2$ catalysts.*

| Product / Catalyst | Propanal | | Acrolein | | Acetaldehyde | | Other | |
|---|---|---|---|---|---|---|---|---|
| | OS ºC | Max % | OS ºC | Max % | OS ºC | Max % | OS ºC | Max % |
| 1Cu-1G-$ZrO_2$ | 230 | 2.6 | - | - | - | - | 420 | 4.4 |
| 1Cu-5G- $ZrO_2$ | 210 | 6.7 | - | - | - | - | 170 | 11.6 |
| 1Cu- $ZrO_2$ | 210 | 4.9 | - | - | - | - | 160 | 91 |
| 5Cu-1G- $ZrO_2$ | 200 | 5.1 | - | - | - | - | - | - |
| 5Cu-5G- $ZrO_2$ | 160 | 36.5 | 160 | 18.3 | - | - | 160 | 25.2 |

## 4.4 Graphene; a promoter or a poison?

Based on the catalytic results of graphene doped metal/metal oxide catalysts given in the previous sections, it can be concluded that graphene has a considerable effect on the selectivity and temperature of evolution of partially oxygenated products. For all cases, the evolution temperature and the amount of product showed a reverse trend to each other. As product selectivity increased, the evolution temperature was observed to be diminished and vice versa in case of a decrease in the selectivity of products. However, there was no common trend in terms of product distribution. Four main partially oxygenated products, namely propanal, acetaldehyde, acrolein and acetone, were observed for different catalyst systems in which the presence of graphene could suppress formation of some products and give rise to the production of others.

Industrially most valuable oxygenated products of propylene are considered as propylene oxide and acrolein. The production of propylene oxide was never observed with our metal oxide catalysts under the applied reaction conditions. Therefore, in order to check the influence of using graphene as a promoter towards the selectivity to acrolein, the catalytic results of graphene impregnated metal/metal oxide catalysts are grouped in Table 11 and 12. Table 11 shows the maximum acrolein selectivity and evolution temperatures on mesoporous oxide supports in the presence or absence of graphene. When graphene was impregnated on $ZrO_2$, a decrease in the acrolein evolution temperature was observed with the increase of graphene loading. In addition, while a small amount of graphene addition (1wt.%) enhanced the acrolein selectivity from 6.8% to 9.8%, further increase in the amount of graphene to 5 wt.% led to a negative effect and diminished the selectivity slightly to 8.8%. $Al_2O_3$ followed a similar trend of $ZrO_2$, while $TiO_2$ showed almost no acrolein selectivity.

*Table 11: Acrolein selectivity and corresponding temperature on different supports.*

| Support | Acrolein selectivity, % | T (°C ) |
|---|---|---|
| $ZrO_2$ | 6.8 | 360 |
| 1G-$ZrO_2$ | 9.8 | 350 |
| 5G-$ZrO_2$ | 8.8 | 330 |
| $Al_2O_3$ | 3.6 | 360 |
| 1G-$Al_2O_3$ | 6.8 | 370 |
| 5G-$Al_2O_3$ | 2.4 | 360 |
| $TiO_2$ | - | - |
| 1G-$TiO_2$ | - | - |
| 5G-$TiO_2$ | 0.7 | 360 |

Analysis of the catalytic performances of metal/mesoporous oxide support composites indicates that sometimes the production of acrolein can be detected at much lower temperatures when graphene is used (Table 12). For instance, while Cu on $Al_2O_3$ produces acrolein at 220 ºC with a maximum selectivity of 14.3%, the addition of graphene can pull the production temperature down to 160 ºC with higher selectivity. Further investigation of

*Table 12: Acrolein selectivity and corresponding temperature on selected catalysts.*

| Support | Acrolein selectivity % | T ºC |
|---|---|---|
| 1Cu-$Al_2O_3$ | 14.3 | 220 |
| 1Cu-1G-$Al_2O_3$ | 16.4 | 220 |
| 1Au-$TiO_2$ | - | - |
| 1Au-5G-$TiO_2$ | 30.8 | 190 |
| 1Cu-$ZrO_2$ | - | - |
| 5Cu-5G-$ZrO_2$ | 18.3 | 160 |

different systems shows that the addition of graphene introduces acrolein on the products map although no acrolein was detected initially.

Figure 4-18 shows the highest acrolein producing catalysts. It can be deduced, from the figure, that mostly high graphene loadings produce high acrolein percentages. In addition, the metal content has an influence on the reaction which might lead to the production of more acrolein.

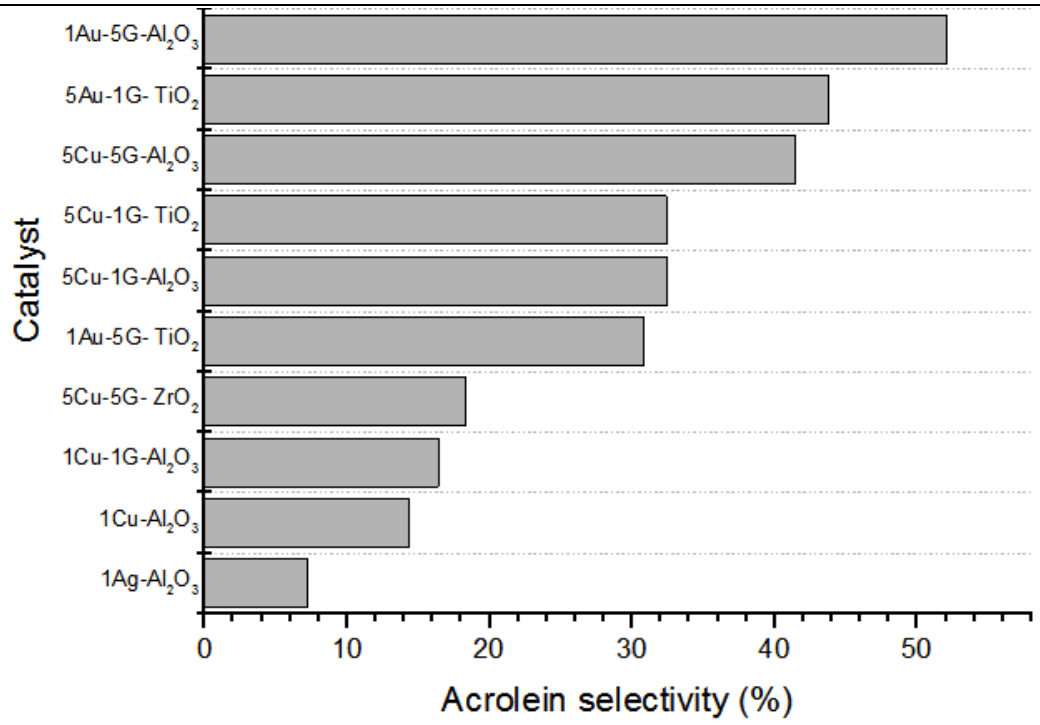



*Figure 4-18 : Acrolein selectivity obtained with different catalysts.*

### 4.4.1 Graphene as a support

In order to investigate the effect of graphene on propylene oxidation, graphene was considered to be used as sole support for metal particles. Initially, a blank experiment was performed with graphene. As illustrated in Figure 4-19, graphene solely was found to be catalytically active in propylene oxidation with up to 1.2% conversion and 26% selectivity towards acrolein. This

observation indicates that the graphene may produce acrolein solely, but the lack of improved acrolein production after the addition of graphene on other catalysts or the supports, as can be seen from Table 11 (*vide supra*), indicated that there could be other factors in play. To understand the effect of graphene further, the metals used were loaded into the graphene and the reaction was carried out under the same conditions to the previous catalysts.

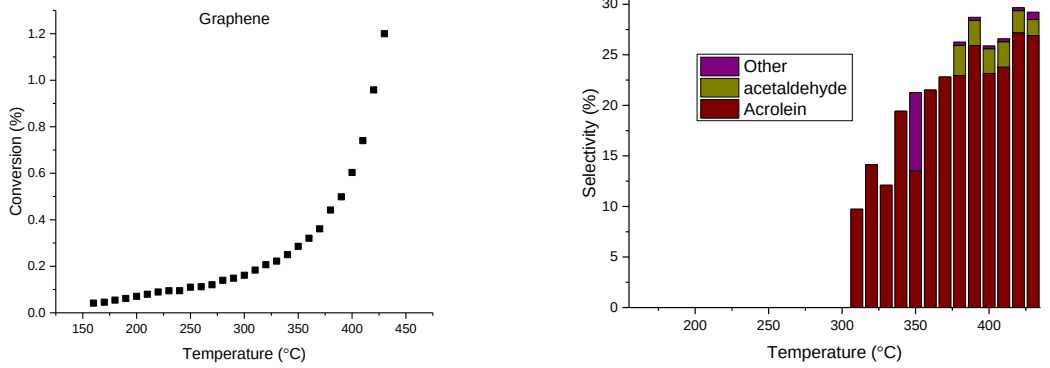



*Figure 4-19: Conversion and products selectivity of graphene in the temperature range of 160 °C - 430 °C.*

#### 4.4.1.1 *Ag-G Catalysts*

Propylene conversion of Ag loaded graphene was found to be much lower than its counterpart metal oxide supports. Introduction of 1% Ag on graphene did not make any noticeable change in the reaction rate and conversion when compared with the catalytic activity of sole graphene; on the other hand, the conversion could be doubled when more silver (5%) was loaded as seen from Figure 4-20.

Similar to silver loaded metal oxide catalysts, Ag on graphene produced different partially oxygenated products, with acetone, acrolein and acetaldehyde being the major ones. Table 13 summarizes the product distribution of Ag-G catalysts revealing the maximum selectivity of the products at corresponding temperatures. Generally, the partially oxygenated products were produced with much higher selectivity at a lower temperature when graphene was used as a sole support than metal oxide supports. The higher amount of Ag on graphene showed a higher

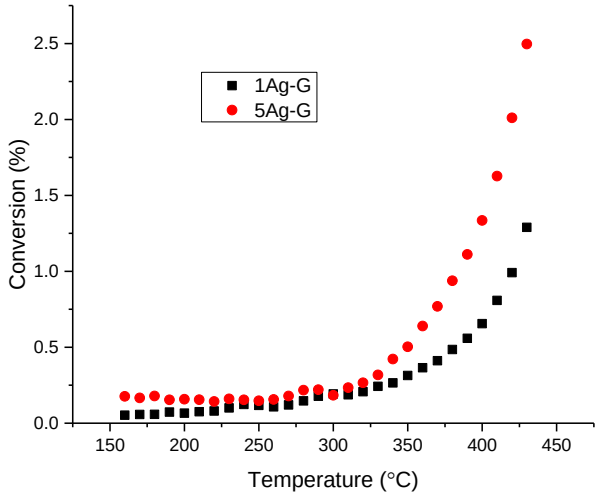



*Figure 4-20: Conversion profiles of 1Ag-G/ 5Ag-G catalysts in the temperature range of 160 °C - 430 °C.*

acetone, but lower acrolein selectivity without any change in their corresponding evolution temperature. Acetaldehyde is also produced with higher selectivity for lower Ag loading but at higher temperatures. The byproducts were only observed at higher metal loading.

*Table 13: Selectivity of 1Ag-G/ 5Ag-G catalysts.*

| Product / Catalyst | Acetone | | Acrolein | | Acetaldehyde | | Other | |
|---|---|---|---|---|---|---|---|---|
| | OS ºC | Max % | OS ºC | Max % | OS ºC | Max % | OS ºC | Max % |
| 1Ag-G | 160 | 29.9 | 280 | 30.6 | 230 | 8.9 | - | - |
| 5Ag-G | 160 | 45.8 | 280 | 22.7 | 170 | 6.9 | 160 | 20.6 |

### 4.4.1.2 *Au-G Catalysts*

The propylene conversion with Au loaded graphene catalysts was found to be similar to its counterpart oxide supports but higher when compared with Ag-G catalysts (Figure 4-21). Increasing the amount of Au on graphene slightly raised the maximum conversion from 2.5%

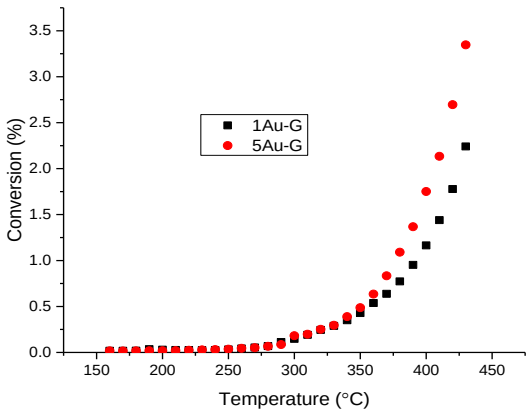



*Figure 4-21: Conversion profiles of 1Au-G/ 5Au-G catalysts in the temperature range of 160 °C - 430 °C.*

to 3% which indicates a higher activity in the presence of higher metal content. In addition, the formation of acetone was inhibited with the introduction of graphene, together with a drastic drop in the selectivity of acrolein as Au content increased (Table 14). Moreover, higher byproducts were produced with higher Au coverage. These results are consistent with previous observations of graphene promoted Au-metal oxide catalysts, which confirms that the presence of graphene alters the catalytic route presumably by changing the electronic and/or structural properties of metals.

*Table 14: Selectivity of 1Au-G/ 5Au-G catalysts.*

| Product / Catalyst | Acetone | | Acrolein | | Acetaldehyde | | Other | |
|---|---|---|---|---|---|---|---|---|
| | OS ºC | Max % | OS ºC | Max % | OS ºC | Max % | OS ºC | Max % |
| 1Au-G | - | - | 290 | 24.4 | 380 | 0.7 | 350 | 4.9 |
| 5Au-G | - | - | 300 | 12.3 | - | - | 300 | 35.8 |

#### 4.4.1.3 *Cu-G Catalysts*

1% Cu on graphene catalysts displayed a comparable conversion performance to those of the metal oxide supports (Figure 4-22). However, higher Cu loading (5%) led to a maximum conversion of around 11% , while lower loading of Cu showed around 8% conversion at the highest point.

Acrolein was the main product with graphene supported Cu independent from the metal

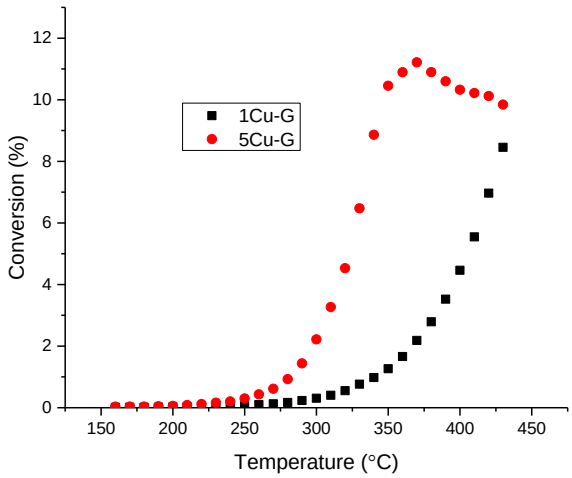



*Figure 4-22: Conversion profiles of 1Cu-G/ 5Cu-G catalysts in the temperature range of 160 °C - 430 °C.*

content. Table 15 shows a higher selectivity towards acrolein and acetaldehyde with low coverage of Cu. It is interesting to notice that propylene oxide was also produced on the 5Cu-G, which may open a new door into the research for a cost effective and environmentally friendly process for the oxidation of propylene that leads to very important products.

*Table 15: Selectivity of 1Cu-G/ 5Cu-G catalysts.*

| Product / Catalyst | Propylene Oxide | | Acrolein | | Acetaldehyde | | Other | |
|---|---|---|---|---|---|---|---|---|
| | OS °C | Max % | OS °C | Max % | OS °C | Max % | OS °C | Max % |
| 1Cu-G | - | - | 250 | 39.4 | 270 | 5.1 | 330 | 1.3 |
| 5Cu-G | 260 | 3.7 | 210 | 34.2 | 260 | 3.9 | 200 | 12 |

## 4.5 Water addition:

In an effort to improve the outcome of the Cu on graphene system, water was introduced into reaction system through bubbling the reaction gas in water then passing it over the catalyst.

### 4.5.1 Cu-G catalyst

First, we started with Cu because it had the highest conversion. Figure 4-23 shows an increase of Cu conversion with water.

The product distribution also changed. Figure 4-24 shows the propanal becomes the major early product of the reaction with water instead of the CO and $CO_2$ that is produced without the water. In addition, a small amount of propylene oxide is formed.

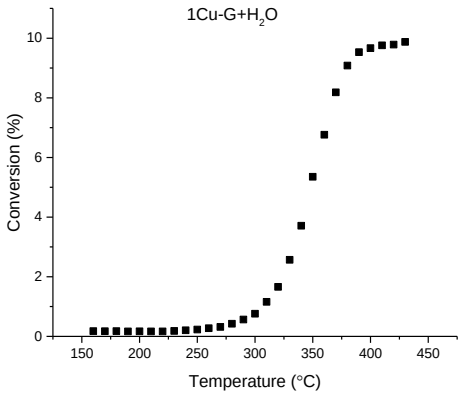



*Figure 4-23: Conversion profile of 1Cu-G+$H_2O$ catalyst in the temperature range of 160 °C - 430 °C.*

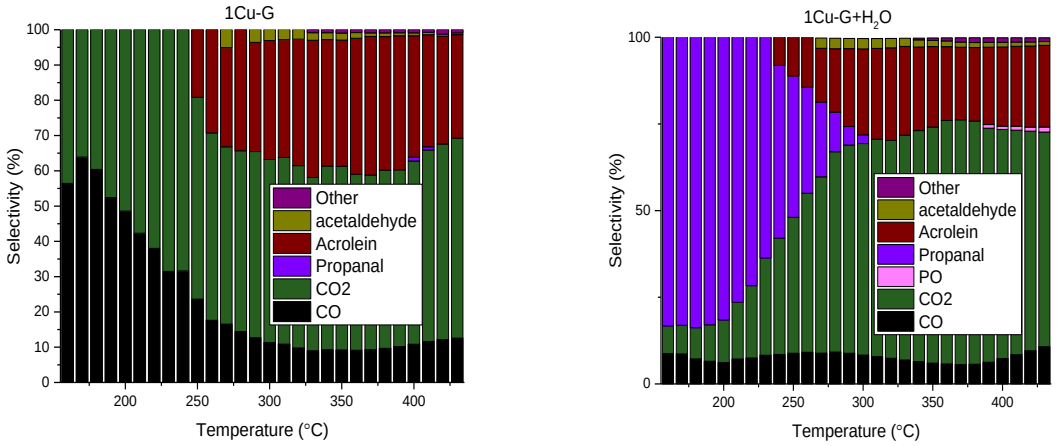



*Figure 4-24: Selectivity of 1Cu-G/ 1Cu-G+$H_2O$ catalysts.*

Upon the success of the use of water with Cu, it was introduced into the reaction stream of the Ag and Au.

### 4.5.2 Ag–G catalyst

Figure 4-25 indicates that the addition of water to Ag-graphene system has not improved the

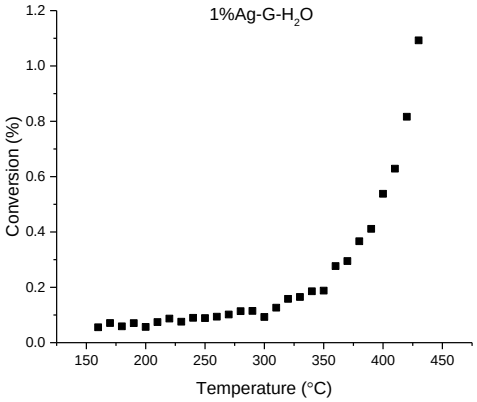



*Figure 4-25: Conversion profile of 1Ag-G+$H_2O$ catalyst in the temperature range of 160 °C - 430 °C.*

conversion. On the other hand, the products distribution has changed. Acetaldehyde has ceased to appear, and other products were introduced into the system as it can be seen from Figure 4-26.

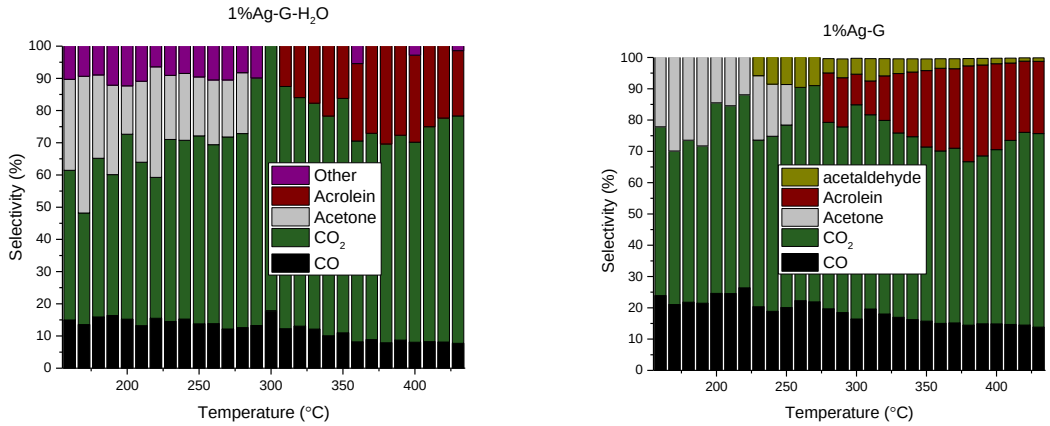



*Figure 4-26: Selectivity of 1Ag-G/ 1Ag-G+$H_2O$ catalysts.*

### 4.5.3 Au-G catalyst

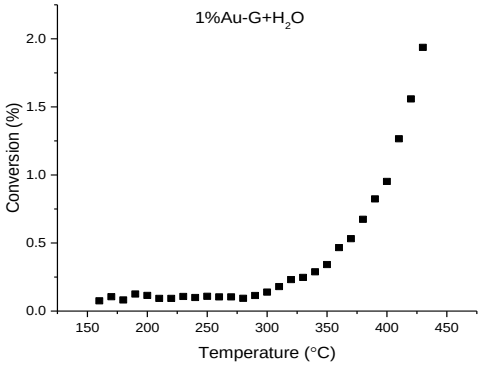



*Figure 4-27: Conversion profile of 1Au-G+$H_2O$ catalyst in the temperature range of 160 °C - 430 °C.*

Similar to Ag, Au shows decreased conversion with the use of water (Figure 4-27), but the products distribution shows a decrease of the combustion products. Alternatively, acetone was produced at lower temperature, as can be seen from Figure 4-28.

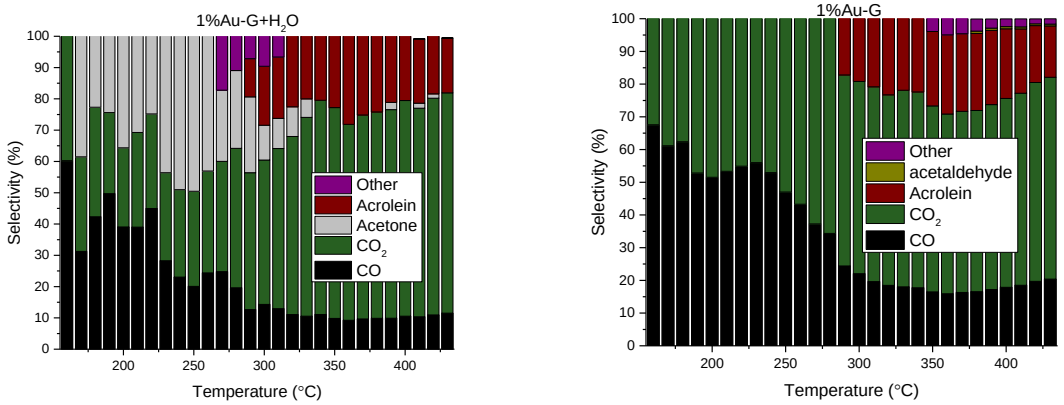



*Figure 4-28: Selectivity of 1Au-G/ 1Au-G+$H_2O$ catalysts.*

## 4.6 Summary of Catalysts Performances towards Acrolein Production

The consensus of literature about the presentation of the activity of catalysts in PO production is based on comparison of their selectivities. This could be due to the challenging gas phase production of PO. In addition, the structural characteristics of PO allow it to be produced mostly at lower temperatures, which is associated with lower conversion. Therefore, generally, the goal is to increase the selectivity at lower temperatures. However, acrolein is usually produced at higher temperatures and is more resistant to heat and pressure. Therefore, herein, we also summarize the performance of prepared catalysts (Table 16) in acrolein production from direct propylene oxidation in terms of % yield.

As seen from the table, Cu catalysts in the presence of graphene exhibit the highest yields. The yield is dependent on the copper loading, with 5% Cu on graphene producing the highest yield followed by 1% Cu on graphene, while the graphene support only produced 0.3 % yield of acrolein. After Cu, other catalysts produced acrolein with direct correlations to the amount of graphene loaded on them. In addition, the amount of metal loading seems to affect the performance of the catalysts, with high yields resulting from higher metal loadings.

*Table 16: Yield percentages of the tested catalysts.*

| Catalyst | Yield % | Catalyst | Yield % | Catalyst | Yield % |
|---|---|---|---|---|---|
| 5Cu-G | 3.40701 | 1Cu-1G-$Al_2O_3$ | 0.14143 | 1Ag-1G-$TiO_2$ | 0.0239 |
| 1Cu-G | 2.4815 | $Al_2O_3$ | 0.12197 | 1Cu-1G-$TiO_2$ | 0.02268 |
| 1Cu-G + $H_2O$ | 2.3269 | 1Ag-5G-$Al_2O_3$ | 0.12091 | 5Au-5G- $ZrO_2$ | 0.02239 |
| 5G-$ZrO_2$ | 0.57621 | 5G-$Al_2O_3$ | 0.08281 | 1Au-1G-$Al_2O_3$ | 0.02084 |
| 5Ag-G | 0.55957 | $ZrO_2$ | 0.07441 | 1Ag-1G-$ZrO_2$ | 0.01632 |
| 1G-$Al_2O_3$ | 0.42647 | 5Au-1G- $TiO_2$ | 0.06344 | 1Ag-5G- $ZrO_2$ | 0.01629 |
| 1G- $ZrO_2$ | 0.41439 | 1Ag-1G-$Al_2O_3$ | 0.06 | 1Ag- $ZrO_2$ | 0.01594 |
| 5Cu-1G-$Al_2O_3$ | 0.40967 | 5Cu-5G- $TiO_2$ | 0.05893 | 5Ag-1G- $ZrO_2$ | 0.01242 |
| 5Cu-1G- $TiO_2$ | 0.40967 | 1Au-5G-$Al_2O_3$ | 0.05886 | 5Au-1G-$Al_2O_3$ | 0 |
| 5Au-G | 0.39743 | 1G-$TiO_2$ | 0.05802 | 1Au- $TiO_2$ | 0 |
| 5Cu-5G-$Al_2O_3$ | 0.37885 | 5Ag-5G- $ZrO_2$ | 0.05701 | 5Au-5G- $TiO_2$ | 0 |
| 1Ag-$Al_2O_3$ | 0.36396 | 5Ag-1G- $TiO_2$ | 0.05511 | 1Au-1G-$ZrO_2$ | 0 |
| 1Au-G | 0.35225 | 1Ag-5G- $TiO_2$ | 0.05198 | 1Au- $ZrO_2$ | 0 |
| 5Ag-1G-$Al_2O_3$ | 0.35109 | 5Au-5G-$Al_2O_3$ | 0.04895 | 5Au-1G- $ZrO_2$ | 0 |
| 1Au-G + $H_2O$ | 0.33934 | 1Au-5G- $TiO_2$ | 0.03642 | 1Cu- $TiO_2$ | 0 |
| 1Au-5G- $ZrO_2$ | 0.33523 | 1Au-1G-$TiO_2$ | 0.03242 | 1Cu-1G-$ZrO_2$ | 0 |
| Graphene | 0.3228 | 5Ag-5G-$Al_2O_3$ | 0.03092 | 1Cu-5G- $ZrO_2$ | 0 |
| 1Ag-G | 0.29796 | 1Cu-5G- $TiO_2$ | 0.03009 | 1Cu- $ZrO_2$ | 0 |
| 1Ag-G + $H_2O$ | 0.22145 | 5Ag-5G- $TiO_2$ | 0.02819 | 5Cu-1G- $ZrO_2$ | 0 |
| 5Cu-5G- $ZrO_2$ | 0.17477 | 1Ag- $TiO_2$ | 0.02703 | 5G-$TiO_2$ | 0 |
| 1Cu-$Al_2O_3$ | 0.17186 | 1Au-$Al_2O_3$ | 0.02523 | $TiO_2$ | 0 |

Comparison of the catalytic performance of other Cu-based catalysts from the literature shows the influence of different supports and additives on the reaction's outcome. Table 17 shows the synergetic effect of V when used with Cu on ZSM-5 which enhanced the production of

acrolein, albeit with low yield (<1%). The change of support also proved to be beneficial for some cases as SBA-15 was capable of producing acrolein while $Al_2O_3$ was incapable. Based on these results, % acrolein yield of our non-porous 5Cu-G is superior to that of Cu/ZSM-5, Cu/AlPO-5 and Cu/$SiO_2$ catalyst systems but still lower than bimetallic CuAu/$SiO_2$ and CuPc-Py-SBA-15 catalysts employed in propylene oxidation.

*Table 17: Yield percentages of different catalysts from literature.*

| Catalyst | Yield % | Catalyst | Yield % | Catalyst | Yield% |
|---|---|---|---|---|---|
| VCu-ZSM-5[94] | 0.7 | VCu-AlPO-5[94] | 0.9 | CuPc-Py-$Al_2O_3$[95] | 0 |
| Cu-ZSM-5[94] | 0 | Cu-$SiO_2$[96] | 0.2 | CuPc-Py-SBA-15[95] | 7.8 |
| Cu-AlPO-5[94] | 0.9 | CuAu-$SiO_2$[96] | 4.7 | Cu-$SiO_2$[48] | 2.7 |

## 4.7 Summary

In summary, various combinations and contents of metal / graphene / metal oxide composites were tested as catalysts in propylene oxidation with molecular oxygen. The catalytic results show the extent of using graphene on the catalyst as a promoter, where it can suppress the formation of some subsequent oxidized products and give rise to the production of more primary oxidized products. In addition, it can be used as a metal free catalyst to produce acrolein with moderate selectivity, albeit low conversions. The metal-free method might lead to low coke deposition and is also cost effective.

Even though, graphene is inherently stable and inert, the defects and edges within the structure can dissociate the oxygen for further reactions.[97] The introduction of metal nanoparticles may increase the number of defects and give rise to more corners and edges leading to more sites for the activation of oxygen.

Water also has a significant effect when cycled with the propylene. It helps to suppress combustion to pave the way to produce useful products. The addition of water into graphene based materials has clearly shown to change the reactivity of the surface.[98]

Among the catalyst systems tested for propylene oxidation Cu / graphene / metal oxide combinations are shown to be highly effective in terms of conversion, selectivity, and yield. These Cu-loaded composite catalysts produce acrolein with high selectivity and even show small extent of propylene oxide formation. In addition, graphene support when loaded with Cu shows a comparable conversion to metal oxide supports. In order to understand the different reactivity behaviors between Cu/G/metal oxide and Cu/G, comprehensive characterization techniques are used. In the following sections, TEM, XPS and $NH_3$-TPD results of these two catalyst systems will be discussed.

## 4.8 TEM

Figure 4-29 exhibits the TEM images of 5Cu-5G-$Al_2O_3$ before and after the propylene

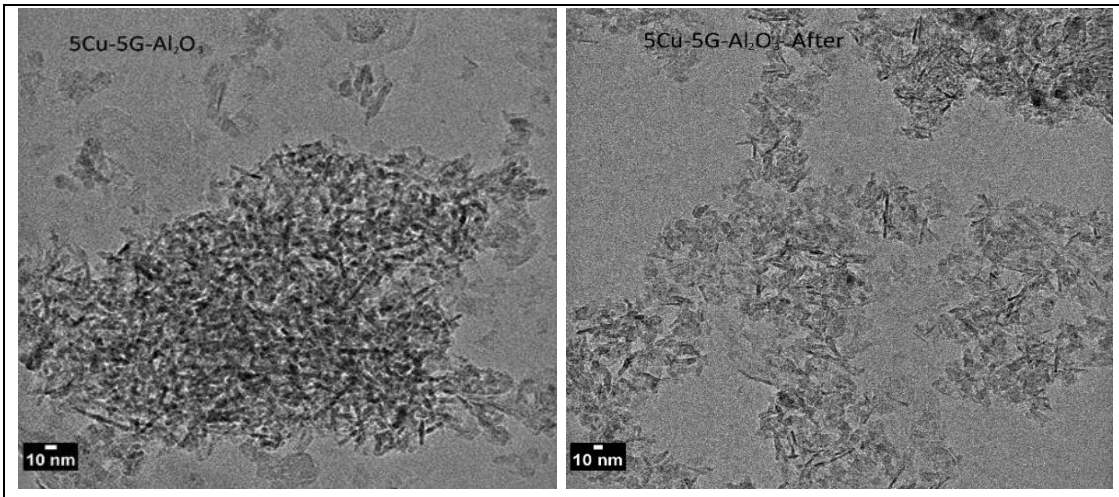



*Figure 4-29: TEM images of 5Cu-5G-$Al_2O_3$ catalyst before and after the reaction.*

oxidation reaction, where the contrast difference allows us to distinguish the species as the darkest being the Cu nanoparticles and the lightest being the graphene which seems to be spread over the catalyst and it's color darkens as the layers increase. TEM analysis performed on 5Cu-5G-$Al_2O_3$ before catalytic reaction showed the presence of nanoparticles homogeneous in shape (spherical) and displaying a narrow size distribution with a mean size of *ca.* 7 nm (Figure 4-30). After the propylene oxidation reaction, larger, polydisperse nanoparticles with an average diameter of *ca.* 8 nm were observed without a significant change in their shape (Figure 4-30).

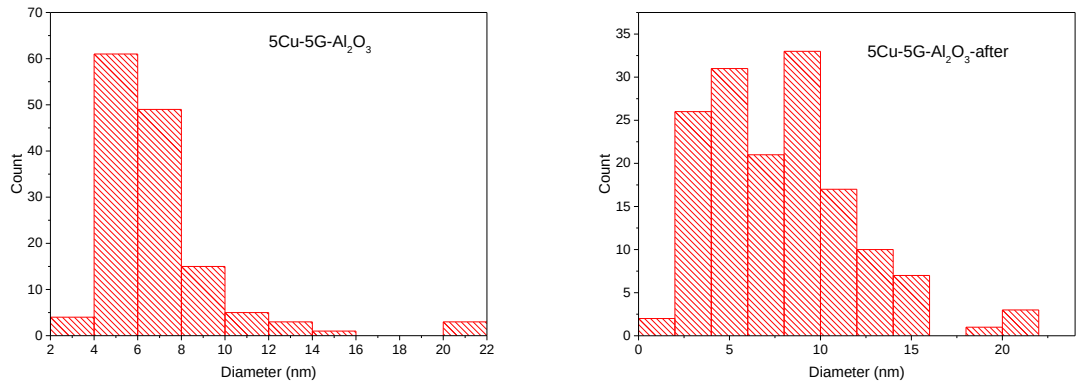



*Figure 4-30: Cu particle size distribution before and after the reaction for 5Cu-5G-$Al_2O_3$ catalyst.*

Cu loaded graphene catalysts were also imaged by TEM in order to shed some light on the nature of the particles between the two catalyst systems. Figure 4-31 demonstrates that spherical Cu nanoparticles with a mean size of *ca.* 25 nm. and are homogeneously distributed on the surface of graphene without aggregation. Similar to the case of 5Cu-5G-$Al_2O_3$ catalyst, Cu nanoparticles deposited on graphene were also found to get larger, *ca.* 35 nm, after propylene oxidation (Figure 4-32).

Comparison between the particles size of the two catalytic systems suggests that O- and OH-functional groups on $Al_2O_3$ can stabilize much smaller nanoparticles than graphene under the same reaction conditions; where they tend to coalesce to minimize their surface energy.[99] On the other hand, graphene could serve as an effective surfactant wrapping around Cu nanoparticles to inhibit their aggregation.

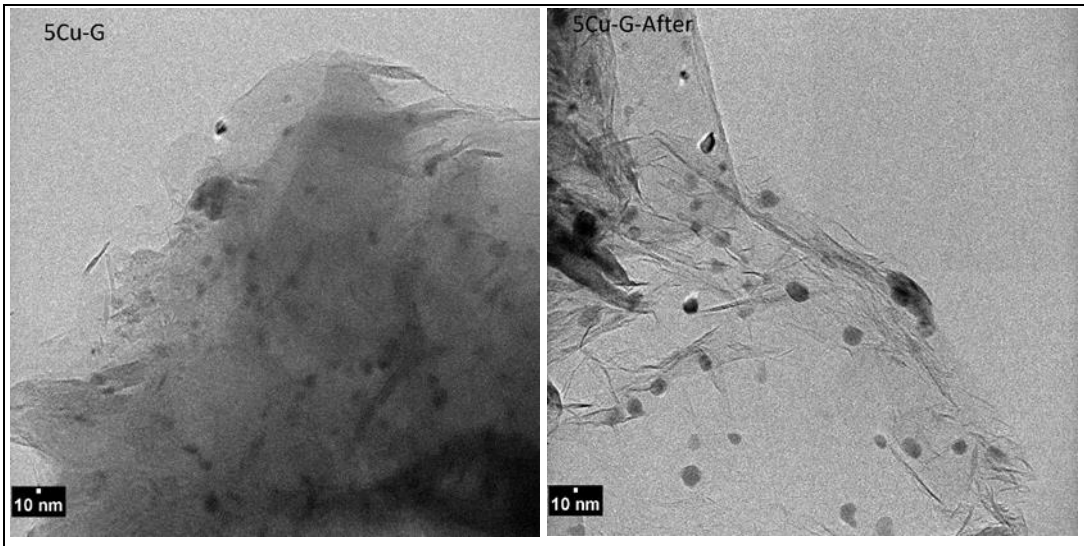



*Figure 4-31: TEM images for 5Cu-G catalyst before and after the reaction.*

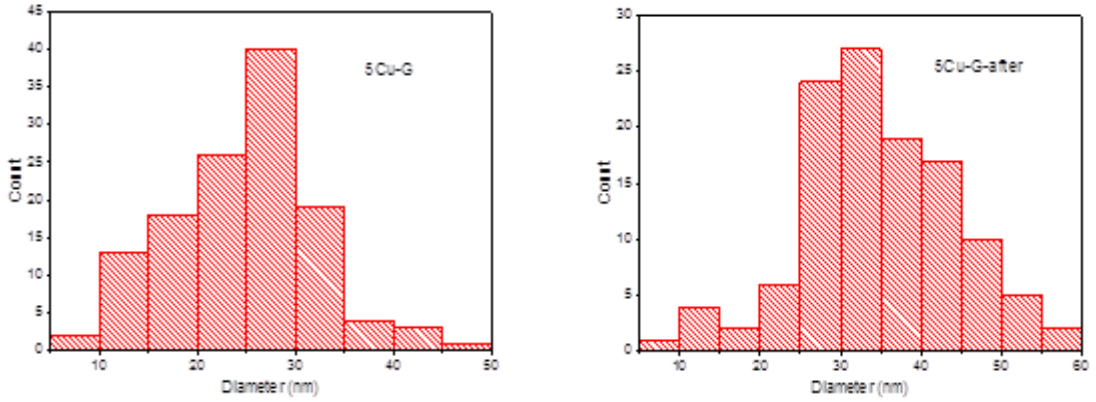



*Figure 4-32: Cu particle size distribution before and after the reaction for 5Cu-G catalyst.*

## 4.9 XPS

XPS analysis is used to gauge the metal support interactions. It can give an idea about the variable electronic effects exhorted on the nanoparticles upon using different supports, poisons or promoters. For this reason, Cu/G/metal oxide composites were analyzed by XPS before and after propylene oxidation reaction.

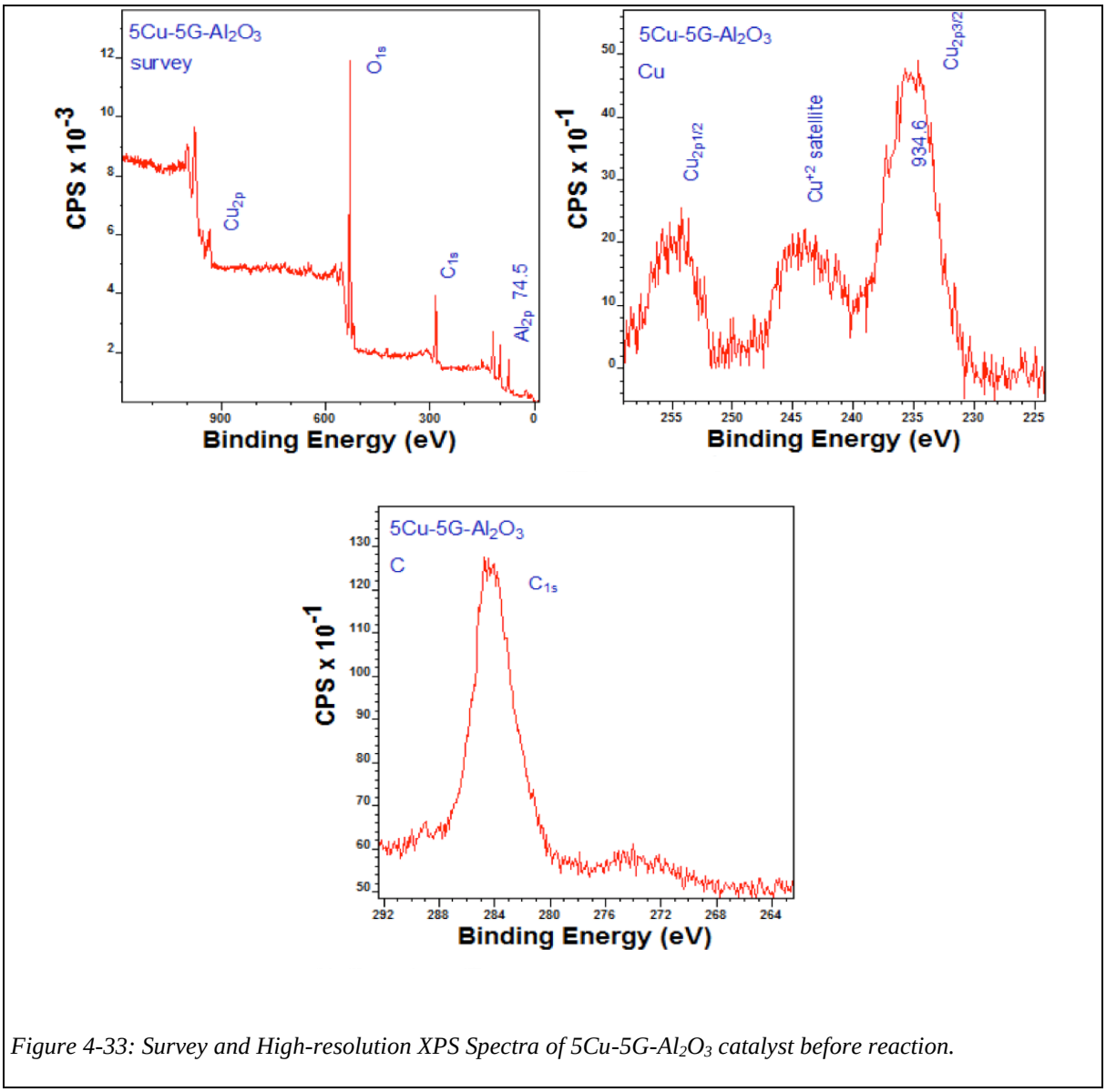



*Figure 4-33: Survey and High-resolution XPS Spectra of 5Cu-5G-$Al_2O_3$ catalyst before reaction.*

The primary XPS region is the Cu2p orbitals. The Cu2p peak is followed by a split spin-orbit component with Δ=19.75 eV. Experiments showed the binding energies for the Cu, $Cu^{+}$ oxide, and $Cu^{2+}$ oxides are 932.5, 932.7 and 933.5 eV respectively. The binding energy differences between the Cu and its oxides are within 1 eV, which makes it difficult to distinguish between their partial oxidation states. One way to identify the peaks is the use of the satellite peaks. $Cu^{2+}$ is accompanied by satellite peaks at Δ=10 eV. The intensity is greatly reduced when the oxidation state is $Cu^{+}$, and nearly vanishes with the metal.[100–107]

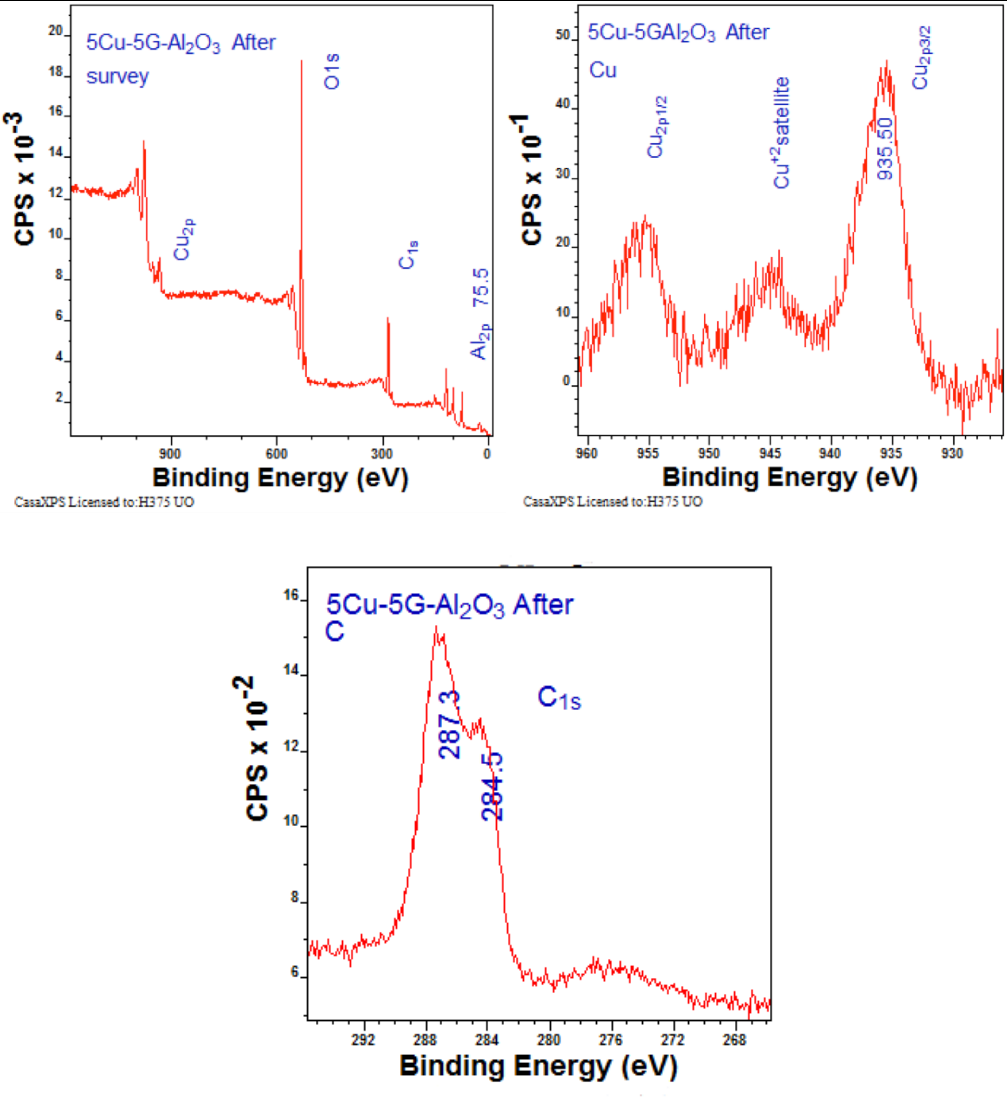



*Figure 4-34: Survey and High-Resolution XPS spectra of 5Cu-5G-$Al_2O_3$ catalyst after reaction.*

XPS data was collected for 5Cu-5G-$Al_2O_3$ before and after the reaction are presented in Figure 4-33 and 4-34. The survey scan shows the sample components which include Al, C, O and Cu. The high-resolution XPS spectrum of Cu shows the $Cu^{2+}$ satellite peak, indicating

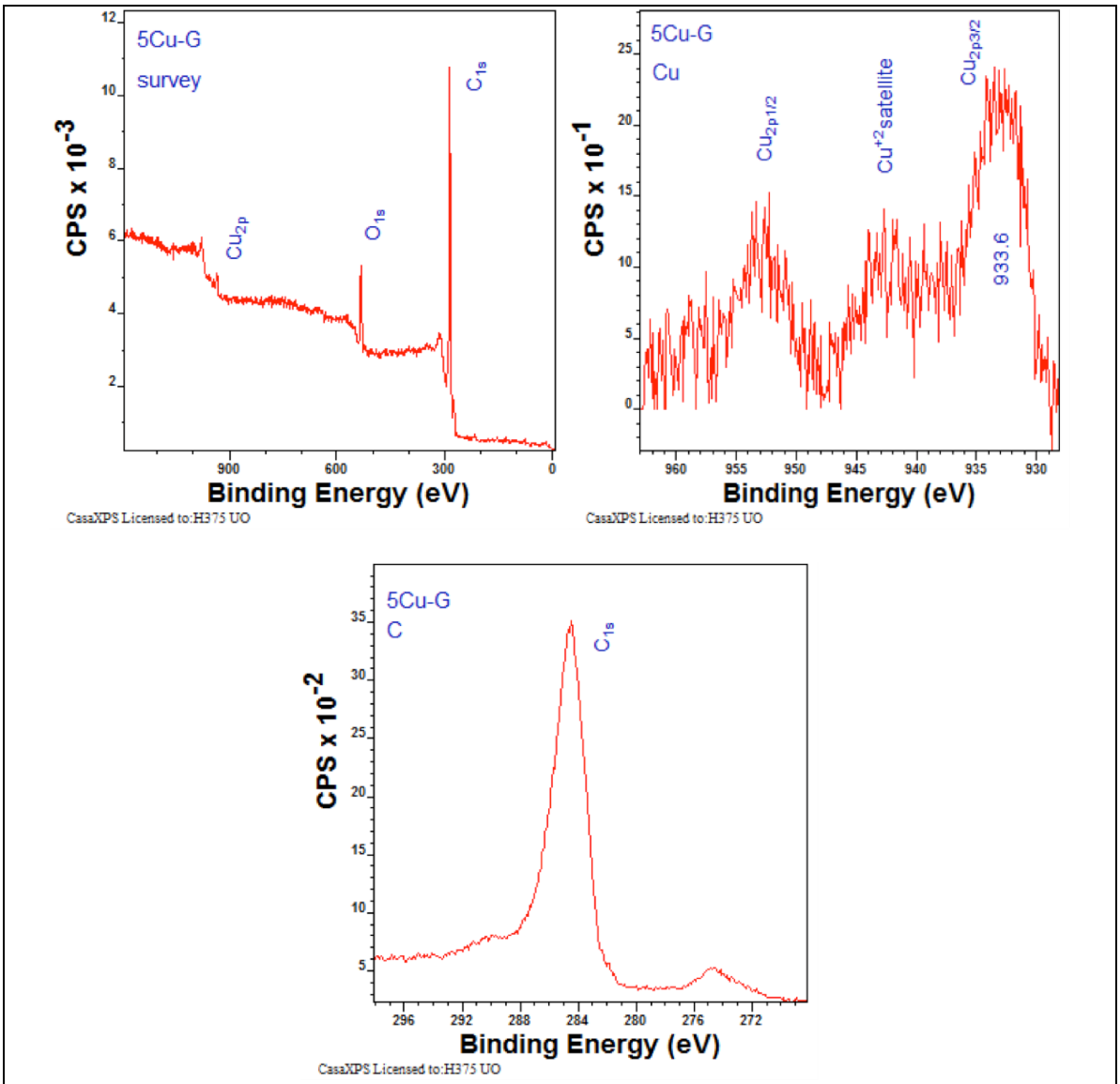



*Figure 4-35: Survey and High-Resolution XPS spectra of 5Cu-G catalyst before reaction.*

the presence of Cu in the form of CuO. Although the Cu precursor (Cu(II) acetylacetonate) impregnated on G-$Al_2O_3$ supports were reduced under $H_2$ flow at elevated temperatures to

form Cu(0) nanoparticles, these nanoparticles are found to be easily re-oxidized under air. The presence of $Cu^{2+}$ satellite peak in the XPS spectrum suggests that the Cu nanoparticles had already been oxidized before propylene oxidation reaction. After propylene oxidation reaction, a decrease of the $Cu^{2+}$ satellite is observed, which could indicate a reduction of the $Cu^{2+}$ due to the use of propylene as a reductant. In addition, a shift to higher binding energy was observed. This could be due to the adsorption of oxygenated hydrocarbon products or water.[108,109]

C1s spectrum exhibits a binding energy at 284.5 eV for C-C bond before the reaction (Figure 4-33), which indicates the presence of graphene on the surface, but after the reaction (Figure 4-34), an additional peak that corresponds to C1s binding energy on C-O bond is formed at 287.3 eV. The formation of C-O bond could have resulted from the adsorption of oxidation products or water on the surface. The new C-O species may have influenced the ionic properties of the alumina and caused an increase of the binding energy of Al 2p from 74.5 eV to 75.5 eV.[110,111]

When graphene was used as a support, an influence in the electronic environment of the Cu nanoparticles was observed. Figure 4-35 shows the binding energy of the $Cu2p_{3/2}$ spectrum. A decrease of the binding energy from that measured on Cu-G-$Al_2O_3$, is observed. The abundance of electron density for the $sp^2$ carbon of the graphene support could be the motive for this decrease.

The Cu nanoparticles when loaded on graphene showed a further decrease (1 eV) of the binding energy after the reaction (Figure 4-36), suggesting an increase in size. This result matches well with our TEM observation which revealed bigger spherical nanoparticles after

the catalytic propylene oxidation reaction. In addition, the intensity of the satellite peaks is reduced, in a similar behavior to the 5Cu-5G-$Al_2O_3$ catalyst.

It is worth noticing that the carbon species for the graphene support does not show a big difference before and after the reaction, contrary to the case of G-$Al_2O_3$ support. This could be due to less deposition of oxygenated partial products when graphene is used. It is also

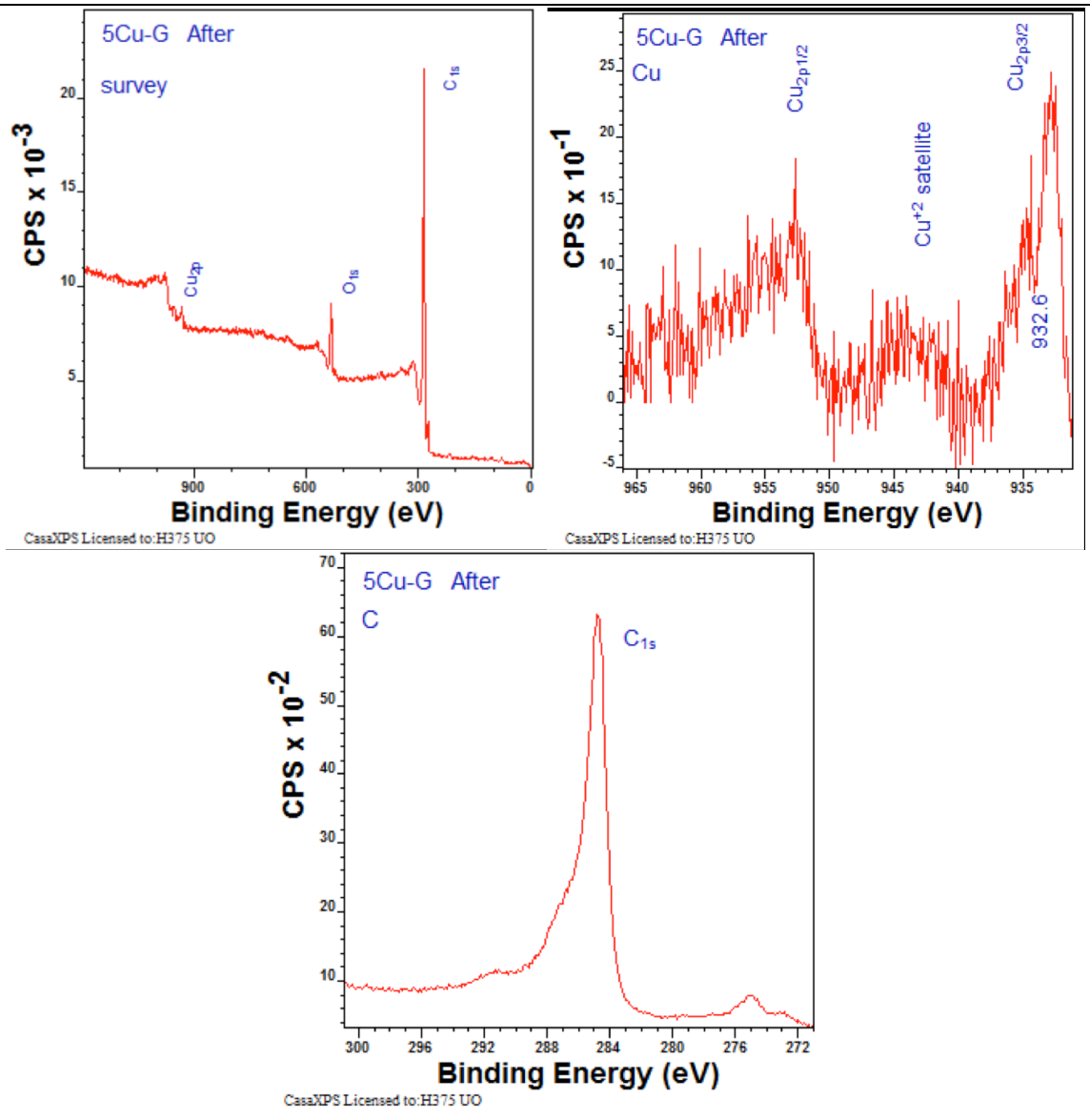



*Figure 4-36: Survey and High-Resolution XPS spectra of 5Cu-G. catalyst after reaction.*

worthy to mention that the Cu spectra on graphene is noisy which could be due to the decreased abundance of the Cu on the graphene when compared with Cu on $Al_2O_3$-G. (0.17 % for Cu-G vs 0.56 % for Cu-G-$Al_2O_3$). In addition, graphene inherently restacks and agglomerates which may cover some of the nanoparticles and reduce the beam intensity reaching the detector.

Overall, XPS analyses reveal a decrease in the binding energies of the Cu species with the increase of amount of graphene. This indicates that there is indeed a strong electronic interaction between the graphene and the Cu nanoparticle, which leads to an overall decrease in electrons hence lowering the binding energy, as originally anticipated.

With the previous observations outlined, it is vital to understand that Cu oxidation state determination using XPS has some limitations. The overlap between the $Cu2p_{3/2}$ peaks makes it impossible to distinguish between them. In addition, ex-situ XPS analysis is very sensitive to the surface composition, and because Cu is easily oxidized even in ambient conditions, this leads to additional complications to the analysis making it difficult to determine the prominent oxidation state.

## 4.10 Ammonia TPD

In previous studies[112], it has been proposed that catalysts with higher surface acidity might be subject to deactivation due to self-poisoning of oxygen containing products. This process is caused by the prolonged adsorption of some species, that might decompose and cause poising of the catalyst. In order to determine the acid properties of our catalysts, $NH_3$-TPD experiments were performed. The $NH_3$-TPD pattern of Cu on $Al_2O_3$ catalyst shows two distinct acidic sites at 113.1 ºC and at 266.1 ºC which might be attributed to weak and strong

acidic sites respectively. On the other hand, only one distinct weak acid site was observed on the Cu-G catalyst which was observed at 149.1 ºC (Figure 4-37). The weaker acidity of the Cu on graphene at elevated temperature might not be subject to self-poisoning hence accounting for higher selectivity towards acrolein with lower combustion products.

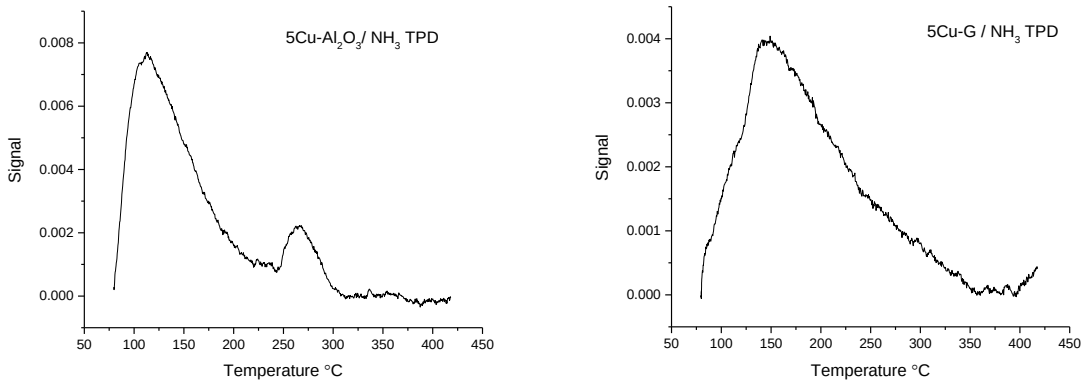



*Figure 4-37: $NH_3$ TPD for 5Cu-$Al_2O_3$ and 5Cu-G catalysts in the range of 60 °C - 430 °C.*

Chapter 5:

# Conclusions and perspectives

# 5 Chapter 5: Conclusions and perspectives

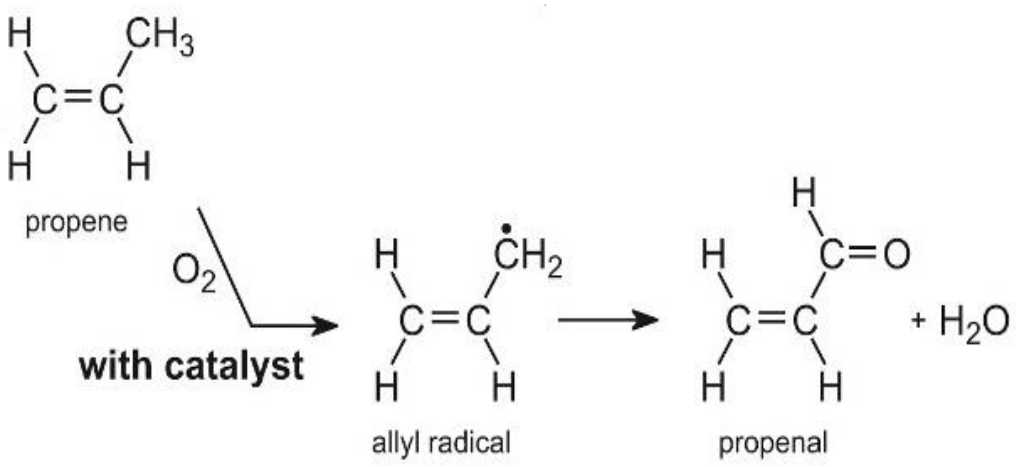
In this thesis, the synthesis, characterization and catalytic application of Metal/Graphene/Metal Oxide composites are reported. This work has been developed in the framework of KACST-Oxford SCET Vapor Project at Inorganic Chemistry Laboratory of University of Oxford under the supervision of Prof. Edman Tsang. The main objective was to study the effect of graphene as a promoter and a support to pave a way for selective propylene oxidation to high value products, in particular to propylene oxide. It is thought the charge of adsorbed oxygen on metal/metal oxide plays an important role in dictating the products. The idea was to use the intrinsic high electronic conductivity of graphene to delocalize the negative charge hence making the oxygen electrophilic for the formation of propylene oxide.

Graphene was therefore synthesized according to modified Hammers' method. Its quality and stability over the reaction thermal conditions were tested by x-ray diffraction and thermogravimetric analysis, respectively, before use. The composite catalysts were prepared by deposition of Ag, Au or Cu via incipient wetness impregnation method on mesoporous metal oxides ($TiO_2$, $ZrO_2$, $Al_2O_3$) and/or graphene supports.

The oxidation of propylene over the prepared composite catalysts was studied in a tubular reactor under atmospheric pressure using molecular oxygen as an oxidant. Later on, water was also introduced to the system to increase the selectivity of partially oxidized products.

In general, the introduction of graphene to the catalytic system enhanced the propylene conversion, as deducted from the comparison of different supports before and after the addition of graphene. Selectivity, on the other hand, did not follow a simple trend. The presence of graphene seems to have influenced the electronic and structural properties of

metal/metal oxide catalyst systems in a different way which led to an enhancement on the selectivity of some oxidized products while suppressing the formation of others.




(3)

The results suggested our original idea of removing the charge of adsorbed oxygen on metal/metal oxide making it electrophilic rather than nucleophilic during propylene-$O_2$ oxidation was not successful. The production of propylene oxide was not observed for most of the studied catalysts. This indicates that the allylic hydrogen of propylene is still activated by the surface oxygen instead of the double bond. However, it did not seem to go always to carbon oxides, unless strong acid sites were present. Instead, it appeared to have further oxidized on the catalyst surface to give acrolein. Thus, we demonstrate a direct production of acrolein from propylene oxidation, which is also an industrially valuable partially oxidized product as shown above (reaction 3), with the introduction of graphene on Ag-$Al_2O_3$, Au-$Al_2O_3$. Au-$TiO_2$, Cu-$Al_2O_3$, Cu-$TiO_2$ and Cu-$ZrO_2$ catalysts. In addition, when graphene was used solely it could facilitate acrolein production. Acrolein selectivity was further enhanced by loading transition metals (Ag, Au or Cu) onto the graphene support together with an increase in conversion from 1% for graphene, to 2.5 %, 3.5 % and 11% for Ag, Au, and Cu

loaded graphene, respectively. The conversion was found to be directly proportional to the metal content, although acrolein selectivity was inversely proportional. The addition of water clearly suppressed the combustion products at early temperatures with Au and Cu and facilitated the production of PO with 1Cu-G catalyst.

Among all composite catalysts, Cu -G-$Al_2O_3$ and Cu-G systems exhibited the best and clearest trend with acrolein and a small amount of PO production. The increase of graphene in Cu-$Al_2O_3$ systems increased the acrolein production, and the increase in Cu content on graphene increased the conversion. PO was produced only with 5Cu-G, So the two systems were elected for further characterization. XPS studies indeed showed modified electronic interactions of Cu on graphene to alter the electronic density of the metal, with the use of graphene as an additive or as a support. This suggests graphene could be used to affect the electron density of the metal by the support interaction. The particle size distribution showed a change of the mean size from 5 nm to 10 nm for the Cu-G-$Al_2O_3$ catalyst during the catalysis, while for Cu-G the mean size changed from 30 nm to 35 nm. The smaller degree of particle agglomeration by using graphene as support may indicate the interesting and stable metal-graphene interaction. In addition, the NH3 -TPD suggested only weaker acidic sites retained for the Cu-G catalyst that did not lead to over-oxidation of the allylic-H activated products as typical in many metal oxide supports.

Overall, with this study, graphene is shown to be a good promoter for the selective oxidation of propylene to acrolein. The obtained results, even if improvements are still needed, are very encouraging and pave the way towards the cost-effective, even metal free, catalyst synthesis. Besides exploring more conditions to increase acrolein or propylene oxide yield, changing the nature of the support/promoter to a material such as carbon nitride, might be of interest to

evaluate the effect of graphitic structures on the conversion and selectivity of propylene oxidation.

# 6 References


(1) Laidler, K. J. *Pure Appl. Chem* **1996**, *68* (1), 149–192.

(2) Ayvali, T. One-pot synthesis and chracterization of colloidally robust rhodium(0) nanoparticles caltalyst: exceptional activity in the dehydrogenation of ammonia borane for chemical hydrogen storage, Middle east technical university, 2011.

(3) Hagen, J. *Industrial catalysis : a practical approach*, Wiley-VCH, **2006**.

(4) Gates, B. C. *Catalytic chemistry*, Wiley, **1992**.

(5) Hagen, J. *Industrial catalysis*, Wiley-VCH Verlag GmbH & Co. KGaA, Weinheim, **2005**.

(6) Anthonsen, T. *Reactions catalyzed by enzymes In applied biocatalysis 2*, Harwood Academic Publishers, **1999**.

(7) John M.; Thomas, W. J. *Principles and practice of heterogeneous catalysis*, Wiley, **2014**.

(8) Hegedus, L. L.; McCabe, R. W. *Stud. Surf. Sci. Catal.* **1980**, *6*, 471–505.

(9) Mann, R.; El-Kady, F. Y. A.; Marzin, R. *Chem. Eng. Sci.* **1985**, *40* (2), 249–257.

(10) McVicker, G. B.; Garten, R. L.; Baker, R. T. K. *J. Catal.* **1978**, *54* (2), 129–142.

(11) Arai, M.; Ishikawa, T.; Nakayama, T.; Nishiyama, Y. *J. Colloid Interface Sci.* **1984**, *97* (1), 254–265.

(12) Wallace, W. T.; Min, B. K.; Goodman, D. W. *J. Mol. Catal. A Chem.* **2005**, *228* (1), 3–

10.

(13) *Peter, E; Linda, AG; Richard, K. Ullmann's Encyclopedia of Industrial Chemistry;Wiley-VCH Verlag GmbH & Co. KGaA: Weinheim, Germany,* ***2000****.*

(14) Baer, H.; Bergamo, M.; Forlin, A.; Pottenger, L. H.; Lindner, J. *Ullmann's Encyclopedia of Industrial Chemistry*; Wiley-VCH Verlag GmbH & Co. KGaA: Weinheim, Germany, **2012**.

(15) Nijhuis, T. A.; Makkee, M.; Moulijn, J. A.; Weckhuysen, B. M. *Ind. Eng. Chem. Res.* **2006**, *45* (10), 3447–3459.

(16) Bassler, P.; Weidenbach, M. *Chem. Eng. Trans.* **2010**, *21*, 571–576.

(17) Huang, J.; Haruta, M. *Res. Chem. Intermed.* **2012**, *38* (1), 1–24.

(18) Campos-Martin, J. M.; Blanco-Brieva, G.; Fierro, J. L. G. *Angew. Chem. Int. Ed.* **2006**, *45* (42), 6962–6984.

(19) Lambert, R. M.; Williams, F. J.; Cropley, R. L.; Palermo, A. *J. Mol. Catal. A Chem.* **2005**, *228* (1–2), 27–33.

(20) Bukhtiyarov, V. I.; Hävecker, M.; Kaichev, V. V; Knop-Gericke, A.; Mayer, R. W.; Schlögl, R. *Phys. Rev. B* **2003**, *67*, 1–12.

(21) Grant, R. B.; Lambert , R. M. *J. Catal.* **1985**, *92*, 364–375.

(22) Carter, E. A.; Goddard, W. A. *J. Catal.* **1988**, 80–92.

(23) Tan, S. *J. Catal.* **1986**, *100* (2), 383–391.

(24) Grant, R. *J. Catal.* **1985**, *92* (2), 364–375.

(25) Palermo, A.; Husain, A.; Lambert, R. M. *Catal. Letters* **2000**, *69* (3), 175–179.

(26) Grant, R. B.; Harbach, C. A. J.; Lambert, R. M.; Tan, S. A. *J. Chem. Soc. Faraday Trans. 1 Phys. Chem. Condens. Phases* **1987**, *83* (7), 2035.

(27) Ozbek, M. O.; Onal, I.; van Santen, R. A. *ChemCatChem* **2013**, *5* (2), 443–451.

(28) Ozbek, M. O.; Onal, I.; Van Santen, R. A. *J. Catal.* **2011**, *284*, 230–235.

(29) De Oliveira, A. L.; Wolf, A.; Schüth, F. *Catal. Letters* **2001**, *73* (2), 157–160.

(30) Wang, C.; Guo, X.; Wang, X.; Wang, R.; Hao, J. *Catal. Letters* **2004**, *96* (1), 79–85.

(31) Wang, R.; Guo, X.; Wang, X.; Hao, J.; Li, G.; Xiu, J. *Appl. Catal. A Gen.* **2004**, *261* (1), 7–13.

(32) Guo, X.; Wang, R.; Wang, X.; Hao, J. *Catal. Today* **2004**, *93*, 211–216.

(33) Sandoval, A.; Aguilar, A.; Louis, C.; Traverse, A.; Zanella, R. *J. Catal.* **2011**, *281* (1), 40–49.

(34) Haruta, M. *Chem. Rec.* **2003**, *3* (2), 75–87.

(35) Bond, G. C.; Sermon, P. A.; Webb, G.; Buchanan, D. A.; Wells, P. B. *J. Chem. Soc. Chem. Commun.* **1973**, 444b-445.

(36) Sault, A. G.; Madix, R. J.; Campbell, C. T. *Surf. Sci.* **1986**, *169* (2–3), 347–356.

(37) Haruta, M.; Kobayashi, T.; Sano, H.; Yamada, N. *Chem. Lett.* **1987**, *16* (2), 405–408.

(38) Hayashi, T.; Tanaka, K.; Haruta, M. *J. Catal.* **1998**, *178* (2), 566–575.

(39) Sinha, A. K.; Seelan, S.; Tsubota, S.; Haruta, M. *Top. Catal.* **2004**, *29* (3-4), 95–102.

(40) Huang, J.; Takei, T.; Akita, T.; Ohashi, H.; Haruta, M. *Appl. Catal. B Environ.* **2010**, *95* (3), 430–438.

(41) Lee, W.-S.; Cem Akatay, M.; Stach, E. A.; Ribeiro, F. H.; Nicholas Delgass, W. *J. Catal.* **2012**, *287*, 178–189.

(42) David H. Wells, J.; Ajay M. Joshi; W. Nicholas Delgass, A.; Thomson, K. T. *J. Phys. Chem. B* **2006**, *110* (30), 14627–14639.

(43) Ajay M. Joshi; W. Nicholas Delgass, A.; Thomson, K. T. *J. Phys. Chem. C* **2007**, *111* (22), 7841–7844.

(44) Haruta, M. *CATTECH* **2002**, *6* (3), 102–115.

(45) Cao, S.; Franklin Tao, ab; Tang, Y.; Li, Y.; Yu, J. *Chem. Soc. Rev. Chem. Soc. Rev* **2016**, *45* (45), 4747–4765.

(46) Haruta, M. *Chem. Rec.* **2003**, *3* (2), 75–87.

(47) Ojeda, M.; Iglesia, E. *Chem. Commun.* **2009**, *95* (3), 352–354.

(48) Vaughan, O.; Kyriakou, G.; Macleod, N.; Tikhov, M.; Lambert, R. *J. Catal.* **2005**, *236* (2), 401–404.

(49) Su, W.; Wang, S.; Ying, P.; Feng, Z.; Li, C. *J. Catal.* **2009**, *268* (1), 165–174.

(50) Zhu, W.; Zhang, Q.; Wang, Y. *J. Phys. Chem. C* **2008**, *112* (20), 7731–7734.

(51) Chu, H.; Yang, L.; Zhang, Q.; Wang, Y. *J. Catal.* **2006**, *241* (1), 225–228.

(52) Seubsai, A.; Kahn, M.; Senkan, S. *ChemCatChem* **2010**, *3* (1), 174–179.

(53) Miller, A.; Zohour, B.; Seubsai, A.; Noon, D.; Senkan, S. *Ind. Eng. Chem. Res* **2013**, *52* (28), 9551–9555.

(54) Cowell, J. J.; Santra, A. K.; Lambert, R. M. *J. Am. Chem. Soc* **2000**, *122* (10), 2381–2382.

(55) Cowell, J. J.; Santra, A. K.; Lindsay, R.; Lambert, R. M.; Baraldi, A.; Goldoni, A. *Surf. Sci.* **1999**, *437* (1–2), 1–8.

(56) Rachael L. Cropley; Federico J. Williams; Andrew J. Urquhart; Owain P. H. Vaughan; Mintcho S. Tikhov, A.; Lambert, R. M. *J. Am. Chem. Soc.* **2005**, *127* (16), 6069–6076.

(57) Liu, L.; Ye, X. P.; Bozell, J. J. *ChemSusChem* **2012**, *5* (7), 1162–1180.

(58) Arntz, D.; Fischer, A.; Höpp, M.; Jacobi, S.; Sauer, J.; Ohara, T.; Sato, T.; Shimizu, N.; Schwind, H. *Ullmann's Encyclopedia of Industrial Chemistry*; Wiley-VCH Verlag GmbH & Co. KGaA: Weinheim, Germany, **2007**.

(59) Ai, M. *Appl. Catal.* **1991**, *77* (1), 123–132.

(60) Imachi, M. *J. Catal.* **1982**, *75* (2), 404–409.

(61) Nakagawa, K.; Teng, Y.; Zhao, Z.; Yamada, Y.; Ueda, A.; Suzuki, T.; Kobayashi, T. *Catal. Letters* **1999**, *63* (1), 79–82.

(62) Cornils, B. *Angew. Chemie Int. Ed.* **2004**, *43* (18), 2324–2325.

(63) Krenzke, L. D. The kinetics and mechanism of propylene oxidation over bismuth-molybdate, The University of Wisconsin, **1977**.

(64) Rase, H. F. *Handbook of commercial catalysts : heterogeneous catalysts*; CRC Press, **2000**.

(65) Saleh-Alhamed, Y. A.; Hudgins, R. R.; Silveston, P. L. *Appl. Catal. A Gen.* **1995**, *127* (1–2), 177–199.

(66) Millet, J. *J. Catal.* **1993**, *142* (2), 381–391.

(67) Krenzke, L. *J. Catal.* **1980**, *61* (2), 316–325.

(68) Adams, C. *J. Catal.* **1963**, *2* (1), 63–68.

(69) Grzybowska, B. *J. Catal.* **1977**, *49* (2), 150–163.

(70) Glaeser, L. C.; Brazdil, J. F.; Hazle, M. A.; Mehicic, M.; Grasselli, R. K. *J. Chem. Soc. Faraday Trans. 1 Phys. Chem. Condens. Phases* **1985**, *81* (11), 2903.

(71) Creten, G. *J. Catal.* **1995**, *154* (1), 151–162.

(72) Schlögl, R. *Top. Catal.* **2016**, *59* (17), 1461–1476.

(73) Hu, C.; Lu, T.; Chen, F.; Zhang, R. *J. Chinese Adv. Mater. Soc.* **2013**, *1* (1), 21–39.

(74) Yao, Y.; Fu, Q.; Zhang, Y. Y.; Weng, X.; Li, H.; Chen, M.; Jin, L.; Dong, A.; Mu, R.; Jiang, P.; Liu, L.; Bluhm, H.; Liu, Z.; Zhang, S. B.; Bao, X. *Proc. Natl. Acad. Sci. U. S. A.* **2014**, *111* (48), 17023–17028.

(75) Davankov, K.; Jinno, G.; Vigh, G. G.; Guilbault, R. E.; Van; Grieken. *Pure &Appl,*

*Chem.* **1993**, *65* (4), 819–872.

(76) McNair, H. M.; Miller, J. M. *Basic gas chromatography*; John Wiley & Sons, **2009**.

(77) Bunaciu, A. A.; gabriela Udriştioiu, E.; Aboul-Enein, H. Y.; Gabriela Udr Stioiu, E.; Aboul-Enein, H. Y. *Crit. Rev. Anal. Chem.* **2015**, *45* (4), 289–299.

(78) Borchardt-Ott, W. *Crystallography: an introduction*; Springer, **2011**.

(79) Pecharsky; Vitalij; Zavalij; Peter. *Fundamentals of Powder Diffraction and Structural Characterization of Materials*; Springer US: Boston, MA, **2009**.

(80) Cullity, B. D. *Elements of x-ray diffraction*; Prentice Hall, **2001**.

(81) Deepak, F. L.; Mayoral, A.; Arenal, R. *Advanced transmission electron microscopy : applications to nanomaterials*; Springer, **2015**.

(82) Che M.; Védrine, J. C. *Characterization of solid materials and heterogeneous catalysts*; Wiley-VCH Verlag GmbH & Co. KGaA: Weinheim, Germany, **2012**.

(83) Leng, Y. *Materials characterization*; John Wiley & Sons, Ltd: Chichester, UK, **2008**.

(84) Gai, P. L.; Boyes, E. D. *Electron microscopy in heterogeneous catalysis*; CRC Press, **2003**.

(85) Wagner, J. M. *X-ray photoelectron spectroscopy*; Nova Science Publishers, **2011**.

(86) Van der Heide, P. *X-ray photoelectron spectroscopy : an introduction to principles and practices*; Wiley-Blackwell, **2012**.

(87) Hummers, W. S.; Offeman, R. E. *J. Am. Chem. Soc.* **1958**, *80* (6), 1339–1339.

(88) Perera, S. D.; Mariano, R. G.; Vu, K.; Nour, N.; Seitz, O.; Chabal, Y.; Balkus, K. J. *ACS Catal.* **2012**, *2* (6), 949–956.

(89) Tong, X.; Wang, H.; Wang, G.; Wan, L.; Ren, Z.; Bai, J.; Bai, J. *J. Solid State Chem.* **2011**, *184* (5), 982–989.

(90) Stobinski, L.; Lesiak, B.; Malolepszy, A.; Mazurkiewicz, M.; Mierzwa, B.; Zemek, J.; Jiricek, P.; Bieloshapka, I. *J. Electron Spectros. Relat. Phenomena* **2014**, *195*, 145–154.

(91) Thamaphat, K.; Limsuwan, P.; Ngotawornchai, B. *Kasetsart J. (Nat. Sci.)* **2008**, *42*, 357–361.

(92) Chen, C.; Xu, K.; Ji, X.; Miao, L.; Jiang, J. *Phys. Chem. Chem. Phys.* **2014**, *16* (22), 11031.

(93) Lee, S.; Molina, L. M.; López, M. J.; Alonso, J. A.; Hammer, B.; Lee, B.; Seifert, S.; Winans, R. E.; Elam, J. W.; Pellin, M. J.; Vajda, S. *Angew. Chemie Int. Ed.* **2009**, *48* (8), 1467–1471.

(94) Bøyesen, K. L.; Kristiansen, T.; Mathisen, K. *Phys. Chem. Chem. Phys.* **2014**, *16* (38), 20451–20463.

(95) Tüysüz, H.; Galilea, J. L.; Schüth, F. *Catal. Letters* **2009**, *131* (1–2), 49–53.

(96) Belin, S.; Bracey, C. L.; Briois, V.; Ellis, P. R.; Hutchings, G. J.; Hyde, T. I.; Sankar, G. *Catal. Sci. Technol* **2013**, *3*, 2944-2957.

(97) Zhang, J.; Su, D.; Zhang, A.; Wang, D.; Schlögl, R.; Hébert, C. *Angew. Chemie Int.*

*Ed.* **2007**, *46* (38), 7319–7323.

(98) Frank, B.; Blume, R.; Rinaldi, A.; Trunschke, A.; Schlögl, R. *Angew. Chemie Int. Ed.* **2011**, *50* (43), 10226–10230.

(99) Grammatikopoulos, P.; Cassidy, C.; Singh, V.; Sowwan, M. *Sci. Rep.*, 4 , **2014**, p. 5779

(100) Espinós, J. P.; J. Morales; A. Barranco; A. Caballero; J. P. Holgado, A.; González-Elipe, A. R. *J. Phys. Chem. B* **2002**, *106* (27), 6921–6929.

(101) Aruna, I.; Mehta, B. R.; Malhotra, L. K.; Shivaprasad, S. M. *J. Appl. Phys.* **2008**, *104* (6), 64308.

(102) Seah, M. P.; Gilmore, I. S.; Spencer, S. J. *Surf. Interface Anal.* **1998**, *26* (9), 617–641.

(103) Seah, M. P.; Gilmore, I. S.; Beamson, G. *Surf. Interface Anal.* **1998**, *26* (9), 642–649.

(104) Wagner, C. D. *Faraday Discuss. Chem. Soc.* **1975**, *60* (0), 291.

(105) Gaarenstroom, S. W.; Winograd, N. *J. Chem. Phys.* **1977**, *67* (8), 3500–3506.

(106) Bird, R. J.; Swift, P. *J. Electron Spectros. Relat. Phenomena* **1980**, *21* (3), 227–240.

(107) Ghijsen, J.; Tjeng, L. H.; van Elp, J.; Eskes, H.; Westerink, J.; Sawatzky, G. A.; Czyzyk, M. T. *Phys. Rev. B* **1988**, *38* (16), 11322–11330.

(108) Hwang, I. C.; Woo, S. I. *J. Phys. Chem. B*, **1997**, *101* (20), 4055–4059.

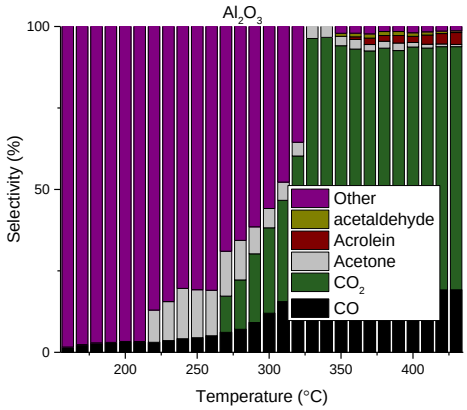
(109) Hu, L.; Liu, X.; Wang, Q.; Zhou, Y. *RSC Adv.*, **2017**, 7, 21507

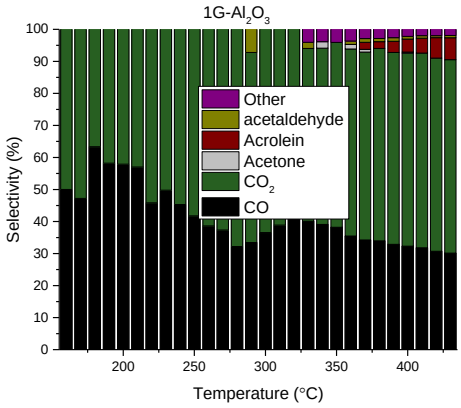
(110) Haverkamp, R. G.; Metson, J. B.; Hyland , M. M.; Welch , B. J. *Surf. Interface Anal.* **1992**, *19*, 139–144.

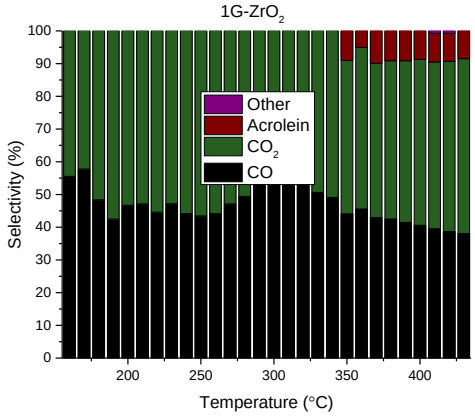
(111) Lizárraga, R.; Holmström, E.; Parker, S. C.; Arrouvel, C. *Phys. Rev. B* **2011**, *83* (9), 94201.

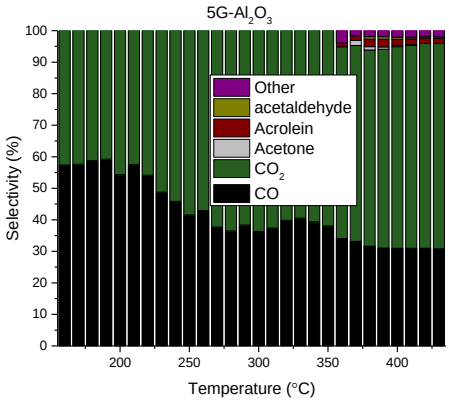
(112) Uphade, B. S.; Akita, T.; Nakamura, T.; Haruta, M. *J. Catal.* **2002**, *209* (2), 331–340.

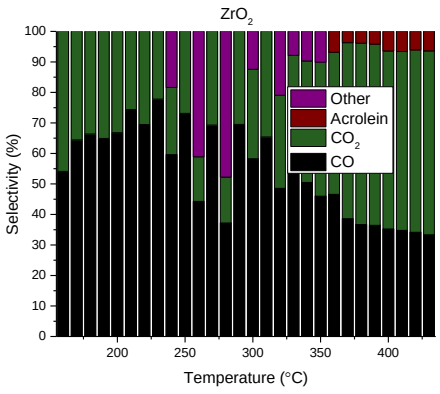
# 7 Appendix A : Catalytic Results

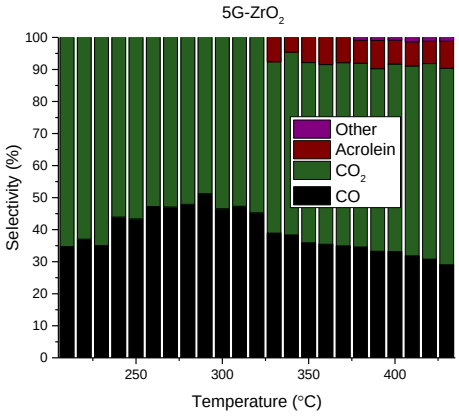


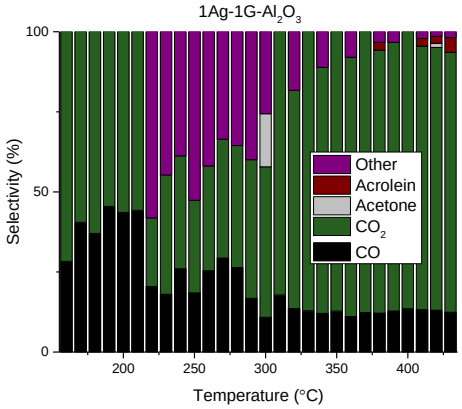



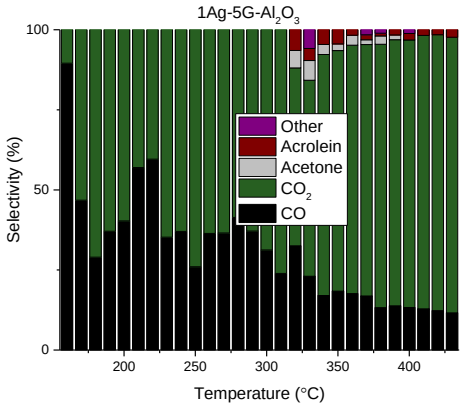



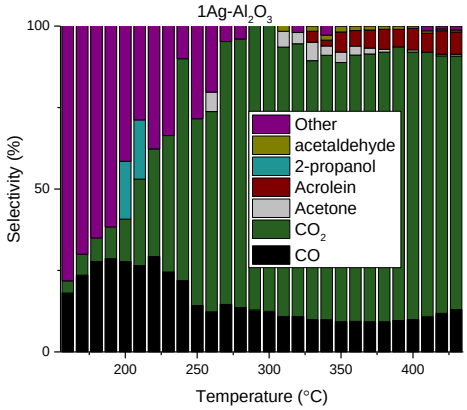



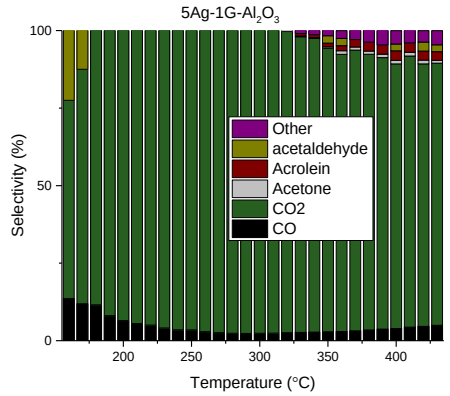



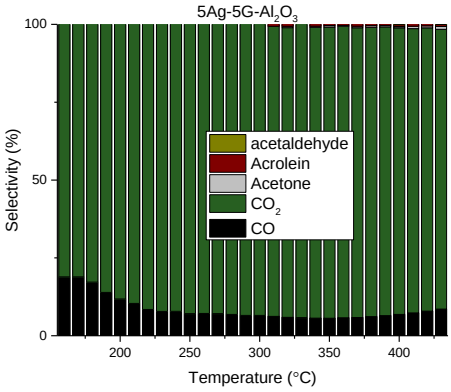



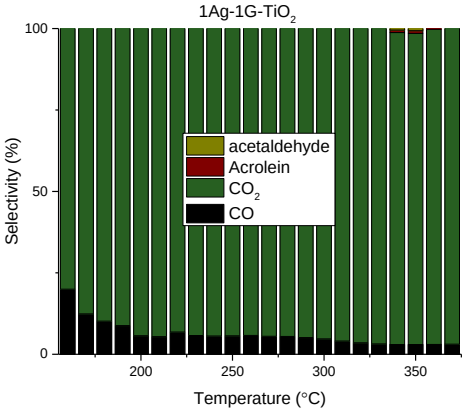

1Ag-1G-Al2O3
Selectivity (%)
Temperature (°C)
Other
Acrolein
Acetone
CO2
CO

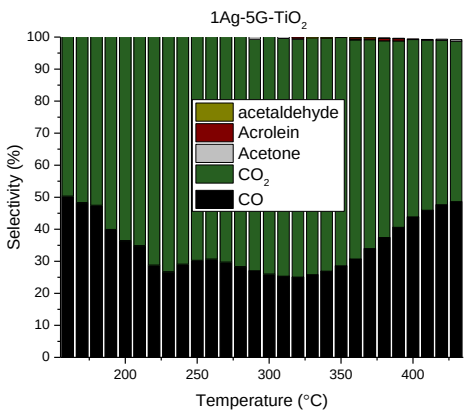

1Ag-5G-Al2O3
Selectivity (%)
Temperature (°C)
Other
Acrolein
Acetone
CO2
CO

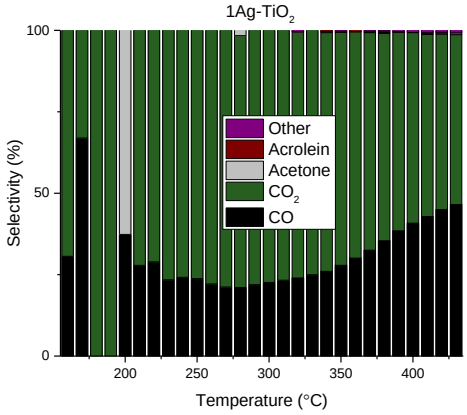

1Ag-Al2O3
Selectivity (%)
Temperature (°C)
Other
acetaldehyde
2-propanol
Acrolein
Acetone
CO2
CO

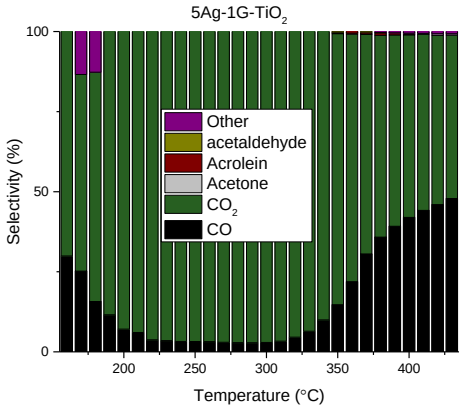

5Ag-1G-Al2O3
Selectivity (%)
Temperature (°C)
Other
acetaldehyde
Acrolein
Acetone
CO2
CO

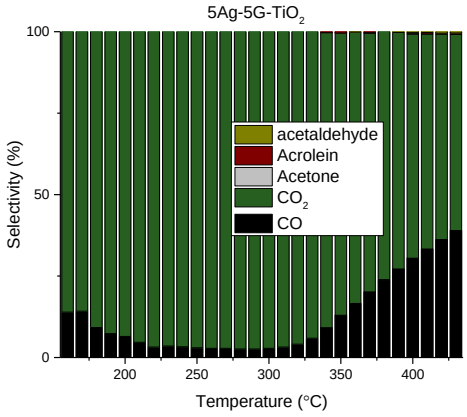

5Ag-5G-Al2O3
Selectivity (%)
Temperature (°C)
acetaldehyde
Acrolein
Acetone
CO2
CO

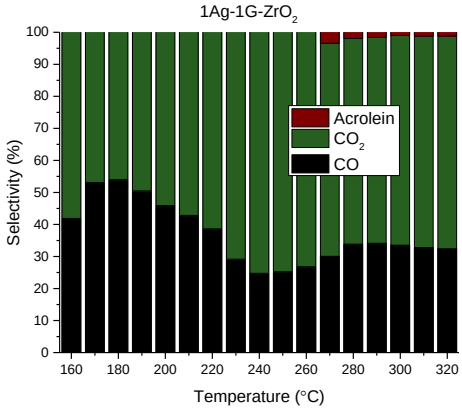

1Ag-1G-TiO2
Selectivity (%)
Temperature (°C)
acetaldehyde
Acrolein
CO2
CO

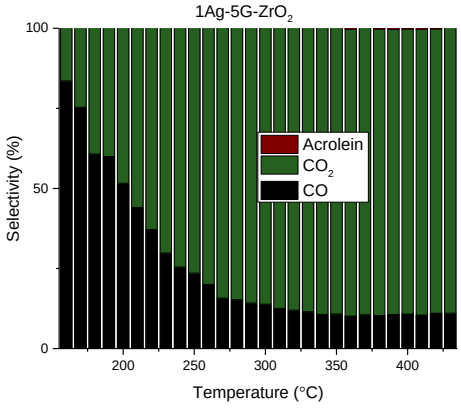

1Ag-5G-TiO2
Selectivity (%)
Temperature (°C)
acetaldehyde
Acrolein
Acetone
CO2
CO

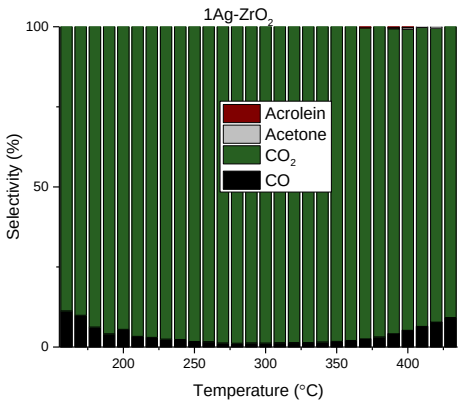

1Ag-TiO2
Selectivity (%)
Temperature (°C)
Other
Acrolein
Acetone
CO2
CO

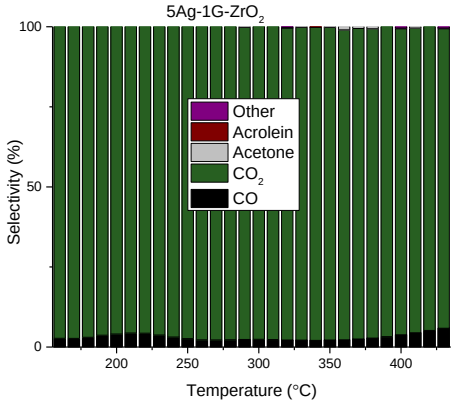

5Ag-1G-TiO2
Selectivity (%)
Temperature (°C)
Other
acetaldehyde
Acrolein
Acetone
CO2
CO

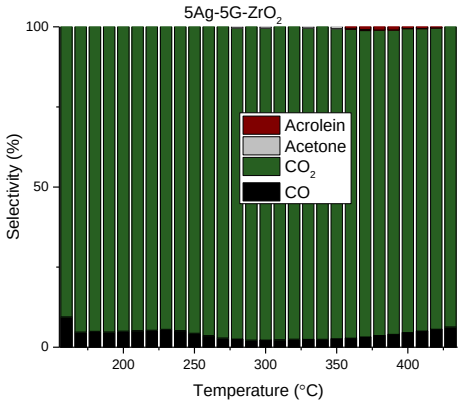

5Ag-5G-TiO2
Selectivity (%)
Temperature (°C)
acetaldehyde
Acrolein
Acetone
CO2
CO

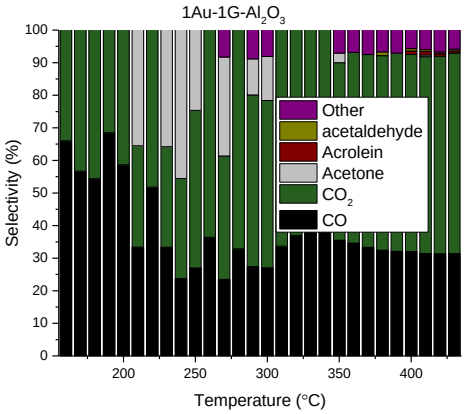

1Ag-1G-ZrO2
Selectivity (%)
Temperature (°C)
Acrolein
CO2
CO

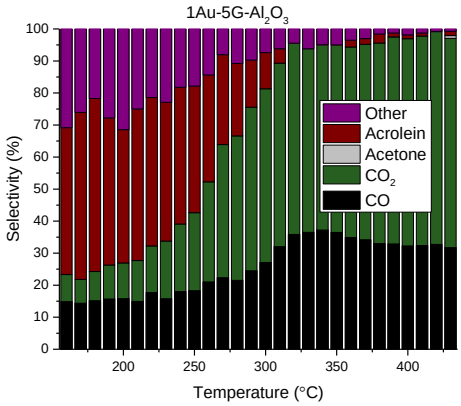

1Ag-5G-ZrO2
Selectivity (%)
Temperature (°C)
Acrolein
CO2
CO

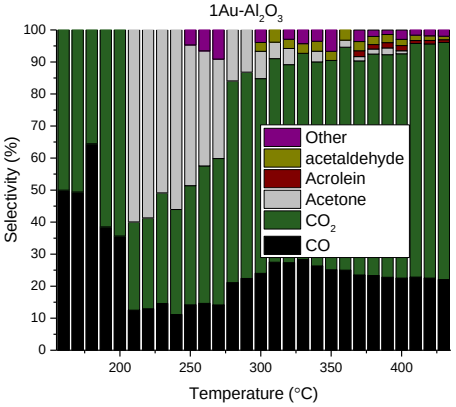

1Ag-ZrO2
Selectivity (%)
Temperature (°C)
Acrolein
Acetone
CO2
CO

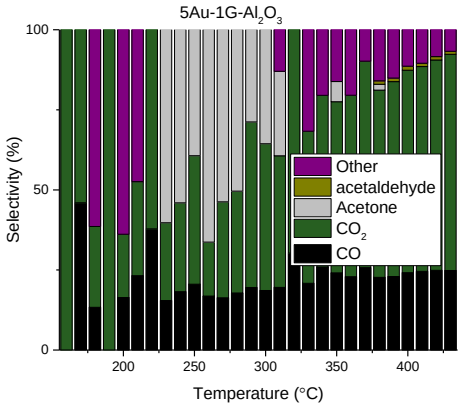

5Ag-1G-ZrO2
Selectivity (%)
Temperature (°C)
Other
Acrolein
Acetone
CO2
CO

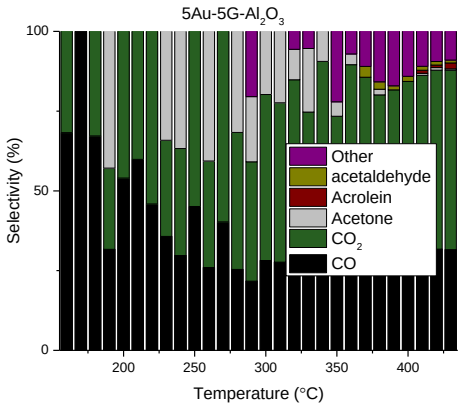

5Ag-5G-ZrO2
Selectivity (%)
Temperature (°C)
Acrolein
Acetone
CO2
CO

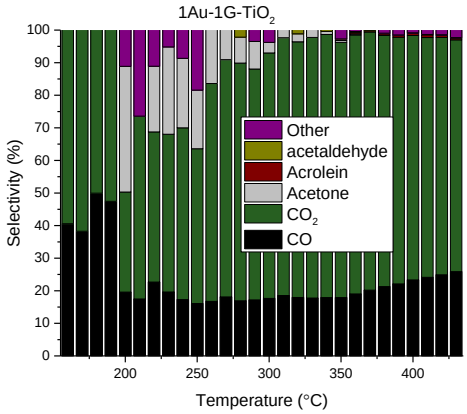

1Au-1G-Al2O3
Selectivity (%)
Temperature (°C)
Other
acetaldehyde
Acrolein
Acetone
CO2
CO

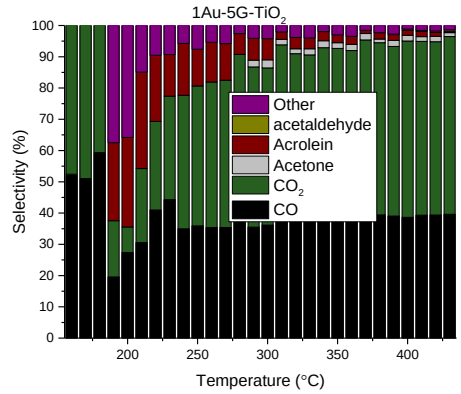

1Au-5G-Al2O3
Selectivity (%)
Temperature (°C)
Other
Acrolein
Acetone
CO2
CO

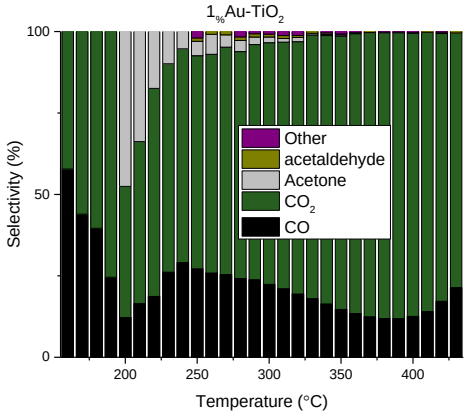

1Au-Al2O3
Selectivity (%)
Temperature (°C)
Other
acetaldehyde
Acrolein
Acetone
CO2
CO

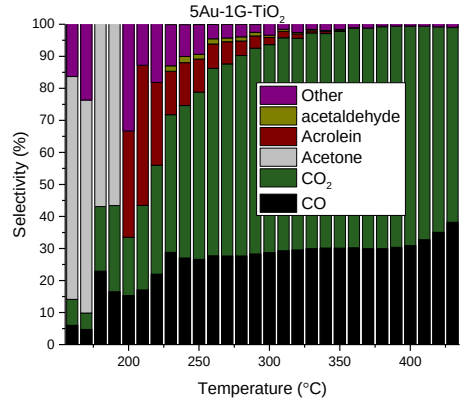

5Au-1G-Al2O3
Selectivity (%)
Temperature (°C)
Other
acetaldehyde
Acetone
CO2
CO

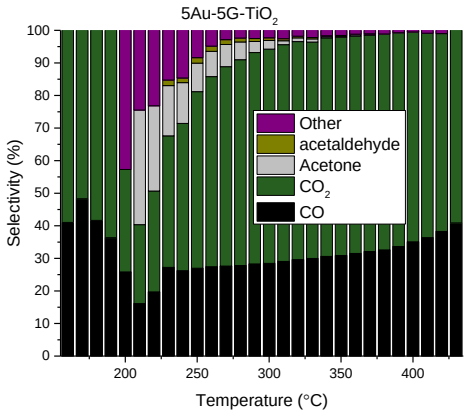

5Au-5G-Al2O3
Selectivity (%)
Temperature (°C)
Other
acetaldehyde
Acrolein
Acetone
CO2
CO

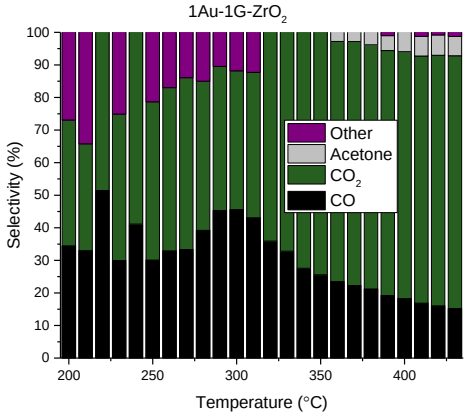

1Au-1G-TiO2
Selectivity (%)
Temperature (°C)
Other
acetaldehyde
Acrolein
Acetone
CO2
CO

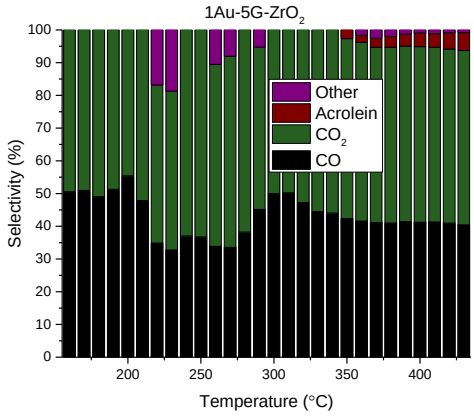

1Au-5G-TiO2
Selectivity (%)
Temperature (°C)
Other
acetaldehyde
Acrolein
Acetone
CO2
CO

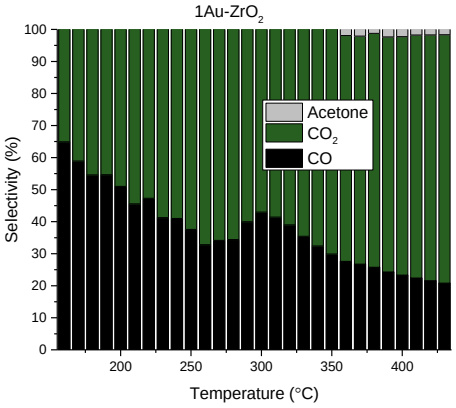

1%Au-TiO2
Selectivity (%)
Temperature (°C)
Other
acetaldehyde
Acetone
CO2
CO

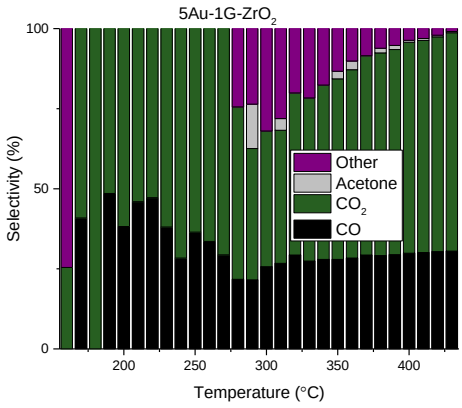

5Au-1G-TiO2
Selectivity (%)
Temperature (°C)
Other
acetaldehyde
Acrolein
Acetone
CO2
CO

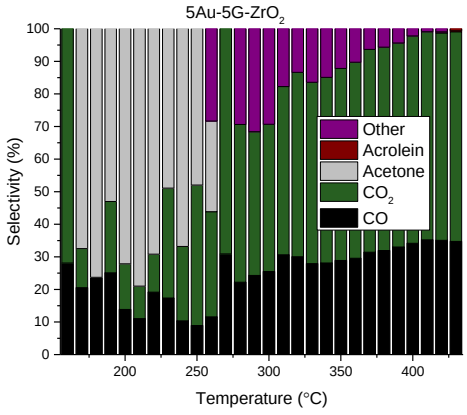

5Au-5G-TiO2
Selectivity (%)
Temperature (°C)
Other
acetaldehyde
Acetone
CO2
CO

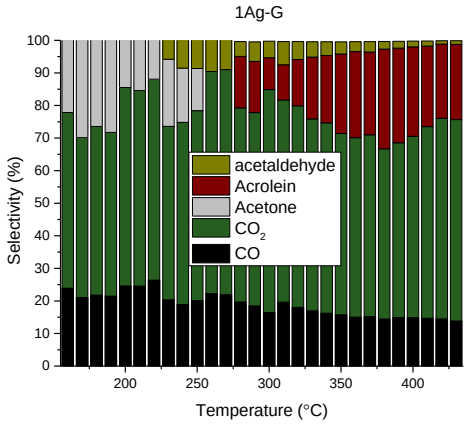

1Au-1G-ZrO2
Selectivity (%)
Temperature (°C)
Other
Acetone
CO2
CO

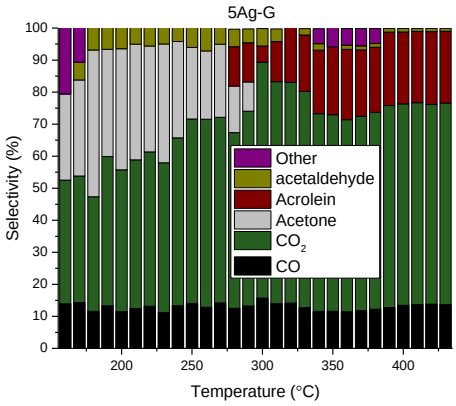

1Au-5G-ZrO2
Selectivity (%)
Temperature (°C)
Other
Acrolein
CO2
CO

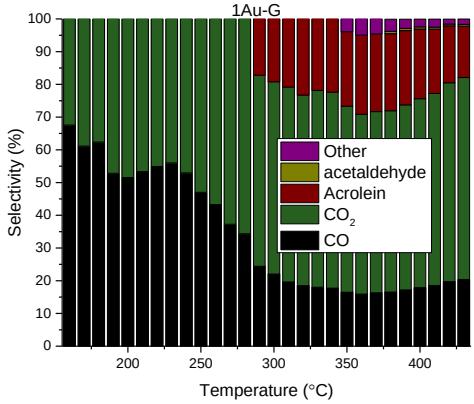

1Au-ZrO2
Selectivity (%)
Temperature (°C)
Acetone
CO2
CO

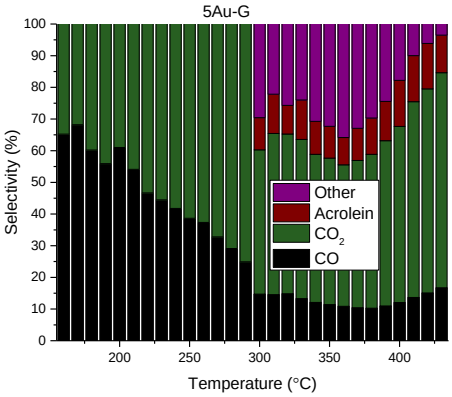

5Au-1G-ZrO2
Selectivity (%)
Temperature (°C)
Other
Acetone
CO2
CO

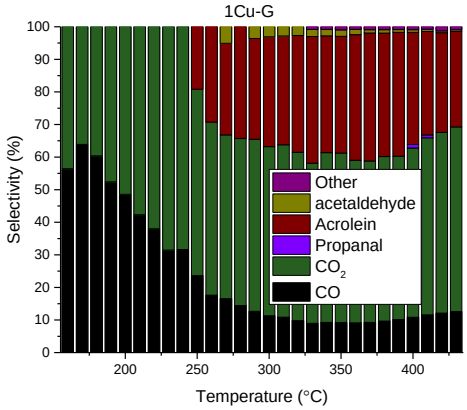

5Au-5G-ZrO2
Selectivity (%)
Temperature (°C)
Other
Acrolein
Acetone
CO2
CO

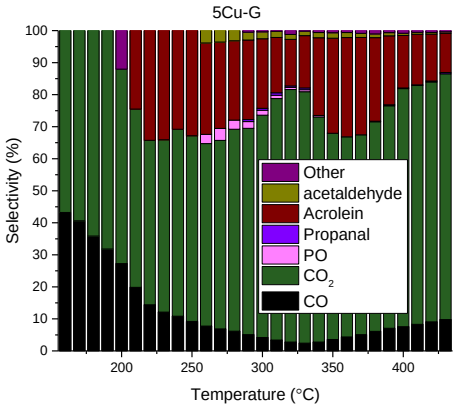

1Ag-G
Selectivity (%)
Temperature (°C)
acetaldehyde
Acrolein
Acetone
CO2
CO

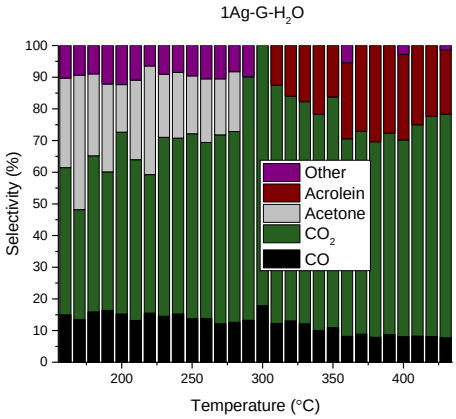

5Ag-G
Selectivity (%)
Temperature (°C)
Other
acetaldehyde
Acrolein
Acetone
CO2
CO

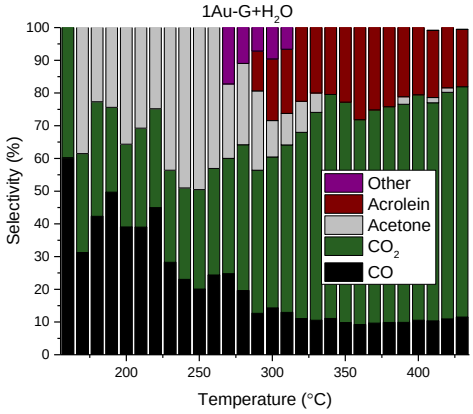

1Au-G
Selectivity (%)
Temperature (°C)
Other
acetaldehyde
Acrolein
CO2
CO

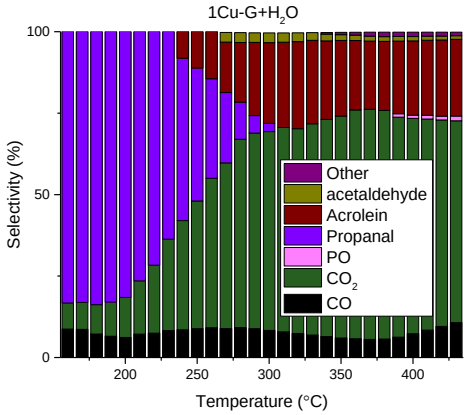

5Au-G
Selectivity (%)
Temperature (°C)
Other
Acrolein
CO2
CO

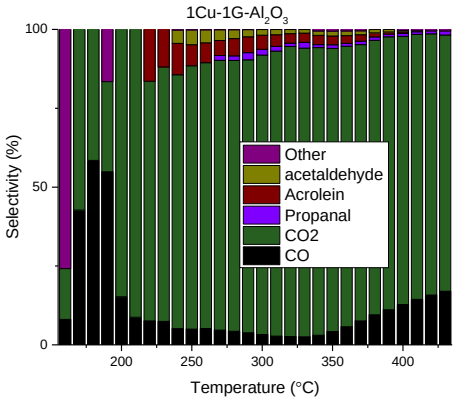

1Cu-G
Selectivity (%)
Temperature (°C)
Other
acetaldehyde
Acrolein
Propanal
CO2
CO

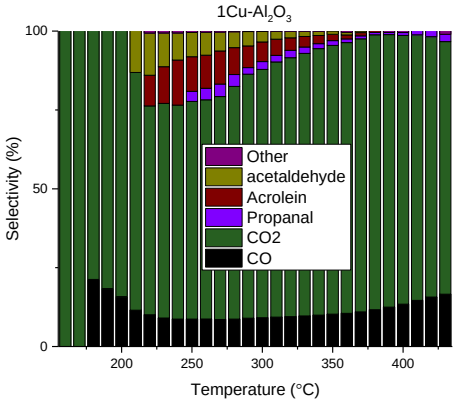

5Cu-G
Selectivity (%)
Temperature (°C)
Other
acetaldehyde
Acrolein
Propanal
PO
CO2
CO

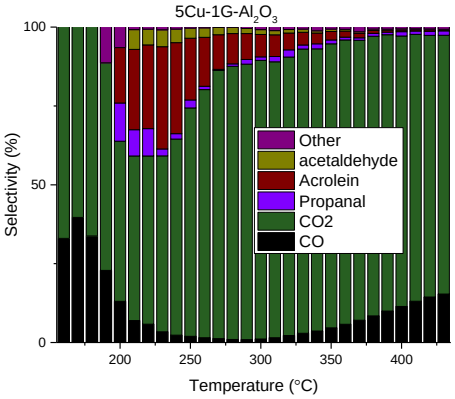

1Ag-G-H2O
Selectivity (%)
Temperature (°C)
Other
Acrolein
Acetone
CO2
CO

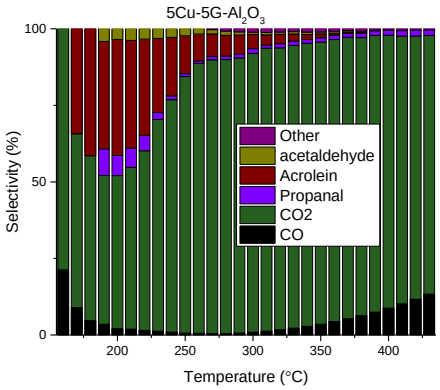

1Au-G+H2O
Selectivity (%)
Temperature (°C)
Other
Acrolein
Acetone
CO2
CO

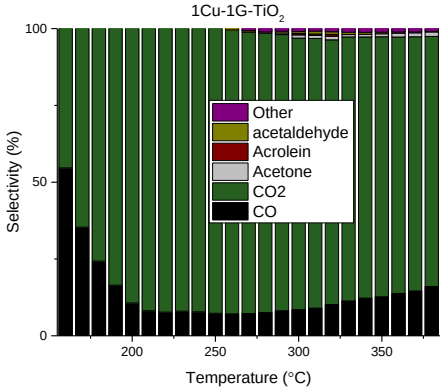

1Cu-G+H2O
Selectivity (%)
Temperature (°C)
Other
acetaldehyde
Acrolein
Propanal
PO
CO2
CO

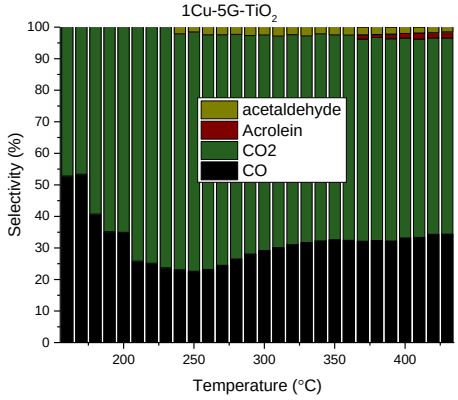

1Cu-1G-Al2O3
Selectivity (%)
Temperature (°C)
Other
acetaldehyde
Acrolein
Propanal
CO2
CO

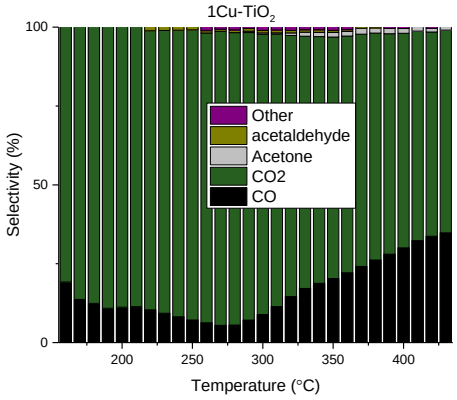

1Cu-Al2O3
Selectivity (%)
Temperature (°C)
Other
acetaldehyde
Acrolein
Propanal
CO2
CO

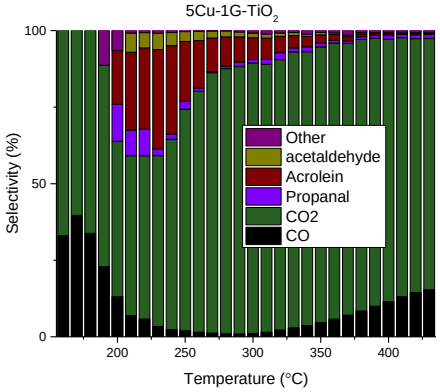

5Cu-1G-Al2O3
Selectivity (%)
Temperature (°C)
Other
acetaldehyde
Acrolein
Propanal
CO2
CO

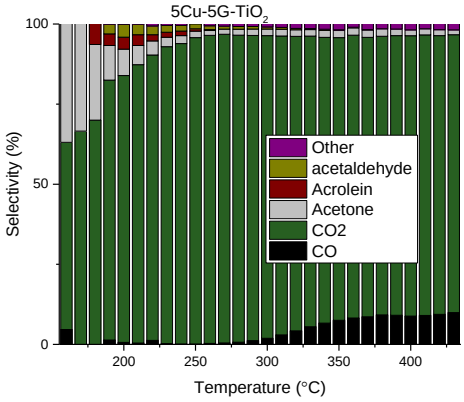

5Cu-5G-Al2O3
Selectivity (%)
Temperature (°C)
Other
acetaldehyde
Acrolein
Propanal
CO2
CO

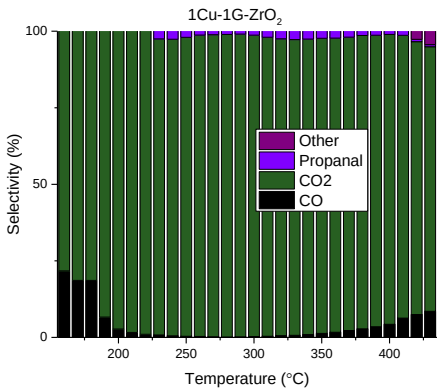

1Cu-1G-TiO2
Selectivity (%)
Temperature (°C)
Other
acetaldehyde
Acrolein
Acetone
CO2
CO

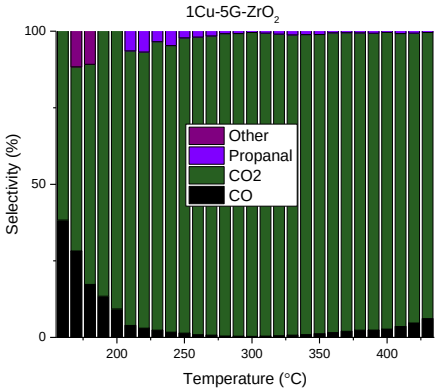

1Cu-5G-TiO2
Selectivity (%)
Temperature (°C)
acetaldehyde
Acrolein
CO2
CO

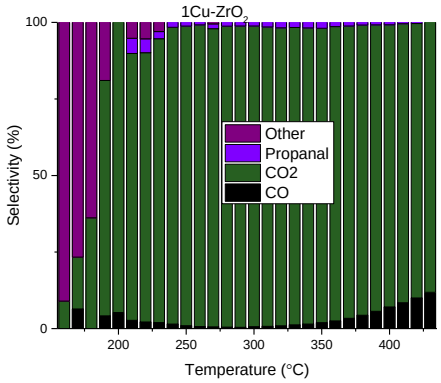

1Cu-TiO2
Selectivity (%)
Temperature (°C)
Other
acetaldehyde
Acetone
CO2
CO

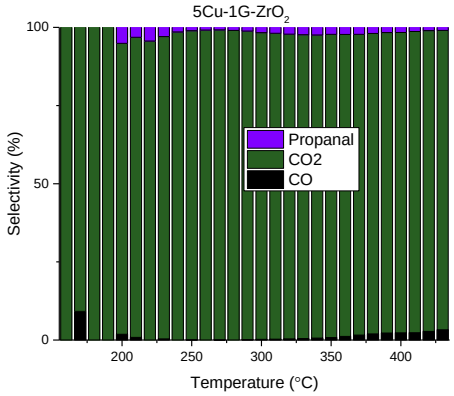

5Cu-1G-TiO2
Selectivity (%)
Temperature (°C)
Other
acetaldehyde
Acrolein
Propanal
CO2
CO

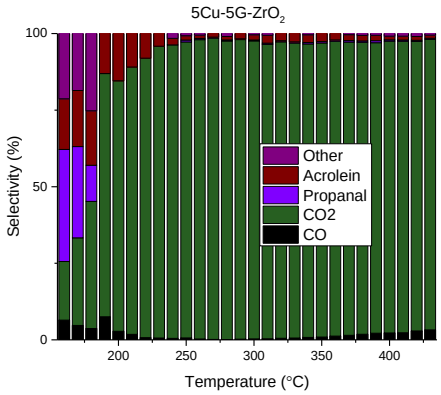

5Cu-5G-TiO2
Selectivity (%)
Temperature (°C)
Other
acetaldehyde
Acrolein
Acetone
CO2
CO


1Cu-1G-ZrO2
Selectivity (%)
Temperature (°C)
Other
Propanal
CO2
CO


1Cu-5G-ZrO2
Selectivity (%)
Temperature (°C)
Other
Propanal
CO2
CO


1Cu-ZrO2
Selectivity (%)
Temperature (°C)
Other
Propanal
CO2
CO


5Cu-1G-ZrO2
Selectivity (%)
Temperature (°C)
Propanal
CO2
CO


5Cu-5G-ZrO2
Selectivity (%)
Temperature (°C)
Other
Acrolein
Propanal
CO2
CO